

國立臺灣海洋大學

河海工程學系

碩士學位論文

指導教授：陳正宗 教授

陳桂鴻 助理教授

正規化無網格法求解多連通邊界值問題
Regularized meshless method for boundary value
problems with multiply-connected domain

研究生：高政宏 撰

中華民國 95 年 6 月

正規化無網格法求解多連通邊界值問題

Regualized meshless method for boundary value problems with multiply-connected domain

研究生：高政宏

Student : Jeng-Hung Kao

指導教授：陳正宗

Advisor : Jeng-Tzong Chen

陳桂鴻

Kue-Hong Chen

國立臺灣海洋大學
河海工程學系
碩士論文

A Thesis
Submitted to Department of Harbor and River Engineering
College of Engineering
National Taiwan Ocean University
In Partial Fulfillment of the Requirements
for the Degree of
Master
in
Harbor and River Engineering
June 2006
Keelung, Taiwan, Republic of China

中華民國 95 年 6 月

國立臺灣海洋大學

博碩士論文全文上網授權書

(提供授權人裝訂於紙本論文書名頁之次頁用)

本授權書所授權之論文為授權人在 國立臺灣海洋大學河海工程學系 94 學年度取得 碩士 學位之論文。

記錄編號：G0M93520009

論文題目：正規化無網格法求解多連通邊界值問題

指導教授：陳正宗 陳桂鴻

■ 同意

茲同意將授權人擁有著作權之上列論文全文電子檔(含摘要)，依下述授權範圍，以非專屬、無償授權國立台灣海洋大學圖書館，不限地域、時間與次數，以微縮、光碟或其他各種數位化方式將上列論文重製，並得將數位化之上列論文及論文電子檔以上載網路方式，提供讀者基於個人非營利性質之線上檢索、閱覽、下載或列印。

■ 讀者基於非營利性質之線上檢索、閱覽、下載或列印上列論文，應依著作權法相關規定辦理。

論文全文上載網路公開之範圍及時間：

校內區域網路	■ 立即公開
校外網際網路	■ 立即公開

授 權 人：高政宏

學 號：M93520009

E-mail: m93520009@mail.ntou.edu.tw

親筆簽名或蓋章：

民 國 九 十 五 年 七 月 二 十 日

國家圖書館

博碩士論文電子檔案上網授權書

本授權書所授權之論文為授權人在國立臺灣海洋大學河海工程學系
94 學年度第 二 學期取得碩士學位之論文。

論文題目：正規化無網格法求解多連通邊界值問題
指導教授：陳正宗 陳桂鴻

茲同意將授權人擁有著作權之上列論文全文（含摘要），非專屬、
無償授權國家圖書館，不限地域、時間與次數，以微縮、光碟或其
他各種數位化方式將上列論文重製，並得將數位化之上列論文及論
文電子檔以上載網路方式，提供讀者基於個人非營利性質之線上檢
索、閱覽、下載或列印。

- 上列論文為授權人向經濟部智慧財產局申請專利之附件或相關文件之一（專利
申請案號： ），請於 年 月 日後再將上列論
文公開或上載網路。
- 因上列論文尚未正式對外發表，請於 年 月 日後再將上列論文公開
或上載網路。

授權人：高政宏

親筆簽名及蓋章：_____ 民國 九十五年 七月 二十 日

身分證字號：

電話： 傳真：

聯絡地址：台中市南屯區東興路三段199號

E-Mail：m93520009@mail.ntou.edu.tw

誌 謝

時光飛逝轉眼間兩年的碩士班生涯即將告一段落，回想當初從雲林科技大學畢業時，承蒙吳文華老師的一句話及靠著一股想提昇自己競爭力的想法，進而決定進入海洋大學力學聲響振動實驗室繼續兩年的碩士班訓練。

論文口試期間，承蒙台灣大學土木工程系 楊德良 教授、成功大學土木工程系 陳東陽 教授與台灣科技大學機械工程系 趙振綱 教授，不吝指教並提供學生寶貴意見，使得文章內容更臻完善，深表謝意。同時也感謝陳正宗老師提供良好的研究環境讓我做研究。

回想這兩年的求學生活，我想最慶幸的應該是認識我的指導教授也是我的學長陳桂鴻。在他有計畫的引導下使我能夠很快的進入狀況，經過兩年的磨練，造就我現在的一點點小成就。另一方面，在生活上他也教導我許許多多做人處事的方法及情緒壓力的管理，使我獲益良多。其次，感謝博士班學長阿德，常在我需要時適時的幫我分析解惑；還有感謝我的同學阿妙、亨利、珮敏與尚津在生活上的幫忙與鼓勵，使我能夠專心的做研究。如今的我可以有一點點小成就，還需要特別感謝我的父母在背後默默的支持及提供相關的援助，使我能夠在毫無顧慮的情況努力向前邁進，雖然做研究很辛苦但在成果出來時卻很令人振奮。最後感謝國科會計畫 NSC-94-2211-E-464-004 提供之碩士生獎學金，讓我於做研究時無經濟之壓力。

這兩年一路走來跌跌撞撞有難過有歡笑，隨著碩士班生涯劃上句點也都將成為回憶的一部分。最後，再次感謝我的父母、吳文華老師、陳桂鴻學長、阿德、阿妙、亨利、珮敏與尚津，一路走來謝謝有你們的陪伴，因為有你們的出現與陪伴使我有現在的成就，這份榮耀希望能與你們大家共同分享，謝謝！

2006/07/20 於海大力學聲響振動實驗室

Regularized meshless method for boundary value problems with multiply-connected domain

Contents

Contents	I
Table captions	III
Figure captions	IV
Notations	VIII
Abstract	XI
中文摘要	XII
Chapter 1 Introduction	
1.1 Motivation of the research	1
1.2 Organization of the thesis	3
Chapter 2 Regularized meshless method for multiply-connected Laplace problem	
Summary	5
2.1 Introduction	5
2.2 Governing equation and boundary conditions	7
2.3 Review of conventional method of fundamental solutions	8
2.4 Regularized meshless method	9
2.5 Construction of influence matrices for arbitrary domain problems	13
2.6 Numerical examples	15
2.7 Concluding remarks	16
Chapter 3 Regularized meshless method for solving antiplane shear problems with multiple inclusions	
Summary	17
3.1 Introduction	18
3.2 Governing equation and boundary conditions	19
3.3 Method of the solution	
3.3.1 Regularized meshless method	20
3.3.2 Construction of influence coefficients for arbitrary domain problems	22
3.3.3 Construction of influence matrices for inclusion problems under antiplane shear	26
3.4 Numerical examples	26
3.5 Concluding remarks	28

Chapter 4	Regularized meshless method for solving antiplane piezoelectricity problems with multiple inclusions	
	Summary	29
	4.1 Introduction	29
	4.2 Governing equation and boundary conditions	31
	4.3 Method of the solution	
	4.3.1 Regularized meshless method	33
	4.3.2 Construction of influence coefficients for problems with arbitrary domain	35
	4.3.3 Construction of influence matrices for piezoelectricity problems	36
	4.4 Numerical examples	36
	4.5 Concluding remarks	39
Chapter 5	Regularized meshless method for solving acoustic eigenproblems with multiply-connected domain	
	Summary	40
	5.1 Introduction	40
	5.2 Governing equation and boundary conditions	43
	5.3 Method of the solution	
	5.3.1 Conventional method of fundamental solutions	43
	5.3.2 Regularized meshless method	45
	5.3.3 Construction of influence matrices for problems with arbitrary domain	49
	5.3.4 Extraction of the eigenvalues	52
	5.3.5 Treatments of spurious eigenvalues	52
	5.3.6 Flowchart of solution procedures	53
	5.4 Numerical examples	53
	5.5 Concluding remarks	56
Chapter 6	Conclusions	
	6.1 Conclusions	57
	6.2 Further research	59
References		60

Table captions

Table 5-1	The former five eigenvalues for a circular domain with two equal holes by using different approaches.	66
Table 5-2	The former five eigenvalues for a circular domain with four equal holes by using different approaches.	66

Figure captions

Fig. 1-1	The conventional MFS and the RMM for the multiply-connected problems,	67
Fig. 1-2	The frame of the thesis.	68
Fig. 2-1	Solution procedures.	69
Fig. 2-2	Problem sketch for the case 2-1 ($r_0 = 2.0$, $r_1 = 0.5$, $r_2 = 0.25$ and $a = 1$).	70
Fig. 2-3	Nodes distribution (200 nodes) for the case 2-1.	70
Fig. 2-4	The norm error along the radius $r = 1.6$ versus the number of nodes for the case 2-1.	71
Fig. 2-5	The error analysis for the field solution along the radius $r = 1.6$ by using the RMM and BEM.	71
Fig. 2-6	Problem sketch for the case 2-2 ($r_0 = 2.0$, $r_1 = 0.25$ and $a = 1.0$).	72
Fig. 2-7	Nodes distribution (175 nodes) for the case 2-2.	72
Fig. 2-8	The norm error along the radius $r = 0.5$ versus the number of nodes for the case 2-2.	73
Fig. 2-9	Absolute error with the exact solution for the entire domain of the case 2-2 (400 nodes).	73
Fig. 2-10	Problem sketch and the exact solution for the case 2-3, (a) problem sketch $r = 0.5$,	74
	(b) the field potential of the exact solution.	74
Fig. 2-11	Nodes distribution (200 nodes) for the case 2-3.	75
Fig. 2-12	The norm error along the radius $r = 0.9$ versus the number of nodes for the case 2-3.	75
Fig. 3-1	Problem sketch for a multiple inclusions problem under remote shear.	76
Fig. 3-2	Decomposition of the problem.	77
Fig. 3-3	Decomposition of the problem of Fig. 3-2 (a).	78
Fig. 3-4	Flowchart of solution procedures.	79
Fig. 3-5	Problem sketch of double inclusions under antiplane shear.	80
Fig. 3-6	Stress concentration along the boundaries of both the matrix and the smaller inclusion, (a) σ_{zr}^m / τ ,	81
	(b) σ_{zr}^i / τ ,	81
	(c) $\sigma_{z\theta}^m / \tau$,	81
	(d) $\sigma_{z\theta}^i / \tau$.	81

Fig. 3-7	The absolute error of stress concentration along the boundaries of both the matrix and the smaller inclusion,	
	(a) σ_{zr}^m / τ and σ_{zr}^i / τ ,	82
	(b) $\sigma_{z\theta}^m / \tau$ and $\sigma_{z\theta}^i / \tau$.	82
Fig. 3-8	Problem sketch of three inclusions under antiplane shear.	83
Fig. 3-9	Stress concentration factor $\sigma_{z\theta}^m / \tau$ along the boundaries of both the left inclusion and matrix for various shear modulus ratios,	
	(a) $\mu_1 / \mu_0 = \mu_2 / \mu_0 = \mu_2 / \mu_0 = 0.0$,	84
	(b) $\mu_1 / \mu_0 = \mu_2 / \mu_0 = \mu_2 / \mu_0 = 0.5$,	84
	(c) $\mu_1 / \mu_0 = \mu_2 / \mu_0 = \mu_2 / \mu_0 = 2.0$,	84
	(d) $\mu_1 / \mu_0 = \mu_2 / \mu_0 = \mu_2 / \mu_0 = 5.0$.	84
Fig. 3-10	The absolute error result of stress concentration along the boundaries of both the matrix and the left inclusion for various shear modulus ratios,	
	(a) $\mu_1 / \mu_0 = \mu_2 / \mu_0 = \mu_2 / \mu_0 = 0.0$ and $\mu_1 / \mu_0 = \mu_2 / \mu_0 = \mu_2 / \mu_0 = 0.5$,	85
	(b) $\mu_1 / \mu_0 = \mu_2 / \mu_0 = \mu_2 / \mu_0 = 2.0$ and $\mu_1 / \mu_0 = \mu_2 / \mu_0 = \mu_2 / \mu_0 = 5.0$.	85
Fig. 4-1	Problem sketch.	86
Fig. 4-2	Decomposition of the problem.	87
Fig. 4-3	Decomposition of the problem of Fig. 4-2 (a).	88
Fig. 4-4	Flowchart of solution procedures.	89
Fig. 4-5	Problem sketch of elastic dielectric matrix with an inclusion.	90
Fig. 4-6	Stress concentration result along the line at $\theta = 0$ versus different elastic modulus ratios for single elastic dielectric inclusion in elastic dielectric matrix,	
	(a) elastic modulus ratio $c_{44}^m / c_{44}^i = 5$,	91
	(b) elastic modulus ratio $c_{44}^m / c_{44}^i = \infty$,	91
	(c) elastic modulus ratio $c_{44}^m / c_{44}^i = 0.1$,	91
	(d) elastic modulus ratio $c_{44}^m / c_{44}^i = 0.3$.	91
Fig. 4-7	Stress concentration result along the line at $\theta = \pi / 2$ versus different elastic modulus ratios for single elastic dielectric inclusion in elastic dielectric matrix,	
	(a) elastic modulus ratio $c_{44}^m / c_{44}^i = 5$,	92
	(b) elastic modulus ratio $c_{44}^m / c_{44}^i = \infty$,	92
	(c) elastic modulus ratio $c_{44}^m / c_{44}^i = 0.1$,	92
	(d) elastic modulus ratio $c_{44}^m / c_{44}^i = 0.3$.	92
Fig. 4-8	Problem sketch of single piezoelectric inclusion.	93
Fig. 4-9	Stress concentration result of single piezoelectric inclusion in piezoelectric matrix for different piezoelectric modulus ratios when	

	$E = -10^6 \text{ V/m}$,	
	(a) stress concentration at $\theta = 0$,	94
	(b) stress concentration at $\theta = \pi/2$.	94
Fig. 4-10	Stress concentration result of single piezoelectric inclusion in piezoelectric matrix for different piezoelectric modulus ratios when $E = 0 \text{ V/m}$,	
	(a) stress concentration at $\theta = 0$,	94
	(b) stress concentration at $\theta = \pi/2$.	94
Fig. 4-11	Stress concentration result of single piezoelectric inclusion in piezoelectric matrix for different piezoelectric modulus ratios when $E = 10^6 \text{ V/m}$,	
	(a) stress concentration at $\theta = 0$,	95
	(b) stress concentration at $\theta = \pi/2$.	95
Fig. 4-12	Contours result of single piezoelectric inclusion in piezoelectric matrix,	
	(a) electric potential ϕ ,	95
	(b) shear stress σ_{zy}^m .	95
Fig. 4-13	Problem sketch of double piezoelectric inclusions.	96
Fig. 4-14	Stress concentration $\sigma_{z\theta}^m / \tau$ result of double piezoelectric inclusions in piezoelectric matrix for different piezoelectric module ratios and electric field,	
	(a) $E_\infty = 10^6 \text{ V/m}$,	97
	(b) $E_\infty = 0.0 \text{ V/m}$,	97
	(c) $E_\infty = -10^6 \text{ V/m}$.	97
Fig. 4-15	Stress concentration σ_{zr}^m / τ result of double piezoelectric inclusions in piezoelectric matrix for different piezoelectric module ratio and electric field,	
	(a) $E_\infty = 10^6 \text{ V/m}$,	98
	(b) $E_\infty = 0.0 \text{ V/m}$,	98
	(c) $E_\infty = -10^6 \text{ V/m}$.	98
Fig. 4-16	Tangential electric field distribution along the boundaries of first inclusion for different ratios d/r_1 with $\beta = \pi/2$,	
	(a) $d/r_1 = 10.0$,	99
	(b) $d/r_1 = 1.0$,	99
	(c) $d/r_1 = 0.1$,	99
	(d) $d/r_1 = 0.02$,	100
	(e) $d/r_1 = 0.01$.	100
Fig. 4-17	Stress concentration for different ratios d/r_1 of piezoelectric constants	

	with $\beta = 0$,	
	(a) $d / r_1 = 10.0$,	101
	(b) $d / r_1 = 1.0$,	101
	(c) $d / r_1 = 0.1$.	101
Fig. 5-1	Flowchart of solution procedures.	102
Fig. 5-2	Problem sketch for the case 5-1.	103
Fig. 5-3	The first minimum singular value versus wave number.	103
Fig. 5-4	Problem sketch for the case 5-2.	104
Fig. 5-5	The first minimum singular value versus wave number,	
	(a) The result of RMM and analytical solution for the Dirichlet BC,	105
	(b) The result of RMM and analytical solution for the Neumann BC,	105
	(c) The result of RMM approach + SVD updating term.	105
Fig. 5-6	Problem sketch for the case 5-3.	106
Fig. 5-7	The eigenmode result of the RMM and BEM for the case 5-3.	107
Fig. 5-8	Problem sketch for the case 5-4.	108
Fig. 5-9	The eigenmode result of the RMM and BEM for the case 5-4.	109

Notations

B	real boundary
B'	fictitious boundary
$B^{\bar{i}}$	Neumann boundary
$B^{\bar{u}}$	Dirichlet boundary
B_p	real boundaries for multiply-connected domain problem ($p = 1, 2, 3 \dots m$)
c	radius of equal holes in a circular domain
c_{44}	shear modulus for piezoelectric materials
c_{44}^m, c_{44}^i	shear moduli for the piezoelectric matrix and inclusions
D	domain
D_x, D_y	electric displacement components in the x and y directions
d	distance between two circular boundaries at the closest points
E	magnitude of applied electric field at infinity
E_∞	magnitude of applied electric field at infinity
E_x, E_y	electric fields in the x and y directions
e	eccentricity
e_{15}	piezoelectric constant for piezoelectric materials
e_{15}^m, e_{15}^i	piezoelectric constants for the piezoelectric matrix and inclusions
$H_n^{(1)}(\cdot)$	the n -th order Hankel function of the first kind
$J_n(\cdot)$	the n -th order Bessel function of the first kind
$J_n'(\cdot)$	derivative of $J_n(\cdot)$
k	wave number
k_i	the i -th eigenvalue
k_s	spurious eigenvalue
$M(s, x)$	kernel function of Laplace problem
$\overline{M}(s, x)$	kernel function of Helmholtz problem
n_j	normal vector at the source point s_j

\bar{n}_x	normal vector at the field point x_i
R	radius of outer boundary
r_i	radius ($i = 1,2$)
r_{ij}	distance between the source point x_i and the field point s_j
s	position vector of the source point
$T(s,x)$	kernel function of Laplace problem
$\bar{T}(s,x)$	kernel function of Helmholtz problem
$t(x)$	normal derivative of $u(x)$
\bar{t}	Neumann boundary condition
$u(x)$	displacement
\bar{u}	Dirichlet boundary condition
u, v, w	displacements in the x, y and z directions
w^∞	magnitude of applied shear displacement at infinity
x	position vector of the field point
$Y_n(\cdot)$	the n -th order Bessel function of the second kind
y_i	$s_i - x_i$
ϕ	electric potential
ϕ^∞	magnitude of applied electric at infinity
τ	magnitude of applied shear stress at infinity
ε_{11}	dielectric constant for piezoelectric materials
$\varepsilon_{11}^m, \varepsilon_{11}^i$	dielectric constants for piezoelectric matrix and inclusions
γ_{zx}, γ_{zy}	shear strains of piezoelectric materials in the x and y directions
α	unknown coefficient
α^m, α^i	unknown coefficient for the matrix and inclusion
α_w^m, α_w^i	unknown coefficient of elastic displacement for the matrix and inclusion
$\alpha_\phi^m, \alpha_\phi^i$	unknown coefficient of electric field for the matrix and inclusion
σ_{zx}, σ_{zy}	shear stress components in the x and y directions
σ_{zy}^m	shear stress components in the y direction applied at matrix
$\sigma_{zr}, \sigma_{z\theta}$	normal and tangential components of shear stress

$\sigma_{zr}^m, \sigma_{z\theta}^m$	normal and tangential components of shear stress in the matrix
$\sigma_{zr}^i, \sigma_{z\theta}^i$	normal and tangential components of shear stress in the inclusion
μ	shear modulus for elastic materials
μ_0	shear modulus for the matrix
μ_k	shear modulus for the k th inclusion ($k = 1,2,3$)
∇^2	Laplacian operator
$\Sigma_{\bar{T}}, \Sigma_{\bar{M}}$	diagonal matrix of SVD
$\Phi_{\bar{T}}, \Phi_{\bar{M}}$	left unitary matrix of SVD
$\Psi_{\bar{T}}, \Psi_{\bar{M}}$	right unitary matrix of SVD

Abstract

In this thesis, the regularized meshless method is adopted to solve Laplace problems and eigenproblems with multiply-connected domain, respectively. Here, the solution is represented by using double-layer potential. The subtracting and adding-back technique is used to regularize the singularity and hypersingularity of the kernel functions. Only boundary nodes on the real boundary are required by using the proposed technique in a different way of conventional MFS by putting singularities on fictitious boundaries. A linear algebraic equation is obtained free of mesh generation. After matching boundary conditions, the unknown densities in the algebraic system can be easily determined. Test of convergence and sensitivity study of the proposed method are also done. Finally, several engineering problems including multiple inclusions problem under antiplane shear, piezoelectricity problems with multiple inclusions and multiply-connected acoustic eigenproblem, were given to demonstrate the validity of the proposed method. Numerical results agree well after comparing with the available exact solution and those of boundary element method, point-matching method and finite element method. A general-purpose program for multiple cavities and inclusions of various shapes and arbitrary positions was developed.

Keywords: Laplace problem, multiple holes, multiply-connected domain, eigenproblem, method of fundamental solution, Regularized meshless method, inclusion, piezoelectricity, eigenproblem, antiplane shear

摘要

本文係利用正規化無網格法分別求解含多連通領域拉普拉斯與特徵值問題。使用雙層勢能來表示整個場解，且使用一加一減技巧來正規化處理奇異及超奇異核函數。使用我們提出的方法有別於傳統基本解法須將源點佈在虛假邊界上，可將奇異源放在真實的邊界上，並可獲得線性代數方程。配合邊界條件，即可輕易的決定出線性代數系統的未知係數。此外，我們也做了收斂測試及敏感度的分析。最後，利用數個多連通的工程算例來驗證我們提出的方法的正確性，包含：多個夾雜受到反平面剪力的問題、多個壓電夾雜的問題及多連通聲場的特徵值問題。將結果與現有的解析解、邊界元素法、配點法及有限元素法資料做比較，都可獲得一致性的結果。最後，我們發展一套含多孔洞及任意夾雜的分析程式。

關鍵字：拉普拉斯問題、多洞、多連通、特徵值問題、基本解法、正規化無網格法、夾雜、壓電材、聲場、反平面剪力。

Chapter 1

Introduction

1.1 Motivation of the research

To simplify complexity of numerical methods in the preprocessor of data preparation, meshless methods were developed to accelerate the speed of model creation. The mesh reduction techniques possess a great promise to replace the FEM and BEM as a dominant numerical method. Because of neither domain nor surface meshing are required for the meshless method, it is very attractive for engineering communities.

The method of fundamental solutions (MFS) is one of the meshless methods as shown in Fig. 1-1 (a) and belongs to a boundary method for boundary value problems, which can be viewed as a discrete type of indirect boundary element method. The MFS was attributed to Kupradze in 1964 [1] and had been applied to potential [2], Helmholtz [3, 4, 5], diffusion [6], biharmonic [7] and elasticity problems [8]. The solution procedure makes use of the fundamental solution which satisfies the governing equation in the interested domain. To avoid the singularity problem, the solution is represented as a set of singular kernels using the single layer potentials on the fictitious boundary. The kernel function is composed of two-point function which is one kind of the radial basis functions (RBFs). The independent variable of two-point function only depends on the distance between the two points. An overview literature on the MFS over the last three decades can be found in Ref. [2]. The diagonal coefficients of influence matrices are infinite when the fictitious boundary approaches the real boundary. Despite singularity-free merit, the influence matrices

become severely ill-posed when the fictitious boundary is far away from the real boundary. It results in an ill-posed problem since the condition number for the influence matrix becomes very large. The MFS is still not a popular method because of the debatable artificial boundary distance of source location in numerical implementation especially for a complicated geometry. Therefore, many scholars put forward schemes to improve this method. Chen *et al.* [5] in Taiwan proposed an imaginary-part BEM to solving eigenproblems. On the other hand, Chen [9] in China independently developed the boundary knot method (BKM), uses the nonsingular general solution to avoid the fictitious boundary outside the physical domain in the method of fundamental solution. In order to use nonsingular solution, Laplace problem was solved by Chen using the Helmholtz equation with small wave number. For the Laplace problem, Young *et al.* [10] developed a new method to improve defects of MFS as shown in Fig. 1-1 (b). Later, they extended to solve Helmholtz problem of exterior acoustics [3] by using the same idea.

Young *et al.* [3, 10] developed a new MFS, namely regularized meshless method (RMM), to solve potential problems including the Laplace and exterior acoustic problems. The proposed singular meshless method behaves like the MFS by improving the singularity evaluation of diagonal terms when the source and observation points are coincident to avoid the ambiguity of off-set distance of the fictitious boundary for the conventional MFS. The RMM eliminates the perplexing artificial boundary in the MFS, which can be arbitrary. The subtracting and adding-back technique [3, 10, 11, 12] can regularize the singularity and hypersingularity of the kernel functions. This method can simultaneously distribute the observation and source points on the real boundary even using the singular kernels instead of non-singular kernels [13, 14]. The diagonal terms of the influence matrices can be determined out by using the proposed technique. However, numerical cases of

above mentioned two papers were limited on problems of simply-connected domain. Also, eigensolution for simply-connected problem was not solved yet by RMM. Our focus is to extend to solve for multiply-connected Laplace and eigenproblems using RMM. For eigenproblems, simply-connected case is tested first in this thesis.

In this thesis, we implement the RMM to investigate some engineering problems including multiple elastic inclusions under anti-plane shear, multiple piezoelectric inclusions under anti-plane shear and in-plane electric field and simply, multiply-connected acoustic eigenproblems.

1.2 Organization of the thesis

The frame of this thesis is shown in Fig. 1-2. In this thesis, the applications of multiply-connected-domain problems with multiple inclusions under remote shear, antiplane piezoelectricity with multiple inclusions and acoustic eigenproblem are investigated. The content of each chapter is summarized below

In chapter 2, we extend the validity of RMM for the Laplace equation to multiply-connected domain problems. The accuracy and stability of the RMM are verified in numerical experiments of the Dirichlet, Neumann, and mixed-type problems containing multiple holes.

In chapter 3, we focus on antiplane problems with multiple inclusions by using the regularized meshless method. We develop a systematic approach for solving antiplane problems with multiple inclusions by using the present method. Finally, the accuracy and stability of the present method are verified by two numerical examples.

In chapter 4, the applications to antiplane piezoelectricity problems with multiple inclusions are considered. The piezoelectricity problem with multiple inclusions

subjected to out-of-plane displacement field and in-plane electric field is solved. The accuracy of the proposed method is demonstrated through numerical examples after comparing with analytical solutions.

In chapter 5, we extend the RMM to acoustic eigenproblems with simply and multiply-connected domains. True and spurious eigenvalues are found by using the present method. Spurious eigenvalue is filtered out by using the technique of SVD updating term. The accuracy and stability of the RMM is also examined in illustrative examples.

Finally, we draw out some conclusions and further research in the chapter 6.

Chapter 2

Regularized meshless method for multiply-connected-domain Laplace problems

Summary

In this chapter, the regularized meshless method (RMM) is developed to solve two-dimensional Laplace problems with multiply-connected domain. The solution is represented by using the double layer potential. The source points can be located on the real boundary by using the proposed technique to regularize the singularity and hypersingularity of the kernel functions. The troublesome singularity in the traditional methods is avoided and the diagonal terms of influence matrices are easily determined. The accuracy and stability of the RMM are verified in numerical experiments of the Dirichlet, Neumann, and mixed-type problems containing multiple holes. The method is found to perform pretty well in comparison with the boundary element method.

2.1 Introduction

In recent years, science and engineering communities have paid much attention to the meshless method in which the element is free. Because of neither domain nor boundary meshing required for the meshless method, it is very attractive for engineers in modeling. Therefore, the meshless method becomes promising in solving engineering problems.

The boundary knot method (BKM) [9, 15, 16, 17, 18], boundary particle method [19] and method of fundamental solutions (MFS) [1, 2, 20] belong to the boundary-discretization-type meshless methods. The boundary knot method (BKM), developed in Ref. [9], uses the nonsingular general solution to avoid the fictitious boundary outside the physical domain in the method of fundamental solution. This idea is similar to the imaginary-part BEM for eigenproblems by Chen's group [21].

Consequently, the stability has greatly been improved, especially in handling multiply-connected problem in the BKM via the dual reciprocity method and the RBF as in the MFS. In particular, the BKM can produce the symmetric interpolation matrix which is often important in some problems (e.g., eigenvalue problem). The boundary particle method [19] is a truly boundary-only meshfree method for inhomogeneous problems, where the fundamental solution or the general solution is used to evaluate the homogeneous solution, while the high-order fundamental solution of the Laplace operator is employed to calculate the particular solution. The method can produce very accurate results with the boundary nodes for problems whose inhomogeneous function can be well represented by a polynomial approximation.

The MFS is attributed to Kupradze in 1964 [1] and had been applied to potential [2], Helmholtz [3, 4, 5], diffusion [6], biharmonic [7] and elasticity problems [8]. In the MFS, the solution is approximated by a set of fundamental solutions which are expressed in terms of sources located outside the physical domain. The unknown coefficients in the linear combination of the fundamental solutions are determined by matching the boundary condition. The method is relatively easy to implement. It is adaptive in the sense that it can take into account sharp changes in the solution and in the geometry of the domain [13, 22] and can easily treat with complex boundary conditions [7]. A survey of the MFS and related method over the last thirty years can be found in Ref. [2]. The equivalence between MFS and Trefftz method was proved by Chen *et al.* [23]. However, the MFS is still not a popular method because of the debatable artificial boundary (fictitious boundary) distance of source location in numerical implementation especially for a complicated geometry. The diagonal coefficients of influence matrices are divergent in the conventional case when the fictitious boundary approaches the physical boundary. Despite singularity-free merit, the influence matrices become severely ill-posed when the fictitious boundary is far away from the real boundary. It results in an ill-posed problem since the condition number for the influence matrix becomes very large.

Recently, Young *et al.* [3, 10] developed a modified MFS, namely regularized meshless method (RMM), to overcome the drawback of MFS for solving the Laplace equation. The RMM eliminates the perplexing artificial boundary in the MFS, which can be arbitrary. The subtracting and adding-back technique [3, 10, 11, 12] is implemented to

regularize the singularity and hypersingularity of the kernel functions. This method can simultaneously distribute the observation and source points on the physical boundary even using the singular kernels instead of non-singular kernels [14, 24]. The diagonal terms of the influence matrices can be extracted out by using the proposed technique.

Following the success of [10] for simply-connected-domain problems, this study makes the first attempt to extend the RMM to the multiply-connected-domain problems [25, 26]. A general-purpose program is developed to solve the multiply-connected Laplace problems. The results will be compared with those of the BEM and analytical solutions. Furthermore, the sensitivity and convergence test will be studied through several examples to show the validity of our method.

2.2 Governing equation and boundary conditions

Consider a boundary value problem with a potential $u(x)$, which satisfies the Laplace equation as follows:

$$\nabla^2 u(x) = 0, \quad x \in D, \quad (2-1)$$

subject to boundary conditions,

$$u(x) = \bar{u}, \quad x \in B_p^{\bar{u}}, \quad p = 1, 2, 3, \dots, m \quad (2-2)$$

$$t(x) = \bar{t}, \quad x \in B_q^{\bar{t}}, \quad p = 1, 2, 3, \dots, m \quad (2-3)$$

where ∇^2 is Laplacian operator, D is the domain of the problem, $t(x) = \frac{\partial u(x)}{\partial n_x}$, m is the total number of boundaries including $m-1$ numbers of inner boundaries and one outer boundary (the m th boundary), $B_p^{\bar{u}}$ is the essential boundary (Dirichlet boundary) of the p th boundary in which the potential is prescribed by \bar{u} and $B_q^{\bar{t}}$ is the natural boundary (Neumann boundary) of the q th boundary in which the flux is prescribed by \bar{t} . Both $B_p^{\bar{u}}$ and $B_q^{\bar{t}}$ construct the whole boundary of the domain D as shown in Fig. 1-1 (a).

2.3 Review of conventional method of fundamental solutions

By employing the RBF technique [17, 27], the representation of the solution for multiply-connected problem as shown in Fig. 1-1 (a) can be approximated in terms of the α_j strengths of the singularities at s_j as

$$\begin{aligned} u(x_i) &= \sum_{j=1}^N T(s_j, x_i) \alpha_j \\ &= \sum_{j=1}^{N_1} T(s_j, x_i) \alpha_j + \sum_{j=N_1+1}^{N_1+N_2} T(s_j, x_i) \alpha_j + \cdots + \sum_{j=N_1+N_2+\cdots+N_{m-1}+1}^N T(s_j, x_i) \alpha_j, \end{aligned} \quad (2-4)$$

$$\begin{aligned} t(x_i) &= \sum_{j=1}^N M(s_j, x_i) \alpha_j \\ &= \sum_{j=1}^{N_1} M(s_j, x_i) \alpha_j + \sum_{j=N_1+1}^{N_1+N_2} M(s_j, x_i) \alpha_j + \cdots + \sum_{j=N_1+N_2+\cdots+N_{m-1}+1}^N M(s_j, x_i) \alpha_j, \end{aligned} \quad (2-5)$$

where x_i and s_j represent i th observation point and j th source point, respectively, α_j are the j th unknown coefficients (strength of the singularity), N_1, N_2, \dots, N_{m-1} are the numbers of source points on $m-1$ numbers of inner boundaries, respectively, N_m is the number of source points on the outer boundary, while N is the total numbers of source points ($N = N_1 + N_2 + \cdots + N_m$) and $M(s_j, x_i) = \frac{\partial T(s_j, x_i)}{\partial n_{x_i}}$. The coefficients $\{\alpha_j\}_{j=1}^N$

are determined so that BCs are satisfied at the boundary points. The distributions of source points and observation points are shown in Fig. 1-1 (a) for the MFS. The chosen bases are the double layer potentials [4, 10, 25] as

$$T(s_j, x_i) = \frac{((x_i - s_j), n_j)}{r_{ij}^2}, \quad (2-6)$$

$$M(s_j, x_i) = \frac{2((x_i - s_j), n_j)((x_i - s_j), \bar{n}_i)}{r_{ij}^4} - \frac{(n_j, \bar{n}_i)}{r_{ij}^2}, \quad (2-7)$$

where (\cdot) is the inner product of two vectors, r_{ij} is $|s_j - x_i|$, n_j is the normal vector at s_j , and \bar{n}_i is the normal vector at x_i .

It is noted that the double layer potentials have both singularity and hypersingularity at source position, which lead to the troublesome artificial boundary in the MFS. The fictitious distance between the fictitious (auxiliary) boundary (B') and the real boundary (B), defined by d , shown in Fig. 1-1 (a) needs to be chosen deliberately. To overcome the abovementioned shortcoming, s_j is distributed on the physical boundary, shown in Fig. 1-1 (b), by using the proposed regularized technique as shown in Section 2.4. The reason for choosing double layer potential instead of the single layer potential as used in the RMM for the form of RBFs is to take advantage of the regularization of the subtracting and adding-back technique, so that no fictitious distance is needed when evaluating the diagonal coefficients of influence matrices which will be elaborated on later in Section 2.4. The single layer potential can not be chosen because the following Eqs. (2-9), (2-12), (2-15) and (2-18) in Section 2.4 for null equations can not be obtained. If the single-layer potential is used, the regularization of subtracting and adding-back technique can not work.

2.4 Regularized meshless method

When the collocation point x_i approaches the source point s_j , the potentials in Eqs. (2-4) and (2-5) become singular. Eqs. (2-4) and (2-5) for multiply-connected problems need to be regularized by using the regularization of subtracting and adding-back technique [3, 10, 11, 12] as follows:

$$\begin{aligned}
u(x_i^I) = & \sum_{j=1}^{N_1} T(s_j^I, x_i^I) \alpha_j + \cdots + \sum_{j=N_1+\cdots+N_{p-1}+1}^{N_1+\cdots+N_p} T(s_j^I, x_i^I) \alpha_j + \cdots \\
& + \sum_{j=N_1+\cdots+N_{m-2}+1}^{N_1+\cdots+N_{m-1}} T(s_j^I, x_i^I) \alpha_j + \sum_{j=N_1+\cdots+N_{m-1}+1}^N T(s_j^O, x_i^I) \alpha_j \\
& - \sum_{j=N_1+\cdots+N_{p-1}+1}^{N_1+\cdots+N_p} T(s_j^I, x_i^I) \alpha_j, \quad x_i^I \in B_p, \quad p = 1, 2, 3, \dots, m-1.
\end{aligned} \tag{2-8}$$

where x_i^I is located on the inner boundary ($p = 1, 2, 3, \dots, m-1$) and the superscripts I and O denote the inward and outward normal vectors, respectively, and

$$\sum_{j=N_1+\dots+N_{p-1}+1}^{N_1+\dots+N_p} T(s_j^I, x_i^I) = 0, \quad x_i^I \in B_p, \quad p = 1, 2, 3, \dots, m-1. \quad (2-9)$$

Therefore, we can obtain

$$\begin{aligned} u(x_i^I) &= \sum_{j=1}^{N_1} T(s_j^I, x_i^I) \alpha_j + \dots + \sum_{j=N_1+\dots+N_{p-1}+1}^{i-1} T(s_j^I, x_i^I) \alpha_j \\ &+ \sum_{j=i+1}^{N_1+\dots+N_p} T(s_j^I, x_i^I) \alpha_j + \dots + \sum_{j=N_1+\dots+N_{m-2}+1}^{N_1+\dots+N_{m-1}} T(s_j^I, x_i^I) \alpha_j \\ &+ \sum_{j=N_1+\dots+N_{m-1}+1}^N T(s_j^O, x_i^I) \alpha_j - \left[\sum_{j=N_1+\dots+N_{p-1}+1}^{N_1+\dots+N_p} T(s_j^I, x_i^I) - T(s_i^I, x_i^I) \right] \alpha_i, \\ &x_i^I \in B_p, \quad p = 1, 2, 3, \dots, m-1. \end{aligned} \quad (2-10)$$

When the observation point x_i^O locates on the outer boundary ($p=m$), Eq. (2-8) becomes

$$\begin{aligned} u(x_i^O) &= \sum_{j=1}^{N_1} T(s_j^I, x_i^O) \alpha_j + \sum_{j=N_1+1}^{N_1+N_2} T(s_j^I, x_i^O) \alpha_j + \dots + \sum_{j=N_1+\dots+N_{m-2}+1}^{N_1+\dots+N_{m-1}} T(s_j^I, x_i^O) \alpha_j \\ &+ \sum_{j=N_1+\dots+N_{m-1}+1}^N T(s_j^O, x_i^O) \alpha_j - \sum_{j=N_1+\dots+N_{m-1}+1}^N T(s_j^I, x_i^I) \alpha_i, \quad x_i^O \text{ and } I \in B_p, \quad p = m. \end{aligned} \quad (2-11)$$

where

$$\sum_{j=N_1+\dots+N_{m-1}+1}^N T(s_j^I, x_i^I) \alpha_i = 0, \quad x_i^I \in B_p, \quad p = m. \quad (2-12)$$

Hence, we obtain

$$\begin{aligned} u(x_i^O) &= \sum_{j=1}^{N_1} T(s_j^I, x_i^O) \alpha_j + \sum_{j=N_1+1}^{N_1+N_2} T(s_j^I, x_i^O) \alpha_j + \dots + \sum_{j=N_1+\dots+N_{m-2}+1}^{N_1+\dots+N_{m-1}} T(s_j^I, x_i^O) \alpha_j \\ &+ \sum_{j=N_1+\dots+N_{m-1}+1}^{i-1} T(s_j^O, x_i^O) \alpha_j + \sum_{j=i+1}^N T(s_j^O, x_i^O) \alpha_j \\ &- \left[\sum_{j=N_1+\dots+N_{m-1}+1}^N T(s_j^I, x_i^I) - T(s_i^O, x_i^O) \right] \alpha_i, \quad x_i^I \text{ and } O \in B_p, \quad p = m. \end{aligned} \quad (2-13)$$

Similarly, the boundary flux is obtained as

$$t(x_i^I) = \sum_{j=1}^{N_1} M(s_j^I, x_i^I) \alpha_j + \dots + \sum_{j=N_1+\dots+N_{p-1}+1}^{N_1+\dots+N_p} M(s_j^I, x_i^I) \alpha_j + \dots \quad (2-14)$$

$$\begin{aligned}
& + \sum_{j=N_1+\dots+N_{m-2}+1}^{N_1+\dots+N_{m-1}} M(s_j^I, x_i^I) \alpha_j + \sum_{j=N_1+\dots+N_{m-1}+1}^N M(s_j^O, x_i^I) \alpha_j \\
& - \sum_{j=N_1+\dots+N_{p-1}+1}^{N_1+\dots+N_p} M(s_j^I, x_i^I) \alpha_j, \quad x_i^I \in B_p, \quad p = 1, 2, 3, \dots, m-1.
\end{aligned}$$

where

$$\sum_{j=N_1+\dots+N_{p-1}+1}^{N_1+\dots+N_p} M(s_j^I, x_i^I) = 0, \quad x_i^I \in B_p, \quad p = 1, 2, 3, \dots, m-1. \quad (2-15)$$

Therefore, we obtain

$$\begin{aligned}
t(x_i^I) &= \sum_{j=1}^{N_1} M(s_j^I, x_i^I) \alpha_j + \dots + \sum_{j=N_1+\dots+N_{p-1}+1}^{i-1} M(s_j^I, x_i^I) \alpha_j \\
& + \sum_{j=i+1}^{N_1+\dots+N_p} M(s_j^I, x_i^I) \alpha_j + \dots + \sum_{j=N_1+\dots+N_{m-2}+1}^{N_1+\dots+N_{m-1}} M(s_j^I, x_i^I) \alpha_j \\
& + \sum_{j=N_1+\dots+N_{m-1}+1}^N M(s_j^O, x_i^I) \alpha_j - \left[\sum_{j=N_1+\dots+N_{p-1}+1}^{N_1+\dots+N_p} M(s_j^I, x_i^I) - M(s_i^I, x_i^I) \right] \alpha_i, \\
& x_i^I \in B_p, \quad p = 1, 2, 3, \dots, m-1.
\end{aligned} \quad (2-16)$$

When the observation point locates on the outer boundary ($p=m$), Eq. (2-14) yields

$$\begin{aligned}
t(x_i^O) &= \sum_{j=1}^{N_1} M(s_j^I, x_i^O) \alpha_j + \sum_{j=N_1+1}^{N_1+N_2} M(s_j^I, x_i^O) \alpha_j + \dots + \sum_{j=N_1+\dots+N_{m-2}+1}^{N_1+\dots+N_{m-1}} M(s_j^I, x_i^O) \alpha_j \\
& + \sum_{j=N_1+\dots+N_{m-1}+1}^N M(s_j^O, x_i^O) \alpha_j - \sum_{j=N_1+\dots+N_{m-1}+1}^N M(s_j^I, x_i^I) \alpha_j, \quad x_i^O \text{ and } x_i^I \in B_p, \quad p = m.
\end{aligned} \quad (2-17)$$

where

$$\sum_{j=N_1+\dots+N_{m-1}+1}^N M(s_j^I, x_i^I) = 0, \quad x_i^I \in B_p, \quad p = m. \quad (2-18)$$

Hence, we obtain

$$\begin{aligned}
t(x_i^O) &= \sum_{j=1}^{N_1} M(s_j^I, x_i^O) \alpha_j + \sum_{j=N_1+1}^{N_1+N_2} M(s_j^I, x_i^O) \alpha_j + \dots + \sum_{j=N_1+\dots+N_{m-2}+1}^{N_1+\dots+N_{m-1}} M(s_j^I, x_i^O) \alpha_j \\
& + \sum_{j=N_1+\dots+N_{m-1}+1}^{i-1} M(s_j^O, x_i^O) \alpha_j + \sum_{j=i+1}^N M(s_j^O, x_i^O) \alpha_j
\end{aligned} \quad (2-19)$$

$$-\left[\sum_{j=N_1+\dots+N_{m-1}+1}^N M(s_j^I, x_i^I) - M(s_i^O, x_i^O) \right] \alpha_i, \quad x_i^O \text{ and } x_i^I \in B_p, \quad p = m.$$

The detailed derivations of Eqs. (2-9), (2-12), (2-15) and (2-18) are given in the reference [10]. According to the dependence of the normal vectors for inner and outer boundaries [10], their relationships are

$$\begin{cases} T(s_j^I, x_i^I) = -T(s_j^O, x_i^O), & i \neq j \\ T(s_j^I, x_i^I) = T(s_j^O, x_i^O), & i = j \end{cases} \quad (2-20)$$

$$\begin{cases} M(s_j^I, x_i^I) = M(s_j^O, x_i^O), & i \neq j \\ M(s_j^I, x_i^I) = M(s_j^O, x_i^O), & i = j \end{cases} \quad (2-21)$$

where the left and right hand sides of the equal sign in Eqs.(2-20) and (2-21) denote the kernels for observation and source points with the inward and outward normal vectors, respectively.

By using the proposed technique, the singular terms in Eqs. (2-4) and (2-5) have been transformed into regular terms $\left(- \left[\sum_{j=N_1+N_2+\dots+N_{p-1}+1}^{N_1+N_2+\dots+N_p} T(s_j^I, x_i^I) - T(s_i^{I \text{ or } O}, x_i^{I \text{ or } O}) \right] \right)$ and $\left[\sum_{j=N_1+\dots+N_{p-1}+1}^{N_1+\dots+N_p} M(s_j^I, x_i^I) - M(s_i^{I \text{ or } O}, x_i^{I \text{ or } O}) \right]$ in Eqs. (2-10), (2-13), (2-16) and (2-19),

respectively, where $p = 1, 2, 3, \dots, m$. The terms of $\sum_{j=N_1+\dots+N_{p-1}+1}^{N_1+\dots+N_p} T(s_j^I, x_i^I)$ and

$\sum_{j=N_1+\dots+N_{p-1}+1}^{N_1+\dots+N_p} M(s_j^I, x_i^I)$ are the adding-back terms and the terms of $T(s_i^{I \text{ or } O}, x_i^{I \text{ or } O})$ and

$M(s_i^{I \text{ or } O}, x_i^{I \text{ or } O})$ are the subtracting terms in the two brackets for regularization. After using the above subtracting and adding-back technique [3, 10, 11, 12], we are able to remove the singularity and hypersingularity of the kernel functions.

2.5 Construction of influence matrices for arbitrary domain problems

By collocating N observation points to match with the BCs from Eqs. (2-10) and (2-13) for the Dirichlet problem, the linear algebraic system is obtained

$$\left\{ \begin{array}{c} \left\{ \begin{array}{c} \bar{u}_1 \\ \vdots \\ \bar{u}_{N_1} \end{array} \right\} \\ \vdots \\ \left\{ \begin{array}{c} \bar{u}_{N_1+N_2+\dots+N_{m-1}+1} \\ \vdots \\ \bar{u}_N \end{array} \right\} \end{array} \right\}_{N \times 1} = \left[\begin{array}{ccc} [T_{11}]_{N_1 \times N_1} & \cdots & [T_{1m}]_{N_1 \times N_m} \\ \vdots & \ddots & \vdots \\ [T_{m1}]_{N_m \times N_1} & \cdots & [T_{mm}]_{N_m \times N_m} \end{array} \right]_{N \times N} \left\{ \begin{array}{c} \left\{ \begin{array}{c} \alpha_1 \\ \vdots \\ \alpha_{N_1} \end{array} \right\} \\ \vdots \\ \left\{ \begin{array}{c} \alpha_{N_1+N_2+\dots+N_{m-1}+1} \\ \vdots \\ \alpha_N \end{array} \right\} \end{array} \right\}_{N \times 1}, \quad (2-22)$$

where

$$[T_{11}] = \left[\begin{array}{ccc} -\left[\sum_{j=1}^{N_1} T(s_j^I, x_1^I) - T(s_1^I, x_1^I) \right] & T(s_2^I, x_1^I) & \cdots & T(s_{N_1}^I, x_1^I) \\ T(s_1^I, x_2^I) & -\left[\sum_{j=1}^{N_1} T(s_j^I, x_2^I) - T(s_2^I, x_2^I) \right] & \cdots & T(s_{N_1}^I, x_2^I) \\ \vdots & \vdots & \ddots & \vdots \\ T(s_1^I, x_{N_1}^I) & T(s_2^I, x_{N_1}^I) & \cdots & -\left[\sum_{j=1}^{N_1} T(s_j^I, x_{N_1}^I) - T(s_{N_1}^I, x_{N_1}^I) \right] \end{array} \right]_{N_1 \times N_1}, \quad (2-23)$$

$$[T_{1m}] = \left[\begin{array}{ccc} T(s_{N_1+\dots+N_{m-1}+1}^O, x_1^I) & T(s_{N_1+\dots+N_{m-1}+2}^O, x_1^I) & \cdots & T(s_N^O, x_1^I) \\ T(s_{N_1+\dots+N_{m-1}+1}^O, x_2^I) & T(s_{N_1+\dots+N_{m-1}+2}^O, x_2^I) & \cdots & T(s_N^O, x_2^I) \\ \vdots & \vdots & \ddots & \vdots \\ T(s_{N_1+\dots+N_{m-1}+1}^O, x_{N_1}^I) & T(s_{N_1+\dots+N_{m-1}+2}^O, x_{N_1}^I) & \cdots & T(s_N^O, x_{N_1}^I) \end{array} \right]_{N_1 \times N_m}, \quad (2-24)$$

$$[T_{m1}] = \left[\begin{array}{ccc} T(s_1^I, x_{N_1+\dots+N_{m-1}+1}^O) & T(s_2^I, x_{N_1+\dots+N_{m-1}+1}^O) & \cdots & T(s_{N_1}^I, x_{N_1+\dots+N_{m-1}+1}^O) \\ T(s_1^I, x_{N_1+\dots+N_{m-1}+2}^O) & T(s_2^I, x_{N_1+\dots+N_{m-1}+2}^O) & \cdots & T(s_{N_1}^I, x_{N_1+\dots+N_{m-1}+2}^O) \\ \vdots & \vdots & \ddots & \vdots \\ T(s_1^I, x_N^O) & T(s_2^I, x_N^O) & \cdots & T(s_{N_1}^I, x_N^O) \end{array} \right]_{N_m \times N_1}, \quad (2-25)$$

$$[T_{mm}] = \left[\begin{array}{ccc} -\left[\sum_{j=N_1+\dots+N_{m-1}+1}^N T(s_j^I, x_{N_1+\dots+N_{m-1}+1}^O) - T(s_{N_1+\dots+N_{m-1}+1}^O, x_{N_1+\dots+N_{m-1}+1}^O) \right] & \cdots & T(s_N^O, x_{N_1+\dots+N_{m-1}+1}^O) \\ \vdots & \ddots & T(s_N^O, x_{N_1+\dots+N_{m-1}+2}^O) \\ T(s_{N_1+\dots+N_{m-1}+1}^O, x_N^O) & \cdots & -\left[\sum_{j=N_1+\dots+N_{m-1}+1}^N T(s_j^I, x_N^O) - T(s_N^O, x_N^O) \right] \end{array} \right]_{N_m \times N_m}, \quad (2-26)$$

For the Neumann problem, Eqs. (2-16) and (2-19) yield

$$\begin{pmatrix} \left\{ \begin{array}{c} \bar{t}_1 \\ \vdots \\ \bar{t}_{N_1} \end{array} \right\} \\ \vdots \\ \left\{ \begin{array}{c} \bar{t}_{N_1+N_2+\dots+N_{m-1}+1} \\ \vdots \\ \bar{t}_N \end{array} \right\} \end{pmatrix}_{N \times 1} = \begin{bmatrix} [M_{11}]_{N_1 \times N_1} & \cdots & [M_{1m}]_{N_1 \times N_m} \\ \vdots & \ddots & \vdots \\ [M_{m1}]_{N_m \times N_1} & \cdots & [M_{mm}]_{N_m \times N_m} \end{bmatrix}_{N \times N} \begin{pmatrix} \left\{ \begin{array}{c} \alpha_1 \\ \vdots \\ \alpha_{N_1} \end{array} \right\} \\ \vdots \\ \left\{ \begin{array}{c} \alpha_{N_1+N_2+\dots+N_{m-1}+1} \\ \vdots \\ \alpha_N \end{array} \right\} \end{pmatrix}_{N \times 1}, \quad (2-27)$$

in which

$$[M_{11}] = \begin{bmatrix} -\left[\sum_{j=1}^{N_1} M(s'_j, x'_1) - M(s'_1, x'_1) \right] & M(s'_2, x'_1) & \cdots & M(s'_{N_1}, x'_1) \\ M(s'_1, x'_2) & -\left[\sum_{j=1}^{N_1} M(s'_j, x'_2) - M(s'_2, x'_2) \right] & \cdots & M(s'_{N_1}, x'_2) \\ \vdots & \vdots & \ddots & \vdots \\ M(s'_1, x'_{N_1}) & M(s'_2, x'_{N_1}) & \cdots & -\left[\sum_{j=1}^{N_1} M(s'_j, x'_{N_1}) - M(s'_{N_1}, x'_{N_1}) \right] \end{bmatrix}_{N_1 \times N_1}, \quad (2-28)$$

$$[M_{1m}] = \begin{bmatrix} M(s_{N_1+\dots+N_{m-1}+1}^O, x'_1) & M(s_{N_1+\dots+N_{m-1}+2}^O, x'_1) & \cdots & M(s_N^O, x'_1) \\ M(s_{N_1+\dots+N_{m-1}+1}^O, x'_2) & M(s_{N_1+\dots+N_{m-1}+2}^O, x'_2) & \cdots & M(s_N^O, x'_2) \\ \vdots & \vdots & \ddots & \vdots \\ M(s_{N_1+\dots+N_{m-1}+1}^O, x'_{N_1}) & M(s_{N_1+\dots+N_{m-1}+2}^O, x'_{N_1}) & \cdots & M(s_N^O, x'_{N_1}) \end{bmatrix}_{N_1 \times N_m}, \quad (2-29)$$

$$[M_{m1}] = \begin{bmatrix} M(s_1^I, x_{N_1+\dots+N_{m-1}+1}^O) & M(s_2^I, x_{N_1+\dots+N_{m-1}+1}^O) & \cdots & M(s_{N_1}^I, x_{N_1+\dots+N_{m-1}+1}^O) \\ M(s_1^I, x_{N_1+\dots+N_{m-1}+2}^O) & M(s_2^I, x_{N_1+\dots+N_{m-1}+2}^O) & \cdots & M(s_{N_1}^I, x_{N_1+\dots+N_{m-1}+2}^O) \\ \vdots & \vdots & \ddots & \vdots \\ M(s_1^I, x_N^O) & M(s_2^I, x_N^O) & \cdots & M(s_{N_1}^I, x_N^O) \end{bmatrix}_{N_m \times N_1}, \quad (2-30)$$

$$[M_{mm}] = \begin{bmatrix} -\left[\sum_{j=N_1+\dots+N_{m-1}+1}^N M(s_j^I, x_{N_1+\dots+N_{m-1}+1}^O) - M(s_{N_1+\dots+N_{m-1}+1}^O, x_{N_1+\dots+N_{m-1}+1}^O) \right] & \cdots & M(s_N^O, x_{N_1+\dots+N_{m-1}+1}^O) \\ \vdots & \ddots & M(s_N^O, x_{N_1+\dots+N_{m-1}+2}^O) \\ M(s_{N_1+\dots+N_{m-1}+1}^O, x_N^O) & \cdots & -\left[\sum_{j=N_1+\dots+N_{m-1}+1}^N M(s_j^I, x_N^O) - M(s_N^O, x_N^O) \right] \end{bmatrix}_{N_m \times N_m}. \quad (2-31)$$

For the mixed-type problem, a linear combination of Eqs. (2-22) and (2-27) is required to satisfy the mixed-type BCs. After the unknown densities $(\{\alpha_j\}_{j=1}^N)$ are obtained by solving the linear algebraic equations, the field solution can be solved by using Eqs. (2-4) and (2-5). The solution procedure using the RMM is shown in Fig. 2-1.

2.6 Numerical examples

In order to show the accuracy and validity of the proposed method, the potential problems with multiply-connected domain subjected to the Dirichlet, Neumann and mixed-type BCs are considered.

Case 2-1: Neumann problem

The multiply-connected Neumann problem is shown in Fig. 2-2, and an analytical solution is

$$u = r^2 \cos(2\theta) + r \sin(\theta). \quad (2-32)$$

The node distribution (200 nodes) is shown in Fig. 2-3 and vector plot denotes the direction of out normal vector. To investigate the error analysis, the norm error is defined

as $\int_0^{2\pi} |u_{exact}(r = 1.6, \theta) - u(r = 1.6, \theta)|^2 d\theta$. The norm error versus the total number N of

source points is plotted in Fig. 2-4 by using the RMM and the BEM, respectively. By collocating 200 boundary points, we can obtain the convergent result and the norm error is less than 10^{-2} . It is found that the data using BEM and present method agree very well when the number of nodes is over 400. The potentials along the radius $r = 1.6$ versus angle are presented in Fig. 2-5 by using the RMM and the BEM, respectively. The RMM and the BEM results perform pretty well in comparison with the exact solution.

Case 2-2: Mixed-type problem

The mixed-type problem for multiply-connected domain is shown in Fig. 2-6, and an analytical solution is available as follows:

$$u = r^3 \cos(3\theta). \quad (2-33)$$

The node distribution (175 nodes) is shown in Fig. 2-7. The norm error is defined as

$\int_0^{2\pi} |u_{exact}(r=0.5, \theta) - u(r=0.5, \theta)|^2 d\theta$. The norm error of the RMM versus the total number N of source points by using the RMM and the BEM, respectively, is shown in Fig. 2-8 and the convergent result is found after distributing 200 points. By adopting 200 boundary points, the norm error is less than 10^{-3} . The absolute errors of the RMM result (400 points) in the entire domain are plotted in Fig. 2-9.

Case 2-3: Arbitrary-shape problem

The arbitrary-shape problem with continuous BCs is given in Fig. 2-10 (a). An analytical solution is available as follows:

$$u = e^x \cos(y). \quad (2-34)$$

The field potential in Eq. (2-34) is shown in Fig. 2-10 (b). The node distribution (200 nodes) is shown in Fig. 2-11. The norm error is defined as $\int_0^{2\pi} |u_{exact}(r=0.9, \theta) - u(r=0.9, \theta)|^2 d\theta$. The norm error versus the total number N of source points is shown in Fig. 2-12 and the convergent result can be found from Fig. 2-12.

2.7 Concluding remarks

In this study, we employed the RMM to solve the Laplace problems with multiply-connected domain subjected to the Dirichlet, Neumann and mixed-type BCs. Only the boundary nodes on the real boundary are required. The perplexing fictitious boundary in the MFS is then circumvented. Despite the presence of singularity and hypersingularity of double layer potential, the finite values of the diagonal terms of the influence matrix can be extracted out by employing subtracting and add-back techniques. The numerical results were obtained by applying the developed program to solve three problems with different BCs and shapes of domain. The convergent result is found from the convergent study in the three cases. Numerical results agree very well with the analytical solutions and those of the BEM.

Chapter 3

Regularized meshless method for solving antiplane shear problems with multiple inclusions

Summary

In this chapter, we employ the regularized meshless method (RMM) to solve antiplane shear problems with multiple inclusions. The solution is represented by a distribution of double layer potentials. The RMM can regularize singularity by using subtracting and adding-back technique. Therefore, the troublesome singularity in the traditional methods is avoided and the diagonal terms of influence matrices are easily determined. An inclusion problem is decomposed into two parts: one is the exterior problem for the matrix with holes subjected to remote shear, the other is the interior problem for each inclusion. The two boundary densities, essential and natural data, along the interface between the inclusion and matrix satisfy the continuity and equilibrium conditions. A linear algebraic system is obtained by matching boundary conditions and interface conditions. Finally, numerical results demonstrate the accuracy of the present solutions. Good agreements are obtained and compared well with analytical solutions and Gong's results.

3.1 Introduction

Engineering materials always contain some defects in the form of inclusions or second-phase particles. The distribution of stress in an infinite medium containing inclusions under antiplane shear has been studied by many investigators [28, 29, 30, 31, 32, 33, 34, 35, 36, 37]. In 1967, Goree and Wilson [28] presented numerical results for an infinite medium containing two inclusions under remote shear. Besides, Sendekyj [29] proposed an iterative scheme for solving problems with multiple inclusions in 1971. In addition, analytical solutions for two identical holes and inclusions were obtained by Stief [30] and by Budiansky and Carrier [31], respectively. Zimmerman [32] employed the Schwartz alternative method for plane problems with two holes or inclusions to obtain a closed-form solution. In 1992, Honein *et al.* [33] derived the analytical solution for two unequal inclusions perfectly bonded to an infinite elastic matrix under anti-plane shear. The solution was obtained via iterations of Möbius transformations involving the complex potential [33]. On the other hand, Bird and Steele [34] used a Fourier series procedure to revisit the antiplane elasticity problems of Honein *et al.s'* paper [33]. For a triangle pattern of three inclusions under antiplane shear, Gong [35] derived the general solution by employing complex potentials and the Laurent series expansion method in 1995. Based on the technique of analytical continuity and the method of successive approximation, Chao and Young [36] studied the stress concentration on a hole surrounded by two inclusions. Recently, Chen *et al.* [37] has successfully solved the anti-plane problem with circular holes and/or inclusions by using the boundary integral equation in conjunction with degenerate kernel and Fourier series. To the author's best knowledge, applications of MFS on this topic were not

found. This chapter may be the first attempt of MFS on inclusion problems under antiplane shear. Based on the same algorithm of chapter 2 [38], we focus on inclusion problems instead of holes in chapter 2.

In this chapter, the RMM is employed to solve antiplane shear problems with multiple inclusions. An inclusion problem can be decomposed into two parts. One is the infinite medium with holes and the other is interior problem for each inclusion. After considering the continuity and equilibrium conditions on the interface, a linear algebraic system can be obtained. The unknown coefficients in the algebraic system can be determined. Furthermore, the field potential and stress can be obtained. Finally, a general-purpose program was developed to solve anti-plane problems with arbitrary number of inclusions by using the present method without any difficulty. The results will be compared with analytical solutions [33] and those of analytical continuity and the Laurent series expansion method [35]. Furthermore, the stress concentration for various shear modulus ratios will be studied through several examples to show the validity of our method.

3.2 Governing equation and boundary conditions

Consider inclusions embedded in an infinite matrix as shown in Fig. 3-1. The inclusions and the matrix have different elastic properties. The matrix is subjected to a remote antiplane shear, $\sigma_{zy} = \tau$. The displacement field of the antiplane deformation is defined as:

$$u = v = 0, \quad w = w(x, y), \quad (3-1)$$

where w is a function of x and y . For a linear elastic body, the stress components are

$$\sigma_{xz} = \sigma_{zx} = \mu \frac{\partial w}{\partial x}, \quad (3-2)$$

$$\sigma_{yz} = \sigma_{zy} = \mu \frac{\partial w}{\partial y}, \quad (3-3)$$

where μ is the shear modulus. The equilibrium equation can be simplified to

$$\frac{\partial \sigma_{zx}}{\partial x} + \frac{\partial \sigma_{zy}}{\partial y} = 0. \quad (3-4)$$

Thus, we have

$$\frac{\partial^2 w}{\partial x^2} + \frac{\partial^2 w}{\partial y^2} = \nabla^2 w = 0. \quad (3-5)$$

The continuity equilibrium conditions across interface of the matrix-inclusion is described as

$$w^m = w^i, \quad (3-6)$$

$$\mu^m \frac{\partial w^m}{\partial n} = -\mu^i \frac{\partial w^i}{\partial n}, \quad (3-7)$$

where the superscripts i and m denote the inclusion and matrix, respectively. The loading is remote shear.

3.3 Methods of the solution

3.3.1 Regularized meshless method

The antiplane shear problem with multiple-inclusions is decomposed into two parts as shown in Fig. 3-2. One is the exterior problem for the matrix with holes subjected to remote shear and the other is the interior problem for each inclusion. The two boundary

data between the matrix and inclusion satisfy the continuity and equilibrium conditions in Eqs. (3-6) and (3-7). Furthermore, the exterior problem for the matrix can be superimposed by two systems as shown in Fig. 3-3. One is the matrix with no hole subjected to remote shear and the other is the matrix with hole. The representations of the two solutions for interior problem ($w(x_i^l)$) and exterior problem ($w(x_i^o)$) can be solved by using the RMM in a unified manner as follows:

(1) *Interior problem*

Following the Eq. (2-10), we obtain

$$\begin{aligned}
w(x_i^l) = & \sum_{j=1}^{N_1} T(s_j^l, x_i^l) \alpha_j + \cdots + \sum_{j=N_1+\cdots+N_{p-1}+1}^{i-1} T(s_j^l, x_i^l) \alpha_j \\
& + \sum_{j=i+1}^{N_1+\cdots+N_p} T(s_j^l, x_i^l) \alpha_j + \cdots + \sum_{j=N_1+\cdots+N_{m-2}+1}^{N_1+\cdots+N_{m-1}} T(s_j^l, x_i^l) \alpha_j \\
& + \sum_{j=N_1+\cdots+N_{m-1}+1}^N T(s_j^l, x_i^l) \alpha_j - \left[\sum_{j=N_1+\cdots+N_{p-1}+1}^{N_1+\cdots+N_p} T(s_j^l, x_i^l) - T(s_i^l, x_i^l) \right] \alpha_i.
\end{aligned} \tag{3-8}$$

Where x_i^l is located on the boundary B_p . p denotes the p th boundary.

Similarly, the boundary flux is obtained as

$$\begin{aligned}
\frac{\partial w(x_i^l)}{\partial n_{x_i^l}} = & \sum_{j=1}^{N_1} M(s_j^l, x_i^l) \alpha_j + \cdots + \sum_{j=N_1+\cdots+N_{p-1}+1}^{i-1} M(s_j^l, x_i^l) \alpha_j \\
& + \sum_{j=i+1}^{N_1+\cdots+N_p} M(s_j^l, x_i^l) \alpha_j + \cdots + \sum_{j=N_1+\cdots+N_{m-2}+1}^{N_1+\cdots+N_{m-1}} M(s_j^l, x_i^l) \alpha_j \\
& + \sum_{j=N_1+\cdots+N_{m-1}+1}^N M(s_j^l, x_i^l) \alpha_j - \left[\sum_{j=N_1+\cdots+N_{p-1}+1}^{N_1+\cdots+N_p} M(s_j^l, x_i^l) - M(s_i^l, x_i^l) \right] \alpha_i, \quad x_i^l \in B_p.
\end{aligned} \tag{3-9}$$

(2) *Exterior problem*

When the observation point x_i^O locates on the boundary B_p , p denotes p th

boundary, Eq. (2-13) becomes

$$\begin{aligned}
w(x_i^O) = & \sum_{j=1}^{N_1} T(s_j^O, x_i^O) \alpha_j + \cdots + \sum_{j=N_1+\cdots+N_{p-1}+1}^{i-1} T(s_j^O, x_i^O) \alpha_j \\
& + \sum_{j=i+1}^{N_1+\cdots+N_p} T(s_j^O, x_i^O) \alpha_j + \cdots + \sum_{j=N_1+\cdots+N_{m-1}+1}^{N_1+\cdots+N_{m-1}} T(s_j^O, x_i^O) \alpha_j \\
& + \sum_{j=N_1+\cdots+N_{m-1}+1}^N T(s_j^O, x_i^O) \alpha_j - \left[\sum_{j=N_1+\cdots+N_{p-1}+1}^{N_1+\cdots+N_p} T(s_j^I, x_i^I) - T(s_i^O, x_i^O) \right] \alpha_i, \\
& x_i^{O \text{ or } I} \in B_p.
\end{aligned} \tag{3-10}$$

Similarly, the boundary flux is obtained as

$$\begin{aligned}
\frac{\partial w(x_i^O)}{\partial n_{x_i^O}} = & \sum_{j=1}^{N_1} M(s_j^O, x_i^O) \alpha_j + \cdots + \sum_{j=N_1+\cdots+N_{p-1}+1}^{i-1} M(s_j^O, x_i^O) \alpha_j \\
& + \sum_{j=i+1}^{N_1+\cdots+N_p} M(s_j^O, x_i^O) \alpha_j + \cdots + \sum_{j=N_1+\cdots+N_{m-1}+1}^{N_1+\cdots+N_{m-1}} M(s_j^O, x_i^O) \alpha_j \\
& + \sum_{j=N_1+\cdots+N_{m-1}+1}^N M(s_j^O, x_i^O) \alpha_j - \left[\sum_{j=N_1+\cdots+N_{p-1}+1}^{N_1+\cdots+N_p} M(s_j^I, x_i^I) - M(s_i^O, x_i^O) \right] \alpha_i, \\
& x_i^{O \text{ or } I} \in B_p.
\end{aligned} \tag{3-11}$$

3.3.2 Construction of influence coefficients for arbitrary domain problems

(1) Interior problem (Inclusion)

From Eqs. (3-8) and (3-9), the linear algebraic system yields

$$\begin{Bmatrix} w_1 \\ \vdots \\ w_N \end{Bmatrix} = [T^I] \begin{Bmatrix} \alpha_1 \\ \vdots \\ \alpha_N \end{Bmatrix} = \begin{bmatrix} [T'_{11}] & \cdots & [T'_{1N}] \\ \vdots & \ddots & \vdots \\ [T'_{N1}] & \cdots & [T'_{NN}] \end{bmatrix} \begin{Bmatrix} \alpha_1 \\ \vdots \\ \alpha_N \end{Bmatrix}, \quad (3-12)$$

$$\begin{Bmatrix} \frac{\partial w_1}{\partial n} \\ \vdots \\ \frac{\partial w_N}{\partial n} \end{Bmatrix} = [M^I] \begin{Bmatrix} \alpha_1 \\ \vdots \\ \alpha_N \end{Bmatrix} = \begin{bmatrix} [M'_{11}] & \cdots & [M'_{1N}] \\ \vdots & \ddots & \vdots \\ [M'_{N1}] & \cdots & [M'_{NN}] \end{bmatrix} \begin{Bmatrix} \alpha_1 \\ \vdots \\ \alpha_N \end{Bmatrix}, \quad (3-13)$$

where

$$[T'_{11}] = \begin{bmatrix} -\left[\sum_{j=1}^{N_1} T(s'_j, x'_1) - T(s'_1, x'_1)\right] & T(s'_2, x'_1) & \cdots & T(s'_{N_1}, x'_1) \\ T(s'_1, x'_2) & -\left[\sum_{j=1}^{N_1} T(s'_j, x'_2) - T(s'_2, x'_2)\right] & \cdots & T(s'_{N_1}, x'_2) \\ \vdots & \vdots & \ddots & \vdots \\ T(s'_1, x'_{N_1}) & T(s'_2, x'_{N_1}) & \cdots & -\left[\sum_{j=1}^{N_1} T(s'_j, x'_{N_1}) - T(s'_{N_1}, x'_{N_1})\right] \end{bmatrix}_{N_1 \times N_1}, \quad (3-14)$$

$$[T'_{1N}] = \begin{bmatrix} T(s'_{N_1+\dots+N_{m-1}+1}, x'_1) & T(s'_{N_1+\dots+N_{m-1}+2}, x'_1) & \cdots & T(s'_N, x'_1) \\ T(s'_{N_1+\dots+N_{m-1}+1}, x'_2) & T(s'_{N_1+\dots+N_{m-1}+2}, x'_2) & \cdots & T(s'_N, x'_2) \\ \vdots & \vdots & \ddots & \vdots \\ T(s'_{N_1+\dots+N_{m-1}+1}, x'_{N_1}) & T(s'_{N_1+\dots+N_{m-1}+2}, x'_{N_1}) & \cdots & T(s'_N, x'_{N_1}) \end{bmatrix}_{N_1 \times N_m}, \quad (3-15)$$

$$[T'_{N1}] = \begin{bmatrix} T(s'_1, x'_{N_1+\dots+N_{m-1}+1}) & T(s'_2, x'_{N_1+\dots+N_{m-1}+1}) & \cdots & T(s'_N, x'_{N_1+\dots+N_{m-1}+1}) \\ T(s'_1, x'_{N_1+\dots+N_{m-1}+2}) & T(s'_2, x'_{N_1+\dots+N_{m-1}+2}) & \cdots & T(s'_N, x'_{N_1+\dots+N_{m-1}+2}) \\ \vdots & \vdots & \ddots & \vdots \\ T(s'_1, x'_N) & T(s'_2, x'_N) & \cdots & T(s'_N, x'_N) \end{bmatrix}_{N_m \times N_1}, \quad (3-16)$$

$$[T'_{NN}] = \begin{bmatrix} -\left[\sum_{j=N_1+\dots+N_{m-1}+1}^N T(s'_j, x'_{N_1+\dots+N_{m-1}+1}) - T(s'_{N_1+\dots+N_{m-1}+1}, x'_{N_1+\dots+N_{m-1}+1})\right] & \cdots & T(s'_{N_1+\dots+N_{m-1}+1}, x'_N) \\ \vdots & \ddots & \vdots \\ T(s'_N, x'_{N_1+\dots+N_{m-1}+1}) & \cdots & -\left[\sum_{j=N_1+\dots+N_{m-1}+1}^N T(s'_j, x'_N) - T(s'_N, x'_N)\right] \end{bmatrix}_{N_m \times N_m}, \quad (3-17)$$

$$[M'_{11}] = \begin{bmatrix} -\left[\sum_{j=1}^{N_1} M(s'_j, x'_1) - M(s'_1, x'_1)\right] & M(s'_2, x'_1) & \cdots & M(s'_{N_1}, x'_1) \\ M(s'_1, x'_2) & -\left[\sum_{j=1}^{N_1} M(s'_j, x'_2) - M(s'_2, x'_2)\right] & \cdots & M(s'_{N_1}, x'_2) \\ \vdots & \vdots & \ddots & \vdots \\ M(s'_1, x'_{N_1}) & M(s'_2, x'_{N_1}) & \cdots & -\left[\sum_{j=1}^{N_1} M(s'_j, x'_{N_1}) - M(s'_{N_1}, x'_{N_1})\right] \end{bmatrix}_{N_1 \times N_1}, \quad (3-18)$$

$$[M'_{1N}] = \begin{bmatrix} M(s'_{N_1+\dots+N_{m-1}+1}, x'_1) & M(s'_{N_1+\dots+N_{m-1}+2}, x'_1) & \dots & M(s'_N, x'_1) \\ M(s'_{N_1+\dots+N_{m-1}+1}, x'_2) & M(s'_{N_1+\dots+N_{m-1}+2}, x'_2) & \dots & M(s'_N, x'_2) \\ \vdots & \vdots & \ddots & \vdots \\ M(s'_{N_1+\dots+N_{m-1}+1}, x'_{N_1}) & M(s'_{N_1+\dots+N_{m-1}+2}, x'_{N_1}) & \dots & M(s'_N, x'_{N_1}) \end{bmatrix}_{N_1 \times N_m}, \quad (3-19)$$

$$[M'_{N1}] = \begin{bmatrix} M(s'_1, x'_{N_1+\dots+N_{m-1}+1}) & M(s'_2, x'_{N_1+\dots+N_{m-1}+1}) & \dots & M(s'_N, x'_{N_1+\dots+N_{m-1}+1}) \\ M(s'_1, x'_{N_1+\dots+N_{m-1}+2}) & M(s'_2, x'_{N_1+\dots+N_{m-1}+2}) & \dots & M(s'_N, x'_{N_1+\dots+N_{m-1}+2}) \\ \vdots & \vdots & \ddots & \vdots \\ M(s'_1, x'_N) & M(s'_2, x'_N) & \dots & M(s'_N, x'_N) \end{bmatrix}_{N_m \times N_1}, \quad (3-20)$$

$$[M'_{NN}] = \begin{bmatrix} - \left[\sum_{j=N_1+\dots+N_{m-1}+1}^N M(s'_j, x'_{N_1+\dots+N_{m-1}+1}) - M(s'_{N_1+\dots+N_{m-1}+1}, x'_{N_1+\dots+N_{m-1}+1}) \right] & \dots & M(s'_{N_1+\dots+N_{m-1}+1}, x'_N) \\ \vdots & \ddots & \vdots \\ M(s'_N, x'_{N_1+\dots+N_{m-1}+1}) & \dots & - \left[\sum_{j=N_1+\dots+N_{m-1}+1}^N M(s'_j, x'_N) - M(s'_N, x'_N) \right] \end{bmatrix}_{N_m \times N_m}. \quad (3-21)$$

(2) Exterior problem (Matrix)

Eqs. (3-10) and (3-11) yield

$$\begin{Bmatrix} w_1 \\ \vdots \\ w_N \end{Bmatrix} = [T^o] \begin{Bmatrix} \alpha_1 \\ \vdots \\ \alpha_N \end{Bmatrix} = \begin{bmatrix} [T'_{11}] & \dots & [T'_{1N}] \\ \vdots & \ddots & \vdots \\ [T'_{N1}] & \dots & [T'_{NN}] \end{bmatrix} \begin{Bmatrix} \alpha_1 \\ \vdots \\ \alpha_N \end{Bmatrix}, \quad (3-22)$$

$$\begin{Bmatrix} \frac{\partial w_1}{\partial n} \\ \vdots \\ \frac{\partial w_N}{\partial n} \end{Bmatrix} = [M^o] \begin{Bmatrix} \alpha_1 \\ \vdots \\ \alpha_N \end{Bmatrix} = \begin{bmatrix} [M'_{11}] & \dots & [M'_{1N}] \\ \vdots & \ddots & \vdots \\ [M'_{N1}] & \dots & [M'_{NN}] \end{bmatrix} \begin{Bmatrix} \alpha_1 \\ \vdots \\ \alpha_N \end{Bmatrix}, \quad (3-23)$$

in which

$$[T'_{11}] = \begin{bmatrix} - \left[\sum_{j=1}^{N_1} T(s'_j, x'_1) - T(s_1^o, x_1^o) \right] & T(s_2^o, x_1^o) & \dots & T(s_{N_1}^o, x_1^o) \\ T(s_1^o, x_2^o) & - \left[\sum_{j=1}^{N_1} T(s'_j, x'_2) - T(s_2^o, x_2^o) \right] & \dots & T(s_{N_1}^o, x_2^o) \\ \vdots & \vdots & \ddots & \vdots \\ T(s_1^o, x_{N_1}^o) & T(s_2^o, x_{N_1}^o) & \dots & - \left[\sum_{j=1}^{N_1} T(s'_j, x'_{N_1}) - T(s_{N_1}^o, x_{N_1}^o) \right] \end{bmatrix}_{N_1 \times N_1}, \quad (3-24)$$

$$[T_{1N}^o] = \begin{bmatrix} T(s_{N_1+\dots+N_{m-1}+1}^o, x_1^o) & T(s_{N_1+\dots+N_{m-1}+2}^o, x_1^o) & \cdots & T(s_N^o, x_1^o) \\ T(s_{N_1+\dots+N_{m-1}+1}^o, x_2^o) & T(s_{N_1+\dots+N_{m-1}+2}^o, x_2^o) & \cdots & T(s_N^o, x_2^o) \\ \vdots & \vdots & \ddots & \vdots \\ T(s_{N_1+\dots+N_{m-1}+1}^o, x_{N_1}^o) & T(s_{N_1+\dots+N_{m-1}+2}^o, x_{N_1}^o) & \cdots & T(s_N^o, x_{N_1}^o) \end{bmatrix}_{N_1 \times N_m}, \quad (3-25)$$

$$[T_{N1}^o] = \begin{bmatrix} T(s_1^o, x_{N_1+\dots+N_{m-1}+1}^o) & T(s_2^o, x_{N_1+\dots+N_{m-1}+1}^o) & \cdots & T(s_{N_1}^o, x_{N_1+\dots+N_{m-1}+1}^o) \\ T(s_1^o, x_{N_1+\dots+N_{m-1}+2}^o) & T(s_2^o, x_{N_1+\dots+N_{m-1}+2}^o) & \cdots & T(s_{N_1}^o, x_{N_1+\dots+N_{m-1}+2}^o) \\ \vdots & \vdots & \ddots & \vdots \\ T(s_1^o, x_N^o) & T(s_2^o, x_N^o) & \cdots & T(s_{N_1}^o, x_N^o) \end{bmatrix}_{N_m \times N_1}, \quad (3-26)$$

$$[T_{NN}^o] = \begin{bmatrix} - \left[\sum_{j=N_1+\dots+N_{m-1}+1}^N T(s_j^I, x_{N_1+\dots+N_{m-1}+1}^I) - T(s_{N_1+\dots+N_{m-1}+1}^o, x_{N_1+\dots+N_{m-1}+1}^o) \right] & \cdots & T(s_{N_1+\dots+N_{m-1}+1}^o, x_N^o) \\ \vdots & \ddots & \vdots \\ T(s_N^o, x_{N_1+\dots+N_{m-1}+1}^o) & \cdots & - \left[\sum_{j=N_1+\dots+N_{m-1}+1}^N T(s_j^I, x_N^I) - T(s_N^o, x_N^o) \right] \end{bmatrix}_{N_m \times N_m}, \quad (3-27)$$

$$[M_{11}^o] = \begin{bmatrix} - \left[\sum_{j=1}^{N_1} M(s_j^I, x_1^I) - M(s_1^o, x_1^o) \right] & M(s_2^o, x_1^o) & \cdots & M(s_{N_1}^o, x_1^o) \\ M(s_1^o, x_2^o) & - \left[\sum_{j=1}^{N_1} M(s_j^I, x_2^I) - M(s_2^o, x_2^o) \right] & \cdots & M(s_{N_1}^o, x_2^o) \\ \vdots & \vdots & \ddots & \vdots \\ M(s_1^o, x_{N_1}^o) & M(s_2^o, x_{N_1}^o) & \cdots & - \left[\sum_{j=1}^{N_1} M(s_j^I, x_{N_1}^I) - M(s_{N_1}^o, x_{N_1}^o) \right] \end{bmatrix}_{N_1 \times N_1}, \quad (3-28)$$

$$[M_{1N}^o] = \begin{bmatrix} M(s_{N_1+\dots+N_{m-1}+1}^o, x_1^o) & M(s_{N_1+\dots+N_{m-1}+2}^o, x_1^o) & \cdots & M(s_N^o, x_1^o) \\ M(s_{N_1+\dots+N_{m-1}+1}^o, x_2^o) & M(s_{N_1+\dots+N_{m-1}+2}^o, x_2^o) & \cdots & M(s_N^o, x_2^o) \\ \vdots & \vdots & \ddots & \vdots \\ M(s_{N_1+\dots+N_{m-1}+1}^o, x_{N_1}^o) & M(s_{N_1+\dots+N_{m-1}+2}^o, x_{N_1}^o) & \cdots & M(s_N^o, x_{N_1}^o) \end{bmatrix}_{N_1 \times N_m}, \quad (3-29)$$

$$[M_{N1}^o] = \begin{bmatrix} M(s_1^o, x_{N_1+\dots+N_{m-1}+1}^o) & M(s_2^o, x_{N_1+\dots+N_{m-1}+1}^o) & \cdots & M(s_{N_1}^o, x_{N_1+\dots+N_{m-1}+1}^o) \\ M(s_1^o, x_{N_1+\dots+N_{m-1}+2}^o) & M(s_2^o, x_{N_1+\dots+N_{m-1}+2}^o) & \cdots & M(s_{N_1}^o, x_{N_1+\dots+N_{m-1}+2}^o) \\ \vdots & \vdots & \ddots & \vdots \\ M(s_1^o, x_N^o) & M(s_2^o, x_N^o) & \cdots & M(s_{N_1}^o, x_N^o) \end{bmatrix}_{N_m \times N_1}, \quad (3-30)$$

$$[M_{NN}^o] = \begin{bmatrix} - \left[\sum_{j=N_1+\dots+N_{m-1}+1}^N M(s_j^I, x_{N_1+\dots+N_{m-1}+1}^I) - M(s_{N_1+\dots+N_{m-1}+1}^o, x_{N_1+\dots+N_{m-1}+1}^o) \right] & \cdots & M(s_{N_1+\dots+N_{m-1}+1}^o, x_N^o) \\ \vdots & \ddots & \vdots \\ M(s_N^o, x_{N_1+\dots+N_{m-1}+1}^o) & \cdots & - \left[\sum_{j=N_1+\dots+N_{m-1}+1}^N M(s_j^I, x_N^I) - M(s_N^o, x_N^o) \right] \end{bmatrix}_{N_m \times N_m}. \quad (3-31)$$

3.3.3 Construction of influence matrices for inclusion problems under antiplane shear

Substituting Eqs. (3-12), (3-13), (3-22) and (3-23) into Eqs. (3-6) and (3-7), the linear algebraic system for the antiplane shear problems can be obtained as:

$$\begin{bmatrix} -[T^I] & [T^O] \\ \frac{\mu^i}{\mu^m}[M^I] & [M^O] \end{bmatrix} \begin{Bmatrix} \{\alpha^i\} \\ \{\alpha^m\} \end{Bmatrix} = \begin{Bmatrix} -\{w^\infty\} \\ -\left\{ \frac{\partial w^\infty}{\partial n} \right\} \end{Bmatrix}, \quad (3-32)$$

where w^∞ denotes the out-of-plane elastic displacement at infinity. After Eq. (3-32) are solved by using the linear algebra solver, the unknown densities ($\{\alpha^i\}$ and $\{\alpha^m\}$) are obtained and the field solution can be solved by using Eq. (2-4). To provide a simple illustration of how the proposed meshless method works, the solution procedure is listed in Fig. 3-4.

3.4 Numerical examples

In order to show the accuracy and validity of the proposed method, the antiplane shear problems with multiple inclusions subjected to the remote shear are considered. Numerical examples containing two and three inclusions under the antiplane shear, respectively, are considered. The numerical results will be compared with analytical solutions [33] and those of the Laurent series expansion method [35], respectively.

Case 3-1: Two inclusions

The antiplane problem with matrix imbedded two inclusions is sketched in Fig. 3-5. The smaller inclusion is centered at the origin of radius r_1 and the larger inclusion of

radius $r_2 = 2r_1$ is centered on the y axis at $r_1 + r_2 + d$ ($d = 0.1r_1$). Stress concentrations along the boundaries of both the matrix and the smaller inclusion with $\tau = 1.0 \text{ Nm}^{-2}$, $\mu_0 = 1.0$, $\mu_1 = \frac{2}{3}\mu_0$ and $\mu_2 = \frac{13}{7}\mu_0$ are plotted in Fig. 3-6 (a)~(d), respectively by using 720 nodes. The results are compared well with analytical solutions. From Fig. 3-6 (a) and (b), both figures show the equilibrium traction along the interface between matrix and smaller inclusion. After comparing with Fig. 3-6 (c) and (d), the maximum stress concentration appears in $\theta = 0^\circ$ as expected. The absolute error of stress concentration along the interface of the smaller inclusion are plotted in Fig. 3-7 (a) and (b).

Case 3-2: Three inclusions

A matrix imbedded three inclusions under antiplane shear is considered as shown in Fig. 3-8. The geometry condition is $d = 2r_1$. The stress concentration $\sigma_{z\theta}^m$ in the matrix around the interface of the left inclusion is evaluated as shown in Fig. 3-9 (a)~(d), respectively, by using 1020 nodes. From Fig. 3-9 (a), it is obvious that the limiting case of holes ($\mu_1 / \mu_0 = \mu_2 / \mu_0 = \mu_3 / \mu_0 = 0.0$) leads to the maximum stress concentration at $\theta = 0^\circ$. Due to the interaction effects, it is larger 2 than single hole [33]. The stress component $\sigma_{z\theta}$ vanishes in the case of more rigid inclusions ($\mu_1 / \mu_0 = \mu_2 / \mu_0 = \mu_3 / \mu_0 = 5.0$), which can be explained by a general analogy between solutions for traction-free holes and those involving rigid inclusions [30]. The results are well compared with those of the Laurent series expansion method [35]. The absolute errors of stress concentration along the interface of the left inclusion for various shear modulus ratios are shown in Fig. 3-10 (a)~(b).

3.5 Concluding remarks

In this chapter, we extended the RMM approach to solve for antiplane shear problems with multiple inclusions. Only boundary nodes on the real boundary are required. The major difficulty of the coincidence of the source and collocation points in the conventional MFS is then circumvented. Furthermore, the controversy of the fictitious boundary outside the physical domain by using the conventional MFS no longer exists. Although it results in the singularity and hypersingularity due to the use of double-layer potentials, the finite values of the diagonal terms for the influence matrices have been extracted out by employing the regularization technique. The numerical results by applying the developed program agreed very well with the analytical solution and those of the Laurent series expansion method.

Chapter 4

Regularized meshless method for solving antiplane piezoelectricity problems with multiple inclusions

Summary

In this chapter, we employ the regularized meshless method (RMM) to solve antiplane piezoelectricity problems with multiple inclusions. The solution is represented by a distribution of double layer potentials. The troublesome singularity in the MFS is avoided and the diagonal terms of influence matrices are determined by using subtracting and adding-back technique. The coupled piezoelectricity system can be decomposed into two potential problems. One is an out-of-plane displacement potential field $w(x, y)$, the other is an in-plane electric potential field $\phi(x, y)$. The solutions of two potential problems are represented by using the RMM, respectively. After matching interface conditions, the linear algebraic system is obtained. Finally, the numerical results demonstrate the accuracy of the solutions after comparing with analytical solutions and those of the method of successive approximations. Good agreements are obtained.

4.1 Introduction

In recent years, the development of piezoelectric materials or structures has been made by the research community. It is well known that piezoelectric materials

undergo deformation when subjected to an electric field and displacement potential field. Bleustein (1968) [39] investigated the antiplane piezoelectric dynamics problem and discovered the existence of Bleustein wave. Pak (1992) [40] has considered a more general case by introducing a piezoelectric inclusion which, in the limiting case of vanishing elastic and piezoelectric constants, become a permeable hole containing free space with electric fields. He obtained an analytical solution by using the alternative method. Later, Honein *et al.* (1995) [41] have visited the problem of two circular piezoelectric fibers subjected to out-of-plane displacement and in-plane electric field. On the other hand, Chung and Ting (1996) [42] has used basic solution [43] approach for solving the problem of an elliptic hole in a solid of anisotropic material. Zhong and Meguid [44] employed the complex variable method to treat the partially-debonded circular inhomogeneity problems in materials under antiplane shear and inplane electric field. In 1997, Chen and Chiang [45] solved for 2D problems of an infinite piezoelectric medium containing a solitary cavity or rigid inclusion of arbitrary shape, subjected to a coupled anti-plane mechanical and in-plane electric load at the matrix by using the conformal mapping techniques. In recent years, Chao and Chang [46] studied the stress concentration and tangential stress distribution on double piezoelectricity inclusions by using the complex variable theory and the method of successive approximations. Wu *et al.* [47] employ conformal mapping and the theorem of analytic continuation for solving the problem of two piezoelectric circular cylindrical inclusions in the infinite piezoelectric medium. To the author's best knowledge, no investigators have solved this problem by using MFS. The first attempt of using MFS to solve piezoelectric inclusion problem under anti-plane load and in-plane electric load will be tried. Based on the same algorithm of Chapter 3, we focus on piezoelectricity problems with inclusions.

In this chapter, the RMM is extended to solve antiplane piezoelectric problems with

multiple piezoelectric inclusions. A general-purpose program was developed to solve antiplane piezoelectric problems with arbitrary number of inclusions. The results are compared with analytical solutions and those by using the method of successive approximations [46]. Furthermore, the tangential electric field distribution and stress concentration for different ratios of piezoelectric module will be studied through several examples to show the validity of our method.

4.2 Governing equation and boundary conditions

Consider piezoelectric inclusions embedded in an infinite domain as shown in Fig. 4-1. The inclusions and matrix have different material properties. The matrix is subjected to a remote antiplane shear, $\sigma_{zy} = \tau$, and a remote inplane electric field, $E_y = E_\infty$. A uniform electric field can be induced in piezoelectric material by applying a potential field $E = E_\infty$.

For this problem, the out-of-plane elastic displacement w and the electric potential ϕ are only functions of x and y , such that

$$w = w(x, y), \quad \phi = \phi(x, y). \quad (4-1)$$

The equilibrium equations for the stresses and the electric displacements are

$$\begin{aligned} \frac{\partial \sigma_{zx}}{\partial x} + \frac{\partial \sigma_{zy}}{\partial y} &= 0, \\ \frac{\partial D_x}{\partial x} + \frac{\partial D_y}{\partial y} &= 0, \end{aligned} \quad (4-2)$$

where σ_{zx} and σ_{zy} are the shear stresses, while D_x and D_y are the electric displacements. For linear piezoelectric materials, the constitutive relations are written as

$$\begin{aligned}
\sigma_{zx} &= c_{44}\gamma_{zx} - e_{15}E_x, \\
\sigma_{zy} &= c_{44}\gamma_{zy} - e_{15}E_y, \\
D_x &= e_{15}\gamma_{zx} + \varepsilon_{11}E_x, \\
D_y &= e_{15}\gamma_{zy} + \varepsilon_{11}E_y,
\end{aligned} \tag{4-3}$$

in which γ_{zx} and γ_{zy} are the shear strains, E_x and E_y are the electric fields, c_{44} is the elastic modulus, e_{15} denotes the piezoelectric modulus and ε_{11} represents the dielectric modulus. The shear strains γ_{zx} and γ_{zy} and the electric fields E_x and E_y are obtained by taking gradient of the displacement potential w and the electric potential ϕ by the following relations:

$$\gamma_{zx} = \frac{\partial w}{\partial x}, \quad \gamma_{zy} = \frac{\partial w}{\partial y}, \quad E_x = -\frac{\partial \phi}{\partial x}, \quad E_y = -\frac{\partial \phi}{\partial y}. \tag{4-4}$$

Substituting Eqs. (4-3) and (4-4) into (4-2), we obtain the following governing equations:

$$\begin{cases} c_{44}\nabla^2 w + e_{15}\nabla^2 \phi = 0 \\ e_{15}\nabla^2 w - \varepsilon_{11}\nabla^2 \phi = 0 \end{cases}. \tag{4-5}$$

From Eq. (4-5), we can obtain the equations as

$$\nabla^2 w = 0, \quad \nabla^2 \phi = 0, \tag{4-6}$$

where ∇^2 is the Laplacian operator. The continuity conditions across the matrix-inclusion interface are written as

$$w^i = w^m, \quad \sigma_{zr}^i = \sigma_{zr}^m, \tag{4-7}$$

$$\phi^i = \phi^m, \quad D_r^i = D_r^m, \tag{4-8}$$

where the superscripts i and m denote the inclusion and material, respectively. The loading is remote shear.

4.3 Method of the solution

4.3.1 Regularized meshless method

The antiplane piezoelectricity problem with multiple inclusions is decomposed into two parts as shown in Fig. 4-2. One is the exterior problem for matrix with holes subjected to the far-displacement field and far-electric field, the other is the interior problem for each inclusion. The two boundary data of matrix and inclusion satisfy the interface conditions in Eqs. (4-7) and (4-8). Furthermore, the exterior problem for matrix with holes subjected to a far-displacement field and far-electric field can be superimposed by two systems as shown in Fig. 4-3. One is an infinite domain with no hole subjected to a far-displacement field and far-electric field, the other is the matrix with holes. The representations of the two solutions for the interior problem ($w(x_i^I)$ and $\phi(x_i^I)$) and exterior problem ($w(x_i^O)$ and $\phi(x_i^O)$) are formulated by using the RMM as follows:

(1) Interior problem

Following Eqs. (3-8) and (3-9), we can obtain

$$\begin{aligned}
 u(x_i^I) = & \sum_{j=1}^{N_1} T(s_j^I, x_i^I) \alpha_j + \cdots + \sum_{j=N_1+\cdots+N_{p-1}+1}^{i-1} T(s_j^I, x_i^I) \alpha_j \\
 & + \sum_{j=i+1}^{N_1+\cdots+N_p} T(s_j^I, x_i^I) \alpha_j + \cdots + \sum_{j=N_1+\cdots+N_{m-2}+1}^{N_1+\cdots+N_{m-1}} T(s_j^I, x_i^I) \alpha_j \\
 & + \sum_{j=N_1+\cdots+N_{m-1}+1}^N T(s_j^I, x_i^I) \alpha_j - \left[\sum_{j=N_1+\cdots+N_{p-1}+1}^{N_1+\cdots+N_p} T(s_j^I, x_i^I) - T(s_i^I, x_i^I) \right] \alpha_i,
 \end{aligned} \tag{4-9}$$

$$x_i^l \in B_p, \quad p=1, 2, 3, \dots, m.$$

where $u(x_i^l)$ can be denoted as $w(x_i^l)$ and $\phi(x_i^l)$, respectively. Similarly, the

boundary flux is obtained as

$$\begin{aligned} t(x_i^l) = & \sum_{j=1}^{N_1} M(s_j^l, x_i^l) \alpha_j + \dots + \sum_{j=N_1+\dots+N_{p-1}+1}^{i-1} M(s_j^l, x_i^l) \alpha_j \\ & + \sum_{j=i+1}^{N_1+\dots+N_p} M(s_j^l, x_i^l) \alpha_j + \dots + \sum_{j=N_1+\dots+N_{m-2}+1}^{N_1+\dots+N_{m-1}} M(s_j^l, x_i^l) \alpha_j \\ & + \sum_{j=N_1+\dots+N_{m-1}+1}^N M(s_j^l, x_i^l) \alpha_j - \left[\sum_{j=N_1+\dots+N_{p-1}+1}^{N_1+\dots+N_p} M(s_j^l, x_i^l) - M(s_i^l, x_i^l) \right] \alpha_i, \end{aligned} \quad (4-10)$$

$$x_i^l \in B_p, \quad p=1, 2, 3, \dots, m.$$

where $t(x_i^l) = \frac{\partial u(x_i^l)}{\partial n_x}$.

(2) Exterior problem

Following Eqs. (3-10) and (3-11), we can obtain

$$\begin{aligned} u(x_i^O) = & \sum_{j=1}^{N_1} T(s_j^O, x_i^O) \alpha_j + \dots + \sum_{j=N_1+\dots+N_{p-1}+1}^{i-1} T(s_j^O, x_i^O) \alpha_j \\ & + \sum_{j=i+1}^{N_1+\dots+N_p} T(s_j^O, x_i^O) \alpha_j + \dots + \sum_{j=N_1+\dots+N_{m-2}+1}^{N_1+\dots+N_{m-1}} T(s_j^O, x_i^O) \alpha_j \\ & + \sum_{j=N_1+\dots+N_{m-1}+1}^N T(s_j^O, x_i^O) \alpha_j - \left[\sum_{j=N_1+\dots+N_{p-1}+1}^{N_1+\dots+N_p} T(s_j^l, x_i^l) - T(s_i^O, x_i^O) \right] \alpha_i, \end{aligned} \quad (4-11)$$

$$x_i^{O \text{ or } I} \in B_p, \quad p=1, 2, 3, \dots, m.$$

Similarly, the boundary flux is obtained as

$$\begin{aligned}
t(x_i^O) &= \sum_{j=1}^{N_1} M(s_j^O, x_i^O) \alpha_j + \cdots + \sum_{j=N_1+\cdots+N_{p-1}+1}^{i-1} M(s_j^O, x_i^O) \alpha_j \\
&+ \sum_{j=i+1}^{N_1+\cdots+N_p} M(s_j^O, x_i^O) \alpha_j + \cdots + \sum_{j=N_1+\cdots+N_{m-1}}^{N_1+\cdots+N_{m-1}} M(s_j^O, x_i^O) \alpha_j \\
&+ \sum_{j=N_1+\cdots+N_{m-1}+1}^N M(s_j^O, x_i^O) \alpha_j - \left[\sum_{j=N_1+\cdots+N_{p-1}+1}^{N_1+\cdots+N_p} M(s_j^I, x_i^I) - M(s_i^O, x_i^O) \right] \alpha_i, \\
x_i^{O \text{ or } I} &\in B_p, \quad p = 1, 2, 3, \dots, m.
\end{aligned} \tag{4-12}$$

4.3.2 Construction of influence coefficients for problems with arbitrary domain

Following Eqs. (4-9)~(4-12), we can obtain linear algebraic system of the interior and exterior problems, respectively.

(1) *Interior problem (Inclusion)*

$$\begin{Bmatrix} u_1 \\ \vdots \\ u_N \end{Bmatrix} = [T_q^I] \begin{Bmatrix} \alpha_1 \\ \vdots \\ \alpha_N \end{Bmatrix} = \begin{bmatrix} [T_{11}^I] & \cdots & [T_{1N}^I] \\ \vdots & \ddots & \vdots \\ [T_{N1}^I] & \cdots & [T_{NN}^I] \end{bmatrix} \begin{Bmatrix} \alpha_1 \\ \vdots \\ \alpha_N \end{Bmatrix}, \quad q \in w \text{ or } \phi, \tag{4-13}$$

$$\begin{Bmatrix} t_1 \\ \vdots \\ t_N \end{Bmatrix} = [M_q^I] \begin{Bmatrix} \alpha_1 \\ \vdots \\ \alpha_N \end{Bmatrix} = \begin{bmatrix} [M_{11}^I] & \cdots & [M_{1N}^I] \\ \vdots & \ddots & \vdots \\ [M_{N1}^I] & \cdots & [M_{NN}^I] \end{bmatrix} \begin{Bmatrix} \alpha_1 \\ \vdots \\ \alpha_N \end{Bmatrix}, \quad q \in w \text{ or } \phi, \tag{4-14}$$

where the influence matrices, $[T^I]$ and $[M^I]$, are equal to influence matrices of Eqs. (3-12) and (3-13), respectively.

(2) *Exterior problem (Matrix)*

$$\begin{Bmatrix} u_1 \\ \vdots \\ u_N \end{Bmatrix} = [T_q^O] \begin{Bmatrix} \alpha_1 \\ \vdots \\ \alpha_N \end{Bmatrix} = \begin{bmatrix} [T_{11}^O] & \cdots & [T_{1N}^O] \\ \vdots & \ddots & \vdots \\ [T_{N1}^O] & \cdots & [T_{NN}^O] \end{bmatrix} \begin{Bmatrix} \alpha_1 \\ \vdots \\ \alpha_N \end{Bmatrix}, \quad q \in w \text{ or } \phi, \tag{4-15}$$

$$\begin{Bmatrix} t_1 \\ \vdots \\ t_N \end{Bmatrix} = [M_q^o] \begin{Bmatrix} \alpha_1 \\ \vdots \\ \alpha_N \end{Bmatrix} = \begin{bmatrix} [M_{11}^o] & \cdots & [M_{1N}^o] \\ \vdots & \ddots & \vdots \\ [M_{N1}^o] & \cdots & [M_{NN}^o] \end{bmatrix} \begin{Bmatrix} \alpha_1 \\ \vdots \\ \alpha_N \end{Bmatrix}, \quad q \in w \text{ or } \phi, \quad (4-16)$$

where the influence matrices $[T^o]$ and $[M^o]$ are equal to influence matrices of Eqs. (3-22) and (3-23), respectively.

4.3.3 Construction of influence matrices for piezoelectricity problems

Substituting Eqs. (4-13), (4-14), (4-15) and (4-16) into Eqs. (4-7) and (4-8), the linear algebraic system for antiplane piezoelectricity problem can be obtained as:

$$\begin{bmatrix} -[T_w^I] & [T_w^o] & 0 & 0 \\ 0 & 0 & -[T_\phi^I] & [T_\phi^o] \\ -\frac{c_{44}^i}{c_{44}^m}[M_w^I] & -[M_w^o] & -\frac{e_{15}^i}{c_{44}^m}[M_\phi^I] & -\frac{e_{15}^m}{c_{44}^m}[M_\phi^o] \\ -[M_w^I] & -\frac{e_{15}^m}{e_{15}^i}[M_w^o] & \frac{\varepsilon_{11}^i}{e_{15}^i}[M_\phi^I] & \frac{\varepsilon_{11}^m}{e_{15}^i}[M_\phi^o] \end{bmatrix}_{4 \times 4} \begin{Bmatrix} \{\alpha_w^i\} \\ \{\alpha_w^m\} \\ \{\alpha_\phi^i\} \\ \{\alpha_\phi^m\} \end{Bmatrix}_{4 \times 1} = \begin{Bmatrix} -\{w^\infty\} \\ -\{\phi^\infty\} \\ \left\{ \frac{\partial w^\infty}{\partial n} \right\} + \frac{e_{15}^m}{c_{44}^m} \left\{ \frac{\partial \phi^\infty}{\partial n} \right\} \\ \left\{ \frac{e_{15}^m}{e_{15}^i} \frac{\partial w^\infty}{\partial n} \right\} - \left\{ \frac{\varepsilon_{11}^m}{e_{15}^i} \frac{\partial \phi^\infty}{\partial n} \right\} \end{Bmatrix}_{4 \times 1}, \quad (4-17)$$

where w and ϕ denote the out-of-plane elastic displacement and electric potential, respectively. The unknown densities ($\{\alpha_w^i\}$, $\{\alpha_w^m\}$, $\{\alpha_\phi^i\}$, $\{\alpha_\phi^m\}$) in Eq. (4-17) can be obtained by implementing the linear algebraic solver and the stress concentration can be solved by using Eq. (4-3). To express clearly, the solution procedure is listed in Fig. 4-4.

4.4 Numerical examples

In order to show the accuracy and validity of the proposed method, the antiplane piezoelectricity problems with multiple inclusions subjected to the remote shear and the far-electric field are considered. Three examples contain single elastic dielectric

inclusion, single piezoelectric inclusion and two piezoelectric inclusions under antiplane shear, respectively.

Case 4-1: Single elastic dielectric inclusion ($e_{15} = 0$) [33, 41]

This case is an elastic dielectric inclusion in elastic dielectric matrix as shown in Fig. 4-5. There is no piezoelectric coupling, i.e., the electric and mechanical effects are uncoupled. The shear stress σ_{zy} along the line $\theta = 0$ is plotted in Fig. 4-6 (a)~(d), and the result along the line $\theta = \pi/2$ is plotted in Fig. 4-7 (a)~(d), respectively. When the matrix is stiffer than the inclusion, $c_{44}^m > c_{44}^i$, the maximum stress concentration occurs in the matrix at $\theta = 0$ as shown in Figs. 4-6 and 4-7. On the contrary, the maximum stress concentration occurs in the matrix at $\theta = \pi/2$ for $c_{44}^i > c_{44}^m$. In the single cavity problem under antiplane shear, the maximum stress concentration is 2 occurring in the matrix of $\theta = 0$. Fig. 4-6 (b) reduce to Fig. 4 in Ref. [33]. Good results are well compared with analytical solutions [41].

Case 4-2: Single piezoelectric inclusion [41]

The single piezoelectric inclusion in a piezoelectric matrix is shown in Fig. 4-8. In this case, the remote shear, shear modulus, piezoelectric modulus, dielectric modulus and elastic modulus are $\tau = 5 \times 10^7 \text{ Nm}^{-2}$, $e_{15}^i = 10.0 \text{ Cm}^{-2}$, $\epsilon_{11}^m = \epsilon_{11}^i = 1.51 \times 10^{-8} \text{ CV}^{-1}\text{m}^{-1}$ and $c_{44}^m = c_{44}^i = 3.53 \times 10^{10} \text{ Nm}^{-2}$, respectively. Stress concentrations versus different piezoelectric modulus ratio are shown in Fig. 4-9 (a)~(b) for the case of $E = -10^6 \text{ V/m}$. Furthermore, two other cases of $E = 0 \text{ V/m}$ and $E = 10^6 \text{ V/m}$ are plotted in Fig. 4-10 (a)~(b) and Fig. 4-11 (a)~(b), respectively. When $E = -10^6 \text{ V/m}$ and $e_{15}^m / e_{15}^i = -10$ for negative poling direction, the negative maximum stress concentration occurs in the matrix of $\theta = 0$ as shown in Fig. 4-9 (a).

However, the positive maximum stress concentration occurs in the matrix of $\theta = \pi/2$ as shown in Fig. 4-9 (b). Contours of electric potential ϕ and shear stress σ_{zy}^m are plotted in Fig. 4-12 (a)~(b), respectively. Good agreement is made after comparing with the analytical solution [41].

Case 4-3: Two piezoelectric inclusions

Two piezoelectric inclusions in piezoelectric matrix are shown in Fig. 4-13. The remote loading and material constants are $\tau = 5 \times 10^7 \text{ Nm}^{-2}$, $c_{44}^m = c_{44}^i = 3.53 \times 10^{10} \text{ Nm}^{-2}$, $\varepsilon_{11}^m = \varepsilon_{11}^i = 1.51 \times 10^{-8} \text{ CV}^{-1}\text{m}^{-1}$ and $e_{15}^i = 10.0 \text{ Cm}^{-2}$, respectively. Stress concentrations σ_{xz}^m/τ versus different piezoelectric modulus ratios are respectively plotted in Fig. 4-14 (a)~(c). On the other hand, stress concentrations $\sigma_{z\theta}^m/\tau$ versus different piezoelectric modulus ratios are plotted in Fig. 4-15 (a)~(c), respectively. The negative maximum stress concentration occurs in the matrix of $\theta = 0$ and $\beta = \frac{\pi}{2}$ as shown in Fig. 4-14 (c) when $E = -10^6 \text{ V/m}$ and $e_{15}^m/e_{15}^i = -10$. However, the maximum stress concentration occurs in the matrix at $\theta = \pi/2$ and $\beta = \pi/2$ as shown in Fig. 4-15 (c). When $E = 10^6 \text{ v/m}$, $e_{15}^m/e_{15}^i = -5$ and $\beta = \pi/2$, the tangential electric field along the boundaries of the matrix distribution function of the different ratios d/r_1 are shown in Fig. 4-16 (a)~(e). It is interesting to find that the tangential electric field is not continuous at $\theta = \pi/2$, when the inclusion approaches another inclusion. Stress concentrations of the different ratios of d/r_1 at $\beta = 0$ versus piezoelectric modulus ratio are shown in Fig. 4-17 (a)~(c). It is found that the stress concentration factor becomes larger, when the two inclusions approach each other inclusion. The results are well compared with those of the method of successive approximations [46].

4.5 Concluding remarks

In this study, we employed the RMM to solve piezoelectricity problems with piezoelectric inclusions under antiplane shear and inplane electric field. Only the boundary nodes on the physical boundary are required. The major difficulty of the coincidence of the source and collocation points in the conventional MFS is then circumvented. Furthermore, the controversy of the fictitious boundary outside the physical domain by using the conventional MFS no longer exists. Although it results in the singularity and hypersingularity due to the use of double layer potential, the finite values of the diagonal terms for the influence matrices have been determined by employing the regularization technique. The numerical results were obtained by applying the developed program to solve piezoelectricity problems through three examples. Numerical results agreed very well with the analytical solution [41] and those of the method of successive approximations [46]. The first attempt to solve piezoelectricity problems using MFS was achieved.

Chapter 5

Regularized meshless method for solving acoustic eigenproblems with multiply-connected domain

Summary

In this chapter, we employ the regularized meshless method (RMM) to search for eigenfrequencies of two-dimension acoustics with multiply-connected domain. The solution is represented by using the double-layer potentials. The source points can be located on the real boundary not alike MFS after using the proposed technique to regularize the singularity and hypersingularity of the kernel functions. The troublesome singularity in the MFS methods is desingularized and the diagonal terms of influence matrices are determined by employing the subtracting and adding-back technique. Spurious eigenvalues are filtered out by using SVD updating term technique. The accuracy and stability of the RMM are verified through the numerical experiments of the Dirichlet and Neumann problems for domains with multiple holes. The method is found to perform pretty well in comparison with analytical solutions and numerical results of boundary element method, finite element method and the point-matching method.

5.1 Introduction

For a multiply-connected problem, spurious eigensolutions always appear, even

when the complex-valued BEM is employed to solve the eigensolutions (Kitahara [70]; Chen *et al.* [71]). In Chen *et al.* [71], the problem of spurious eigensolutions of the singular and hypersingular BEMs was studied by using circulants for an annular case and treated by using the Burton & Miller approach in a discrete system. Chen and Liu [72, 73] studied the spurious and true eigensolutions for a multiply connected problem by using BIE, BEM and dual BEM. Also, spurious eigensolutions were examined in the MFS for annular eigenproblems. In this study, we implement a novel meshless method to solve multiply-connected eigenproblem. Spurious eigenvalues are extracted out by employing SVD updating term technique.

Several meshless methods have been reported in the literature, for example, the domain-based methods of the reproducing kernel method [48], and boundary type methods of collocation approach [14, 24], the method of fundamental solution (MFS) approach [1, 2], the meshless local Petrov-Galerkin approach [49], the RBF approach [22, 23, 24] and the boundary knot method (BKM) etc. Since neither domain nor boundary meshing is required for the meshless method, it is very attractive for engineers in modeling. Therefore, the meshless method becomes promising in solving engineering problems.

In the MFS, the solution is approximated by a set of fundamental solutions of the governing equations which are expressed in terms of sources located outside the physical domain. The method is relatively easy to implement. However, the MFS is still not a popular method because of the debatable artificial boundary (fictitious boundary) distance of source location in numerical implementation especially for a complicated geometry. The diagonal coefficients of influence matrices are divergent in the conventional case when the fictitious boundary approaches the physical boundary. In spite of its gain of singularity free, the influence matrices become ill-posed when the fictitious boundary is far away from the real boundary. It results in

an ill-posed problem since the condition number for the influence matrix becomes very large.

To distribute singularities on the real boundary, imaginary-part kernel method was adopted [14]. Later, Chen independently employed nonsingular fundamental solution to solve PDE using the similar idea [5]. Later, Young *et al.* [3, 10] proposed the novel meshless method, namely regularized meshless method (RMM), to deal with 2-D problems including the Laplace problem and Helmholtz problem of exterior acoustics.

The RMM can be seen as one kind of MFS. The RMM is successful to overcome the drawback of MFS for solving the Helmholtz equation [3]. The method eliminates the well-known drawback of equivocal artificial boundary. The subtracting and adding-back technique [3, 10, 11, 12] can regularize the singularity and hypersingularity of the kernel functions. This method can simultaneously distribute the observation and source points on the real boundary even using the singular kernels instead of non-singular kernels [17, 24]. The diagonal terms of the influence matrices can be extracted out by using the proposed technique. However, previous paper [3] were limited to the exterior acoustic problem with a simply-connected domain.

Following the success of previous applications [3], we investigate the eigenfrequency of interior acoustics with multiply-connected domain by using the RMM in this chapter. The rationale for choosing double-layer potential as radius basic function (RBF) instead of the single-layer potential in the RMM is to take the advantage of the regularization of the subtracting and adding-back technique. A general-purpose program was developed to solve the multiply-connected eigenproblems of Laplace operator. True and spurious eigenvalues are found by using the proposed method. Spurious eigenvalues are filtered out by using SVD updating term technique. Furthermore, the results will be compared with analytical solutions and those of BEM, FEM and PM to show the validity of our method.

5.2 Governing equation and boundary conditions

Consider an eigenproblem with an acoustic pressure field $u(x)$, which satisfies the Helmholtz equation as follows:

$$(\nabla^2 + k^2)u(x) = 0, \quad x \in D, \quad (5-1)$$

subject to boundary conditions,

$$u(x) = \bar{u} = 0, \quad x \in B_p^{\bar{u}}, \quad p = 1, 2, 3, \dots, m \quad (5-2)$$

$$t(x) = \bar{t} = 0, \quad x \in B_q^{\bar{t}}, \quad q = 1, 2, 3, \dots, m \quad (5-3)$$

where ∇^2 is the Laplacian operator, k is the wave number, D is the domain of the problem, $t(x) = \frac{\partial u(x)}{\partial n_x}$, m is the total number of boundaries including $m-1$ numbers of

inner boundaries and one outer boundary (the m th boundary), $B_p^{\bar{u}}$ is the essential boundary (Dirichlet boundary) of the p th boundary in which the potential is prescribed by \bar{u} and $B_q^{\bar{t}}$ is the natural boundary (Neumann boundary) of the q th boundary in which the flux is prescribed by \bar{t} . Both $B_p^{\bar{u}}$ and $B_q^{\bar{t}}$ construct the whole boundary of the domain D as shown in Fig. 1-1 (a).

5.3 Method of the solution

5.3.1 Conventional method of fundamental solutions

By employing the RBF technique [17, 22, 24, 27], the representation of the solution for multiply-connected problem as shown in Fig. 1-1 (a) can be approximated in terms

of the α_j strengths of the singularity at s_j as

$$\begin{aligned} u(x_i) &= \sum_{j=1}^N \overline{T}(s_j, x_i) \alpha_j \\ &= \sum_{j=1}^{N_1} \overline{T}(s_j, x_i) \alpha_j + \sum_{j=N_1+1}^{N_1+N_2} \overline{T}(s_j, x_i) \alpha_j + \cdots + \sum_{j=N_1+N_2+\cdots+N_{m-1}+1}^N \overline{T}(s_j, x_i) \alpha_j, \end{aligned} \quad (5-4)$$

$$\begin{aligned} t(x_i) &= \sum_{j=1}^N \overline{M}(s_j, x_i) \alpha_j \\ &= \sum_{j=1}^{N_1} \overline{M}(s_j, x_i) \alpha_j + \sum_{j=N_1+1}^{N_1+N_2} \overline{M}(s_j, x_i) \alpha_j + \cdots + \sum_{j=N_1+N_2+\cdots+N_{m-1}+1}^N \overline{M}(s_j, x_i) \alpha_j, \end{aligned} \quad (5-5)$$

where x_i and s_j represent the i th observation point and the j th source point, respectively, α_j are the j th unknown coefficients (strength of the singularity), N_1, N_2, \dots, N_{m-1} are the numbers of source points on $m-1$ numbers of inner boundaries, respectively, N_m is the number of source points on the outer boundary, while N is the total numbers of source points ($N = N_1 + N_2 + \cdots + N_m$) and

$\overline{M}(s_j, x_i) = \frac{\partial \overline{T}(s_j, x_i)}{\partial n_{x_i}}$. After BCs are satisfied at the boundary points, the coefficients

$\{\alpha_j\}_{j=1}^N$ are determined. The distributions of source points and observation points are

shown in Fig. 1-1 (a) for the MFS. The chosen bases are the double-layer potentials [3]

as

$$T(s_j, x_i) = -\frac{i\pi k}{2} H_1^{(1)}(kr_{ij}) \frac{((x_i - s_j), n_j)}{r_{ij}}, \quad (5-6)$$

$$M(s_j, x_i) = \frac{i\pi k}{2} \{kH_2^{(1)}(kr_{ij}) \frac{((x_i - s_j), n_j)((x_i - s_j), \overline{n_i})}{r_{ij}^2} - H_1^{(1)}(kr_{ij}) \frac{n_k \overline{n_k}}{r_{ij}}\}, \quad (5-7)$$

where (\cdot) is the inner product of two vectors, $H_2^{(1)}(kr_{ij})$ is the second-order Hankel

function of the first kind, $r_{ij} = |s_j - x_i|$, n_j is the normal vector at s_j , and $\overline{n_i}$ is the

normal vector at x_i .

It is noted that the double layer potentials have both singularity and hypersingularity when source and field points coincide, which lead to difficulty in the conventional MFS. The fictitious distance between the fictitious (auxiliary) boundary (B') and the physical boundary (B), defined by d , shown in Fig. 1-1 (a) needs to be chosen deliberately. To overcome the above mentioned shortcoming, s_j is distributed on the real boundary, as shown in Fig. 1-1 (b), by using the proposed regularized technique as stated in the following Section 5.3.2.

5.3.2 Regularized meshless method

When the collocation point x_i approaches the source point s_j , the potentials in Eqs. (5-6) and (5-7) are approximated by:

$$\lim_{x_i \rightarrow s_j} \bar{T}(s_j, x_i) = T(s_j, x_i) = \frac{n_k y_k}{r_{ij}^2}, \quad (5-8)$$

$$\lim_{x_i \rightarrow s_j} \bar{M}(s_j, x_i) = M(s_j, x_i) + \frac{k^2}{4} i = \left(2 \frac{y_k y_l n_k n_l}{r_{ij}^4} - \frac{n_k n_k}{r_{ij}^2} \right) + \frac{k^2}{4} i, \quad (5-9)$$

by using the limiting form for small arguments and the identities form the generalized function as shown below [74]

$$\lim_{r_{ij} \rightarrow 0} H_1^{(1)}(kr_{ij}) = \frac{kr_{ij}}{2} + \frac{2}{\pi kr_{ij}} i, \quad (5-10)$$

$$\lim_{r_{ij} \rightarrow 0} H_2^{(1)}(kr_{ij}) = \frac{(kr_{ij})^2}{8} + \frac{4}{\pi (kr_{ij})^2} i. \quad (5-11)$$

The kernels in Eqs. (5-8) and (5-9) have the same singularity order as the Laplace equation. Therefore, Eqs. (5-4) and (5-5) for the multiply-connected domain problems can be regularized by using the above mentioned regularization of subtracting and

adding-back technique [3, 10, 11, 12] as follows:

$$\begin{aligned}
u(x_i^I) = & \sum_{j=1}^{N_1} \bar{T}(s_j^I, x_i^I) \alpha_j + \cdots + \sum_{j=N_1+\cdots+N_{p-1}+1}^{N_1+\cdots+N_p} \bar{T}(s_j^I, x_i^I) \alpha_j + \cdots \\
& + \sum_{j=N_1+\cdots+N_{m-2}+1}^{N_1+\cdots+N_{m-1}} \bar{T}(s_j^I, x_i^I) \alpha_j + \sum_{j=N_1+\cdots+N_{m-1}+1}^N \bar{T}(s_j^O, x_i^I) \alpha_j \\
& - \sum_{j=N_1+\cdots+N_{p-1}+1}^{N_1+\cdots+N_p} T(s_j^I, x_i^I) \alpha_j, \quad x_i^I \in B_p, \quad p = 1, 2, 3, \dots, m-1.
\end{aligned} \tag{5-12}$$

where x_i^I is located on the inner boundary ($p = 1, 2, 3, \dots, m-1$) and the

superscripts I and O denote the inward and outward normal vectors, respectively,

and

$$\sum_{j=N_1+\cdots+N_{p-1}+1}^{N_1+\cdots+N_p} T(s_j^I, x_i^I) = 0, \quad x_i^I \in B_p, \quad p = 1, 2, 3, \dots, m-1. \tag{5-13}$$

Therefore, we can obtain

$$\begin{aligned}
u(x_i^I) = & \sum_{j=1}^{N_1} \bar{T}(s_j^I, x_i^I) \alpha_j + \cdots + \sum_{j=N_1+\cdots+N_{p-1}+1}^{i-1} \bar{T}(s_j^I, x_i^I) \alpha_j \\
& + \sum_{j=i+1}^{N_1+\cdots+N_p} \bar{T}(s_j^I, x_i^I) \alpha_j + \cdots + \sum_{j=N_1+\cdots+N_{m-2}+1}^{N_1+\cdots+N_{m-1}} \bar{T}(s_j^I, x_i^I) \alpha_j \\
& + \sum_{j=N_1+\cdots+N_{m-1}+1}^N \bar{T}(s_j^O, x_i^I) \alpha_j - \left[\sum_{j=N_1+\cdots+N_{p-1}+1}^{N_1+\cdots+N_p} T(s_j^I, x_i^I) - \bar{T}(s_i^I, x_i^I) \right] \alpha_i,
\end{aligned} \tag{5-14}$$

$$x_i^I \in B_p, \quad p = 1, 2, 3, \dots, m-1.$$

When the observation point x_i^O locates on the outer boundary ($p=m$), Eq. (5-12)

becomes

$$u(x_i^O) = \sum_{j=1}^{N_1} \bar{T}(s_j^I, x_i^O) \alpha_j + \sum_{j=N_1+1}^{N_1+N_2} \bar{T}(s_j^I, x_i^O) \alpha_j + \cdots + \sum_{j=N_1+\cdots+N_{m-2}+1}^{N_1+\cdots+N_{m-1}} \bar{T}(s_j^I, x_i^O) \alpha_j \tag{5-15}$$

$$+ \sum_{j=N_1+\dots+N_{m-1}+1}^N \bar{T}(s_j^O, x_i^O) \alpha_j - \sum_{j=N_1+\dots+N_{m-1}+1}^N T(s_j^I, x_i^I) \alpha_j, \quad x_i^O \text{ and } x_i^I \in B_p, \quad p = m.$$

where

$$\sum_{j=N_1+\dots+N_{m-1}+1}^N T(s_j^I, x_i^I) \alpha_j = 0, \quad x_i^I \in B_p, \quad p = m. \quad (5-16)$$

Hence, we obtain

$$\begin{aligned} u(x_i^O) &= \sum_{j=1}^{N_1} \bar{T}(s_j^I, x_i^O) \alpha_j + \sum_{j=N_1+1}^{N_1+N_2} \bar{T}(s_j^I, x_i^O) \alpha_j + \dots + \sum_{j=N_1+\dots+N_{m-2}+1}^{N_1+\dots+N_{m-1}} \bar{T}(s_j^I, x_i^O) \alpha_j \\ &+ \sum_{j=N_1+\dots+N_{m-1}+1}^{i-1} \bar{T}(s_j^O, x_i^O) \alpha_j + \sum_{j=i+1}^N \bar{T}(s_j^O, x_i^O) \alpha_j \\ &- \left[\sum_{j=N_1+\dots+N_{m-1}+1}^N T(s_j^I, x_i^I) - \bar{T}(s_i^O, x_i^O) \right] \alpha_i, \quad x_i^I \text{ and } x_i^O \in B_p, \quad p = m. \end{aligned} \quad (5-17)$$

Similarly, the boundary flux is obtained as

$$\begin{aligned} t(x_i^I) &= \sum_{j=1}^{N_1} \bar{M}(s_j^I, x_i^I) \alpha_j + \dots + \sum_{j=N_1+\dots+N_{p-1}+1}^{N_1+\dots+N_p} \bar{M}(s_j^I, x_i^I) \alpha_j + \dots \\ &+ \sum_{j=N_1+\dots+N_{m-2}+1}^{N_1+\dots+N_{m-1}} \bar{M}(s_j^I, x_i^I) \alpha_j + \sum_{j=N_1+\dots+N_{m-1}+1}^N \bar{M}(s_j^O, x_i^I) \alpha_j \\ &- \sum_{j=N_1+\dots+N_{p-1}+1}^{N_1+\dots+N_p} M(s_j^I, x_i^I) \alpha_j, \quad x_i^I \in B_p, \quad p = 1, 2, 3, \dots, m-1. \end{aligned} \quad (5-18)$$

where

$$\sum_{j=N_1+\dots+N_{p-1}+1}^{N_1+\dots+N_p} M(s_j^I, x_i^I) = 0, \quad x_i^I \in B_p, \quad p = 1, 2, 3, \dots, m-1. \quad (5-19)$$

Therefore, we obtain

$$\begin{aligned} t(x_i^I) &= \sum_{j=1}^{N_1} \bar{M}(s_j^I, x_i^I) \alpha_j + \dots + \sum_{j=N_1+\dots+N_{p-1}+1}^{i-1} \bar{M}(s_j^I, x_i^I) \alpha_j \\ &+ \sum_{j=i+1}^{N_1+\dots+N_p} \bar{M}(s_j^I, x_i^I) \alpha_j + \dots + \sum_{j=N_1+\dots+N_{m-2}+1}^{N_1+\dots+N_{m-1}} \bar{M}(s_j^I, x_i^I) \alpha_j \end{aligned} \quad (5-20)$$

$$+ \sum_{j=N_1+\dots+N_{m-1}+1}^N \overline{M}(s_j^O, x_i^I) \alpha_j - \left[\sum_{j=N_1+\dots+N_{p-1}+1}^{N_1+\dots+N_p} M(s_j^I, x_i^I) - \overline{M}(s_i^I, x_i^I) \right] \alpha_i,$$

$$x_i^I \in B_p, \quad p = 1, 2, 3, \dots, m-1.$$

When the observation point locates on the outer boundary ($p=m$), Eq. (5-18) yields

$$\begin{aligned} t(x_i^O) = & \sum_{j=1}^{N_1} \overline{M}(s_j^I, x_i^O) \alpha_j + \sum_{j=N_1+1}^{N_1+N_2} \overline{M}(s_j^I, x_i^O) \alpha_j + \dots + \sum_{j=N_1+\dots+N_{m-2}+1}^{N_1+\dots+N_{m-1}} \overline{M}(s_j^I, x_i^O) \alpha_j \\ & + \sum_{j=N_1+\dots+N_{m-1}+1}^N \overline{M}(s_j^O, x_i^O) \alpha_j - \sum_{j=N_1+\dots+N_{m-1}+1}^N M(s_j^I, x_i^I) \alpha_i, \quad x_i^O \text{ and } I \in B_p, \quad p = m. \end{aligned} \quad (5-21)$$

where

$$\sum_{j=N_1+\dots+N_{m-1}+1}^N M(s_j^I, x_i^I) = 0, \quad x_i^I \in B_p, \quad p = m. \quad (5-22)$$

Hence, we obtain

$$\begin{aligned} t(x_i^O) = & \sum_{j=1}^{N_1} \overline{M}(s_j^I, x_i^O) \alpha_j + \sum_{j=N_1+1}^{N_1+N_2} \overline{M}(s_j^I, x_i^O) \alpha_j + \dots + \sum_{j=N_1+\dots+N_{m-2}+1}^{N_1+\dots+N_{m-1}} \overline{M}(s_j^I, x_i^O) \alpha_j \\ & + \sum_{j=N_1+\dots+N_{m-1}+1}^{i-1} \overline{M}(s_j^O, x_i^O) \alpha_j + \sum_{j=i+1}^N \overline{M}(s_j^O, x_i^O) \alpha_j \\ & - \left[\sum_{j=N_1+\dots+N_{m-1}+1}^N M(s_j^I, x_i^I) - \overline{M}(s_i^O, x_i^O) \right] \alpha_i, \quad x_i^O \text{ and } I \in B_p, \quad p = m. \end{aligned} \quad (5-23)$$

The detailed derivations of Eqs. (5-13), (5-16), (5-19) and (5-22) can be found in the reference [3]. According to the dependence of normal vectors for inner and outer boundaries [10], their relationships are

$$\begin{cases} \overline{T}(s_j^I, x_i^I) = -\overline{T}(s_j^O, x_i^O), & i \neq j \\ \overline{T}(s_j^I, x_i^I) = \overline{T}(s_j^O, x_i^O), & i = j \end{cases} \quad (5-24)$$

$$\begin{cases} \overline{M}(s_j^I, x_i^I) = \overline{M}(s_j^O, x_i^O), & i \neq j \\ \overline{M}(s_j^I, x_i^I) = \overline{M}(s_j^O, x_i^O), & i = j \end{cases} \quad (5-25)$$

where the left and right hand sides of the equal sign in Eqs. (5-24) and (5-25) denote the kernels for observation and source point with the inward and outward normal

vectors, respectively.

By using the proposed technique, the singular terms in Eqs. (5-4) and (5-5) have been transformed into regular terms $\left(-\left[\sum_{j=N_1+N_2+\dots+N_{p-1}+1}^{N_1+N_2+\dots+N_p} T(s_j^I, x_i^I) - \bar{T}(s_i^{I \text{ or } O}, x_i^{I \text{ or } O})\right]\right)$ and $\left(-\left[\sum_{j=N_1+\dots+N_{p-1}+1}^{N_1+\dots+N_p} M(s_j^I, x_i^I) - \bar{M}(s_i^{I \text{ or } O}, x_i^{I \text{ or } O})\right]\right)$ in Eqs. (5-14), (5-17), (5-20) and (5-23),

respectively, where $p = 1, 2, 3, \dots, m$. The terms of $\sum_{j=N_1+\dots+N_{p-1}+1}^{N_1+\dots+N_p} T(s_j^I, x_i^I)$ and

$\sum_{j=N_1+\dots+N_{p-1}+1}^{N_1+\dots+N_p} M(s_j^I, x_i^I)$ are the adding-back terms and the terms of $\bar{T}(s_i^{I \text{ or } O}, x_i^{I \text{ or } O})$ and

$\bar{M}(s_i^{I \text{ or } O}, x_i^{I \text{ or } O})$ are the subtracting terms in the two brackets for regularization.

After used the above mentioned method of regularization of subtracting and adding-back technique [3, 74], we are able to remove the singularity and hypersingularity of the kernel functions.

5.3.3 Construction of influence matrices for problems with arbitrary domain

By collocated N observation points to match the BCs from Eqs. (5-14) and (5-17) for the Dirichlet problem, the linear algebraic equation is obtained

$$\{\bar{u}\} = \{0\} = [\bar{T}]\{\alpha\} \Leftrightarrow$$

$$\left\{ \begin{matrix} 0 \\ \vdots \\ 0 \end{matrix} \right\}_{N \times 1} = \left[\begin{matrix} [\bar{T}_{11}]_{N_1 \times N_1} & \cdots & [\bar{T}_{1m}]_{N_1 \times N_m} \\ \vdots & \ddots & \vdots \\ [\bar{T}_{m1}]_{N_m \times N_1} & \cdots & [\bar{T}_{mm}]_{N_m \times N_m} \end{matrix} \right]_{N \times N} \left\{ \begin{matrix} \alpha_1 \\ \vdots \\ \alpha_{N_1} \\ \vdots \\ \alpha_{N_1+N_2+\cdots+N_{m-1}+1} \\ \vdots \\ \alpha_N \end{matrix} \right\}_{N \times 1}, \quad (5-26)$$

where

$$[\bar{T}_{11}] = \left[\begin{matrix} -\left[\sum_{j=1}^{N_1} T(s_j^I, x_1^I) - \bar{T}(s_1^I, x_1^I) \right] & \bar{T}(s_2^I, x_1^I) & \cdots & \bar{T}(s_{N_1}^I, x_1^I) \\ \bar{T}(s_1^I, x_2^I) & -\left[\sum_{j=1}^{N_1} T(s_j^I, x_2^I) - \bar{T}(s_2^I, x_2^I) \right] & \cdots & \bar{T}(s_{N_1}^I, x_2^I) \\ \vdots & \vdots & \ddots & \vdots \\ \bar{T}(s_1^I, x_{N_1}^I) & \bar{T}(s_2^I, x_{N_1}^I) & \cdots & -\left[\sum_{j=1}^{N_1} T(s_j^I, x_{N_1}^I) - \bar{T}(s_{N_1}^I, x_{N_1}^I) \right] \end{matrix} \right]_{N_1 \times N_1}, \quad (5-27)$$

$$[\bar{T}_{1m}] = \left[\begin{matrix} \bar{T}(s_{N_1+\cdots+N_{m-1}+1}^O, x_1^I) & \bar{T}(s_{N_1+\cdots+N_{m-1}+2}^O, x_1^I) & \cdots & \bar{T}(s_N^O, x_1^I) \\ \bar{T}(s_{N_1+\cdots+N_{m-1}+1}^O, x_2^I) & \bar{T}(s_{N_1+\cdots+N_{m-1}+2}^O, x_2^I) & \cdots & \bar{T}(s_N^O, x_2^I) \\ \vdots & \vdots & \ddots & \vdots \\ \bar{T}(s_{N_1+\cdots+N_{m-1}+1}^O, x_{N_1}^I) & \bar{T}(s_{N_1+\cdots+N_{m-1}+2}^O, x_{N_1}^I) & \cdots & \bar{T}(s_N^O, x_{N_1}^I) \end{matrix} \right]_{N_1 \times N_m}, \quad (5-28)$$

$$[\bar{T}_{m1}] = \left[\begin{matrix} \bar{T}(s_1^I, x_{N_1+\cdots+N_{m-1}+1}^O) & \bar{T}(s_2^I, x_{N_1+\cdots+N_{m-1}+1}^O) & \cdots & \bar{T}(s_{N_1}^I, x_{N_1+\cdots+N_{m-1}+1}^O) \\ \bar{T}(s_1^I, x_{N_1+\cdots+N_{m-1}+2}^O) & \bar{T}(s_2^I, x_{N_1+\cdots+N_{m-1}+2}^O) & \cdots & \bar{T}(s_{N_1}^I, x_{N_1+\cdots+N_{m-1}+2}^O) \\ \vdots & \vdots & \ddots & \vdots \\ \bar{T}(s_1^I, x_N^O) & \bar{T}(s_2^I, x_N^O) & \cdots & \bar{T}(s_{N_1}^I, x_N^O) \end{matrix} \right]_{N_m \times N_1}, \quad (5-29)$$

$$[\bar{T}_{mm}] = \left[\begin{matrix} -\left[\sum_{j=N_1+\cdots+N_{m-1}+1}^N T(s_j^I, x_{N_1+\cdots+N_{m-1}+1}^O) - \bar{T}(s_{N_1+\cdots+N_{m-1}+1}^O, x_{N_1+\cdots+N_{m-1}+1}^O) \right] & \cdots & \bar{T}(s_N^O, x_{N_1+\cdots+N_{m-1}+1}^O) \\ \vdots & \ddots & \vdots \\ \bar{T}(s_{N_1+\cdots+N_{m-1}+1}^O, x_N^O) & \cdots & -\left[\sum_{j=N_1+\cdots+N_{m-1}+1}^N T(s_j^I, x_N^O) - \bar{T}(s_N^O, x_N^O) \right] \end{matrix} \right]_{N_m \times N_m}. \quad (5-30)$$

For the Neumann problem, Eqs. (5-20) and (5-23) yield

$$\{\bar{t}\} = \{0\} = [\bar{M}]\{\alpha\} \Leftrightarrow$$

$$\left\{ 0 \right\}_{N \times 1} = \begin{bmatrix} [\bar{M}_{11}]_{N_1 \times N_1} & \cdots & [\bar{M}_{1m}]_{N_1 \times N_m} \\ \vdots & \ddots & \vdots \\ [\bar{M}_{m1}]_{N_m \times N_1} & \cdots & [\bar{M}_{mm}]_{N_m \times N_m} \end{bmatrix}_{N \times N} \left\{ \begin{array}{c} \alpha_1 \\ \vdots \\ \alpha_{N_1} \\ \vdots \\ \alpha_{N_1+N_2+\cdots+N_{m-1}+1} \\ \vdots \\ \alpha_N \end{array} \right\}_{N \times 1}, \quad (5-31)$$

in which

$$[\bar{M}_{11}] = \begin{bmatrix} -\left[\sum_{j=1}^{N_1} M(s'_j, x'_1) - \bar{M}(s'_1, x'_1) \right] & \bar{M}(s'_2, x'_1) & \cdots & \bar{M}(s'_{N_1}, x'_1) \\ \bar{M}(s'_1, x'_2) & -\left[\sum_{j=1}^{N_1} M(s'_j, x'_2) - \bar{M}(s'_2, x'_2) \right] & \cdots & \bar{M}(s'_{N_1}, x'_2) \\ \vdots & \vdots & \ddots & \vdots \\ \bar{M}(s'_1, x'_{N_1}) & \bar{M}(s'_2, x'_{N_1}) & \cdots & -\left[\sum_{j=1}^{N_1} M(s'_j, x'_{N_1}) - \bar{M}(s'_{N_1}, x'_{N_1}) \right] \end{bmatrix}_{N_1 \times N_1}, \quad (5-32)$$

$$[\bar{M}_{1m}] = \begin{bmatrix} \bar{M}(s'_{N_1+\cdots+N_{m-1}+1}, x'_1) & \bar{M}(s'_{N_1+\cdots+N_{m-1}+2}, x'_1) & \cdots & \bar{M}(s'_{N_1}, x'_1) \\ \bar{M}(s'_{N_1+\cdots+N_{m-1}+1}, x'_2) & \bar{M}(s'_{N_1+\cdots+N_{m-1}+2}, x'_2) & \cdots & \bar{M}(s'_{N_1}, x'_2) \\ \vdots & \vdots & \ddots & \vdots \\ \bar{M}(s'_{N_1+\cdots+N_{m-1}+1}, x'_{N_1}) & \bar{M}(s'_{N_1+\cdots+N_{m-1}+2}, x'_{N_1}) & \cdots & \bar{M}(s'_{N_1}, x'_{N_1}) \end{bmatrix}_{N_1 \times N_m}, \quad (5-33)$$

$$[\bar{M}_{m1}] = \begin{bmatrix} \bar{M}(s'_1, x'_{N_1+\cdots+N_{m-1}+1}) & \bar{M}(s'_2, x'_{N_1+\cdots+N_{m-1}+1}) & \cdots & \bar{M}(s'_{N_1}, x'_{N_1+\cdots+N_{m-1}+1}) \\ \bar{M}(s'_1, x'_{N_1+\cdots+N_{m-1}+2}) & \bar{M}(s'_2, x'_{N_1+\cdots+N_{m-1}+2}) & \cdots & \bar{M}(s'_{N_1}, x'_{N_1+\cdots+N_{m-1}+2}) \\ \vdots & \vdots & \ddots & \vdots \\ \bar{M}(s'_1, x'_N) & \bar{M}(s'_2, x'_N) & \cdots & \bar{M}(s'_{N_1}, x'_N) \end{bmatrix}_{N_m \times N_1}, \quad (5-34)$$

$$[\bar{M}_{mm}] = \begin{bmatrix} -\left[\sum_{j=N_1+\cdots+N_{m-1}+1}^N M(s'_j, x'_{N_1+\cdots+N_{m-1}+1}) - \bar{M}(s'_{N_1+\cdots+N_{m-1}+1}, x'_{N_1+\cdots+N_{m-1}+1}) \right] & \cdots & \bar{M}(s'_N, x'_{N_1+\cdots+N_{m-1}+1}) \\ \vdots & \ddots & \vdots \\ \bar{M}(s'_{N_1+\cdots+N_{m-1}+1}, x'_N) & \cdots & -\left[\sum_{j=N_1+\cdots+N_{m-1}+1}^N M(s'_j, x'_N) - \bar{M}(s'_N, x'_N) \right] \end{bmatrix}_{N_m \times N_m}. \quad (5-35)$$

For the mixed-type problem, a linear combination of Eqs. (5-26) and (5-31) is required to satisfy the mixed-type BCs.

5.3.4 Extraction of the eigenvalues

In order to sort out the eigenvalues, the SVD technique is utilized [5, 22]. We obtain Eqs. (5-26) and (5-31) by used the double-layer potentials approach for the Dirichlet and Neumann problems, respectively. Form Eqs. (5-26) and (5-31), we can obtain eigenvalues by using the SVD technique as follows:

$$\left[\bar{T}\right] = \left[\Phi_{\bar{T}}\right] \left[\Sigma_{\bar{T}}\right] \left[\Psi_{\bar{T}}\right]^H, \quad (5-36)$$

$$\left[\bar{M}\right] = \left[\Phi_{\bar{M}}\right] \left[\Sigma_{\bar{M}}\right] \left[\Psi_{\bar{M}}\right]^H, \quad (5-37)$$

where the superscript H denotes the transpose and conjugate, $\Sigma_{\bar{T}}$ and $\Sigma_{\bar{M}}$ are diagonal matrices with diagonal elements of positive or zero singular values and $\left[\Phi_{\bar{T}}\right]$, $\left[\Phi_{\bar{M}}\right]$, $\left[\Psi_{\bar{T}}\right]$ and $\left[\Psi_{\bar{M}}\right]$ are the left and right unitary matrices corresponding with $\left[\bar{T}\right]$ and $\left[\bar{M}\right]$, respectively. Thus the minimum singular value of $\left[\bar{T}\right]$ or $\left[\bar{M}\right]$ as a function of k can be utilized to detect the eigenvalue and eigenmodes by using right unitary vectors. However, spurious eigenvalue are imbedded in those eigenvalues for multi-domain eigenproblem. Spurious eigenvalue can be extracted out by SVD updating term techniques as descriptively as next section.

5.3.5 Treatments of spurious eigenvalues

In order to sort out spurious eigenvalues, the SVD updating term is utilized [5, 22]. We can combine Eqs. (5-26) and (5-31) by using the SVD updating term as follows:

$$\left[P\right]\{\alpha\} = \begin{bmatrix} \left[\bar{T}\right]_{N \times N} \\ \left[\bar{M}\right]_{N \times N} \end{bmatrix} \{\alpha\} = \{0\}. \quad (5-38)$$

The rank of the matrix $[P]$ must be smaller than $2N$ to have a spurious mode [22].

By using the SVD technique, the matrix in Eq. (5-38) can be decomposed into

$$[P] = \begin{bmatrix} \Phi_{\bar{T}} & 0 \\ 0 & \Phi_{\bar{M}} \end{bmatrix} \begin{bmatrix} \Sigma_{\bar{T}} & 0 \\ 0 & \Sigma_{\bar{M}} \end{bmatrix} \begin{bmatrix} \Psi_{\bar{T}} & 0 \\ 0 & \Psi_{\bar{M}} \end{bmatrix}^H, \quad (5-39)$$

Based on the equivalence between the SVD technique and the least-squares method, we extract out the spurious eigenvalue by detecting zero singular value for $[P]$ matrix.

5.3.6 Flowchart of solution procedures

Following the Section 5.3.2 to Section 5.3.5, the flowchart of solution procedures by using the RMM is shown in Fig. 5-1.

5.4 Numerical examples

In order to show the accuracy and validity of the proposed method, four cases with simply-connected and multiply-connected domains subjected to the Dirichlet and Neumann BCs are considered.

Case 5-1: Square problem (simply-connected case)

The length of the square domain is $L = 1.0$. All the boundary conditions are the Dirichlet type ($u = 0$) as shown in Fig. 5-2. The analytical solution of true eigenequations [76] for this case is shown below:

$$k_{mn} = \pi \sqrt{(m/L)^2 + (n/L)^2}, \quad m, n = 1, 2, 3, \dots, \quad (5-40)$$

The former five eigenvalues for the Dirichlet BC by using our proposed method is

shown in Fig. 5-3. The maximum relative error of eigenvalue is 1%. Good agreement is obtained after comparing with analytical solutions. Since the domain is simply connected, no spurious eigenvalue is found by using proposed method.

Case 5-2: Annular problem

The inner and outer radii of domain are $r_1 = 0.5$ and $r_2 = 2.0$, respectively. All the boundary conditions are the Dirichlet type ($u = 0$) and Neumann type ($t = 0$) as shown in Fig. 5-4. The analytical solution of true eigenequations [73] for Dirichlet and Neumann types, respectively, is shown below:

$$J_n(kr_1)Y_n(kr_2) - J_n(kr_2)Y_n(kr_1) = 0, \text{ (Dirichlet)} \quad (5-41)$$

$$J_n'(kr_1)Y_n'(kr_2) - J_n'(kr_2)Y_n'(kr_1) = 0, \text{ (Neumann)}. \quad (5-42)$$

The analytical solutions of spurious eigenequations [73] for both types are the same as:

$$J_n'(kr_1) = 0. \quad (5-43)$$

The minimum singular value versus wave number by using our proposed method for the Dirichlet and Neumann BCs are shown in Figs. 5-5 (a) and (b), respectively. The maximum relative error of eigenvalue is 3%. Good agreement is obtained after comparing with analytical solutions. The spurious eigenvalues for Dirichlet and Neumann problems are found out by employing SVD updating term as shown in Fig. 5-5 (c). From Fig. 5-5 (c), we find that one spurious eigenvalue appear at $k_s = 3.68$ (J_1^{n1}) in the range of $0 < k \leq 5$. This spurious eigenvalue is found to be the true eigenvalue of eigenproblem of interior circular of radius 0.5.

Case 5-3: A circular domain with two equal holes [72]

In this case, the eigenvalues were obtained in the Ref. [72] by using the

point-matching (PM) approach. The radius R of the outer boundary is 1.0 and the eccentricity e and radius c of the inner circular boundaries are 0.5 and 0.3, respectively, as shown in Fig. 5-6. All the boundary conditions are the Dirichlet type ($u = 0$). Numerical data of eigenvalues for RMM, BEM, FEM and PM, are shown in Table 5-1. In Table 5-1, the (S) and (A) symbols denote the symmetric and antisymmetric with respect to the x- and y-axis, respectively [15]. It is easy to find that the mode shapes of RMM, BEM and PM approach matched well. In this case, the first spurious eigenvalue $k_s = 6.14$ is found by comparing with analytical solution J_1^1 . From Table 5-1, it is found that the former five eigenvalues match well with those of RMM and BEM. On the other hand, the former five eigenmodes are shown in Fig. 5-7, respectively, by using the RMM and the BEM approach. The results match well with the BEM results.

Case 5-4: A circular domain with four equal holes [72]

The radius R of outer boundary domain is 1.0 and the eccentricity e and radius c of the inner circular boundaries are 0.5 and 0.1, respectively. Dirichlet problem is considered as shown in Fig. 5-8. The former five eigenvalues by using the RMM, BEM, FEM and PM are listed in Table 5-2, where the results of PM miss the eigenvalues of k_2 and k_3 . In this case, no spurious eigenvalue is found in the range of $0 < k < 6$ sine the first spurious eigenvalue is 18.412 (J_1^1). The eigenvalues of k_2 and k_3 are roots of multiplicity two by finding the second successive zero singular value in SVD by using RMM and BEM. Besides, the symmetry of the fourth mode shape by using the point-matching method is quite different with the results of RMM and BEM. The former five eigenmodes of the RMM and the BEM are shown in Fig. 5-9. Agreeable results of the RMM are obtained by comparing with the BEM data.

5.5 Concluding remarks

In this study, we used the RMM to solve the acoustic eigenproblems with multiply-connected domain subjected to the Dirichlet and Neumann BCs, respectively. Only the boundary nodes on the physical boundary are required. The perplexing fictitious boundary in the MFS is then circumvented. Despite the presence of singularity and hypersingularity of double layer potentials, the finite values of the diagonal terms of the influence matrix can be extracted out by employing subtracting and add-back techniques. Four numerical experiments were performed to demonstrate not only the occurring mechanism of spurious eigenvalue due to inner boundaries but also the suppression of the spurious eigenvalue by using SVD techniques of updating term. The numerical results were obtained by applying the developed program in four examples of simply-connected and multiply-connected domain subjected to Dirichlet and Neumann BCs. Numerical results agreed very well with analytical solutions and those of BEM, FEM and the PM.

Chapter 6

Conclusions

6.1 Conclusions

Based on the proposed formulation for solving boundary value problems involving arbitrary boundaries in different branches of engineering applications, some concluding remarks are itemized as follows:

1. The present method is a new version of method of fundamental solutions. Only the boundary nodes on the physical boundary are required. Although it results in the singularity and hypersingularity due to using the double layer potential, the finite values of the diagonal terms for the influence matrices have been extracted out by the subtracting and adding-back technique to regularize the singularity and hypersingularity of the kernel functions. Convergence test and sensitivity study of the proposed method were also done.
2. A systematic approach to solve the Laplace and eigenproblems with multiply-connected domain was proposed successfully in this thesis by using the regularized meshless method. Problems involving infinite domains with arbitrary boundaries of inclusion were examined to check the accuracy of the present formulation for different branches of engineering applications including antiplane shear problems with multiple inclusions, piezoelectric problems with multiple inclusions. Eigenproblems with multiply-connected domain as well as

simply-connected case were also solved.

3. Stress concentration for an infinite medium with multiple inclusions under antiplane remote shear was studied by using the present formulation. The maximum stress concentration appears in the matrix of $\theta = 0^\circ$ as expected in the two inclusions.
4. The stress concentration for an infinite piezoelectric medium with multiple inclusions under out-of-plane displacement field and in-plane electric field was studied by using the present formulation. The stress at the neighbor point becomes larger as the two inclusions approach each other. To verify our accuracy, our results are found to match well with the Pak's and Chao *et al.s'* results.
5. The results of the eigenproblems containing multiply-connected domain show the superiority of our method over other numerical methods, *e.g.* boundary element method, point-matching method and finite element method on the basis of the same number of degrees of freedom. Spurious eigenvalue is filtered out by using the technique of SVD updating term. Although our approach can solve eigenproblems with arbitrary number of holes, one, two and four holes were tested in this thesis. Since analytical solutions are not always available, our numerical results may provide a datum for other researchers' reference. To verify our accuracy, our results were compared with those of BEM, FEM and PM.
6. A general-purpose program for solving Laplace problems involving infinite domain with multiple inclusions and/or several holes of various shapes and

arbitrary positions was developed. Also, the eigenproblem of multiply-connected domain as well as simply-connected case can be solved by replacing kernels in the program. Its possible applications in engineering are very broad, not only limited on the three topics of our thesis.

6.2 Further research

In this thesis, our the novel meshless method has been applied to solve Laplace and eigenproblems with multiply-connected domain on three topics of engineering applications by using the fundamental solutions for boundary densities. However, there are several interested issues which need further investigations:

1. According to our successful experiences in antiplane shear problems with multiple inclusions, it is straightforward to extend this concept to antiplane shear problems with multiple inclusions in an anisotropic medium by using proposed method.
2. According to our successful experiences in two-dimensional problems with multiple inclusions, it is possible to extend this concept to 3-D cases.
3. Although eigenproblem was solved in this thesis, the possible applications to exterior acoustics of multiple radiators or scatters deserve further study.

References

- [1]. Kupradze VD and Aleksidze MA. The method of functional equations for the approximate solution of certain boundary value problems. U.S.S.R. Computational Mathematics and Mathematical Physics 1964; **4**: 199-205.
- [2]. Fairweather G and Karageorghis A. The method of fundamental solutions for elliptic boundary value problems. Advances in Computational Mathematics 1998; **9**: 69-95.
- [3]. Young DL, Chen KH and Lee CW. Singular meshless method using double layer potentials for exterior acoustics, The Journal of the Acoustical Society of America 2006; **119**: 96-107.
- [4]. Karageorghis A. The method of fundamental solutions for the calculation of the eigenvalues of the Helmholtz equation. Applied Mathematics Letters 2001; **14**: 837-842.
- [5]. Chen JT, Chen IL and Lee YT. Eigensolutions of multiply connected membranes using the method of fundamental solutions. Engineering Analysis with Boundary Elements 2005; **29**: 166-174.
- [6]. Chen CS, Golberg MA and Hon YC. The method of fundamental solutions and quasi-Monte-Carlo method for diffusion equations. International Journal for Numerical Methods in Engineering 1998; **43**: 1421-1435.
- [7]. Poullikkas A, Karageorghis A and Georgiou G. Methods of fundamental solutions for harmonic and biharmonic boundary value problems. Computational Mechanics 1998; **21**: 416-423.
- [8]. Cheng AHD, Chen CS, Golberg MA and Rashed YF. BEM for thermoelasticity and elasticity with body force: a revisit. Engineering Analysis with Boundary Elements 2001; **25**: 377-387.
- [9]. Chen W. Symmetric boundary knot method. Engineering Analysis with Boundary Elements 2002; **26**: 489-494.
- [10]. Young DL, Chen KH and Lee CW. Novel meshless method for solving the potential problems with arbitrary domain. Journal of Computational Physics 2005; **209**: 290-321.
- [11]. Hwang WS, Hung LP and Ko CH. Non-singular boundary integral formulations for plane interior potential problems. International Journal for Numerical Methods in Engineering 2002; **53**: 1751-1762.
- [12]. Tournour MA and Atalla N. Efficient evaluation of the acoustic radiation using multipole expansion. International Journal for Numerical Methods in Engineering 1999; **46**: 825-837.
- [13]. Chen JT, Kuo SR, Chen KH and Cheng YC. Comments on vibration analysis of

- arbitrary shaped membranes using nondimensional dynamic influence function. *Journal of Sound and Vibration* 2000; **235**: 156-171.
- [14].Chen JT, Chang MH, Chen KH and Lin SR. The boundary collocation method with meshless concept for acoustic eigenanalysis of two-dimensional cavities using radial basis function. *Journal of Sound and Vibration* 2002; **257**: 667-711.
- [15].Hon YC and Chen W. Boundary knot method for 2D and 3D Helmholtz and the convection-diffusion problems with complicated geometry. *International Journal for Numerical Methods in Engineering* 2003; **56**: 1931-1948.
- [16].Chen W and Hon YC. Numerical investigation on convergence of boundary knot method in the analysis of homogeneous Helmholtz, modified Helmholtz, and convection–diffusion problems. *Computer Methods in Applied Mechanics and Engineering* 2003; **192**: 1859-1875.
- [17].Chen W and Tanaka M. A meshfree integration-free and boundary-only RBF technique. *Computers & Mathematics with Applications* 2002; **43**: 379-391.
- [18].Jin B and Chen W. Boundary knot method based on geodesic distance for anisotropic problems. *Journal of Computational Physics* 2006; **215**: 614-629.
- [19].Chen W. Meshfree boundary particle method applied to Helmholtz problems. *Engineering Analysis with Boundary Elements* 2002; **26**: 577-581.
- [20].Cheng AHD, Young DL and Tsai CC. The solution of Poisson’s equation by iterative DRBEM using compactly supported, positive definite radial basis function. *Engineering Analysis with Boundary Elements* 2000; **24**: 549-557.
- [21].Chen JT, Lin SY, Lee YT and Chen IL. Analytical and numerical studies of free vibrations of plate by imaginary-part BEM formulations. *Journal of Sound and Vibration* 2006; **293**: 380-408.
- [22].Chen JT, Chen IL, Chen KH, Yeh YT and Lee YT. A meshless method for free vibration of arbitrarily shaped plates with clamped boundaries using radial basis function. *Engineering Analysis with Boundary Elements* 2004; **28**: 535-545.
- [23].Chen JT, Wu CS and Lee YT. On the equivalence of the Trefftz method and method of fundamental solutions for Laplace and biharmonic equations. *Computers and Mathematics with Applications*, accepted.
- [24].Chen JT, Chang MH, Chen KH and Chen IL. Boundary collocation method for acoustic eigenanalysis of three-dimensional cavities using radial basis function. *Computational Mechanics* 2002; **29**: 392-408.
- [25].Baker GR and Shelley MJ. Boundary Integral Techniques for Multi-connected Domains. *Journal of Computational Physics* 1986; **64**: 112-132.
- [26].Bird MD and Steele CR. A solution procedure for Laplace’s equation on multiply-connected circular domain. *ASME Journal of Applied Mechanics* 1992; **59**: 398-404.

- [27].Cheng AHD. Particular solutions of Laplacian, Helmholtz-type, and polyharmonic operators involving higher order radial basis functions. *Engineering Analysis with Boundary Elements* 2000; **24**: 531-538.
- [28].Goree JG and Wilson HB Jr. Transverse shear loading in an elastic matrix containing two circular cylindrical inclusions. *ASME Journal of Applied Mechanics* 1967; **34**: 511-513.
- [29].Sendekyj GP. Multiple circular inclusion problems in longitudinal shear deformation. *Journal of Elasticity* 1971; **1**: 83-86.
- [30].Steif PS. Shear stress concentration between holes. *ASME Journal of Applied Mechanics* 1989; **56**: 719-721.
- [31].Budiansky B and Carrier GF. High shear stresses in stiff-fiber composites. *ASME Journal of Applied Mechanics* 1984; **51**: 733-735.
- [32].Zimmerman RW. Second-order approximation for the compression of an elastic plate containing a pair of circular holes. *Zeitschrift fur Angewandte Mathematik und Mechanik* 1988; **68**: 575-577.
- [33].Honein E, Honein T and Herrmann G. On two circular inclusions in harmonic problems. *Quarterly of Applied Mathematics* 1992; **50**: 479-499.
- [34].Bird MD and Steele CR. A solution procedure for Laplace's equation on multiply-connected circular domains. *ASME Journal of Applied Mechanics* 1992; **59**: 398-404.
- [35].Gong SX. Antiplane interaction among multiple circular inclusions. *Mechanics Research Communications* 1995; **22**: 257-262.
- [36].Chao CK and Young CW. On the general treatment of multiple inclusions in antiplane elastostatics. *International Journal of Solids and Structures* 1998; **35**: 3573-3593.
- [37].Chen JT and Wu AC. Null-field integral equation approach for stress field around circular holes and/or inclusions under anti-plane shear 2006; accepted.
- [38].Chen KH, Kao JH, Chen JT, Young DL and Lu MC, Regularized meshless method for multiply-connected-domain Laplace problems, *Engineering Analysis with Boundary Elements* 2006; accepted.
- [39].Bleustein JL. New surface wave in piezoelectric materials. *Applied Physics Letters* 1968; **13**: 412-413.
- [40].Pak YE. Circular inclusion problem in antiplane piezoelectricity. *International Journal of Solids and Structures* 1992; **29**: 2403-2419.
- [41].Honein T and Honein BV. On the interaction of two piezoelectric fibers embedded in an intelligent material. *Journal of Intelligent Material Systems and Structures* 1995; **6**: 229-236.
- [42].Chung MY and Ting TCT. Piezoelectric solid with an elliptic inclusion or hole.

- International Journal of Solids and Structures 1996; **33**: 3343-3361.
- [43].Stroh AN. Steady state problems in anisotropic elasticity. Journal of Mathematics and Physics 1962; **41**: 77-103.
- [44].Zhong Z and Meguid SA. Interfacial debonding of a circular inhomogeneity in piezoelectric materials. International Journal of Solids and Structures 1997; **34**: 1965-1984.
- [45].Chen T and Chiang SC. Electroelastic fields and effective moduli of a medium containing cavities or rigid inclusions of arbitrary shape under anti-plane mechanical and in-plane electric fields. Acta Mechanica 1997; **121**: 79-96.
- [46].Chao CK and Chang KJ. Interacting circular inclusion in antiplane piezoelectricity. International Journal of Solids and Structures 1999; **36**: 3349-3373.
- [47].Wu L, Chen J and Meng Q. Two piezoelectric circular cylindrical inclusions in the infinite piezoelectric medium. International Journal of Engineering Science 2000; **38**: 879-892.
- [48].Liu WK, Jun S, Li S, Adee J and Belytschko T. Reproducing kernel particle methods for structural dynamics. International Journal for Numerical Methods in Engineering 1995; **38**: 1655-1679.
- [49].Atluri SN and Zhu TL. The meshless local Petrov-Galerkin (MLPG) approach for solving problems in elasto-statics. Computational Mechanics 2000; **25**: 169-179.
- [50].Partridge PW, Brebbia CA and Wrobel LC. The dual reciprocity boundary element method. Southampton: Computational Mechanics Publications 1992.
- [51].Kamiya N and Andoh E. A note on multiple reciprocity integral formulation for Helmholtz equation. Communications in Numerical Methods in Engineering 1993; **9**: 9-13.
- [52].Nowak AJ and Brebbia CA. The multiple reciprocity method|a new approach for transforming BEM domain integrals to the boundary. Engineering Analysis with Boundary Elements 1989; **6**: 164-167.
- [53].Nowak AJ and Neves AC (eds). Multiple reciprocity boundary element method. Southampton: Computational Mechanics Publications 1994.
- [54].Itagaki M and Brebbia CA. Source iterative multiple reciprocity technique for Helmholtz eigenvalue problems with boundary elements. In Proc. 5th Japan-China Symp. Boundary Element Methods, Current Research in Japan and China, Sapporo, 1993; 79-88. Elsevier.
- [55].Itagaki M and Brebbia CA. Application of the multiple reciprocity boundary element method to neutron diffusion problems. In The multiple reciprocity boundary element method. Southampton: Computational Mechanics Publications

1994.

- [56]. Itagaki M, Nishiyama S, Tomioka S, Enoto T and Sahashi N. Power iterative multiple reciprocity boundary element method for solving three-dimensional Helmholtz equation. *Engineering Analysis with Boundary Elements* 1997; **20**: 113-121.
- [57]. Kamiya N, Andoh E and Nogae K. A new complex-valued formulation and eigenvalue analysis of the Helmholtz equation by boundary element method. *Advances in Engineering Software* 1996; **26**: 219-227.
- [58]. Tai GRG and Shaw RP. Helmholtz equation eigenvalues and eigenmodes for arbitrary domains. *The Journal of the Acoustical Society of America* 1974; **56**: 796-804.
- [59]. De Mey G. Calculation of the Helmholtz equation by an integral equation. *International Journal for Numerical Methods in Engineering* 1976; **10**: 59-66.
- [60]. De Mey G. A simplified integral equation method for the calculation of the eigenvalues of Helmholtz equation. *International Journal for Numerical Methods in Engineering* 1977; **11**: 1340-1342.
- [61]. Hutchinson JR. An alternative BEM formulation applied to membrane vibrations. In *Boundary elements VII* (ed. C. A. Brebbia & G. Maier) 1985. Springer.
- [62]. Hutchinson JR. Vibration of plates, in *boundary elements X* (ed. C. A. Brebbia), 1988; **4**: 415-430. Springer.
- [63]. Hutchinson JR. Analysis of plates and shells by boundary collocation. In *Boundary elements analysis of plates and shells* (ed. D. E. Beskos) 1991; 314-368. Springer.
- [64]. Chen JT, Huang CX and Wong FC. Determination of spurious eigenvalues and multiplicities of true eigenvalues in the dual multiple reciprocity method using the singularvalue decomposition technique. *Journal of Sound and Vibration* 2000a; **230**: 219-230.
- [65]. Kuo SR, Yeih W and Wu YC. Applications of the generalized singular-value decomposition method on the eigenproblem using the incomplete boundary element formulation. *Journal of Sound and Vibration* 2000b; **235**: 813-845.
- [66]. Golub GH and Van Loan CF. *Matrix computations*, 2nd ed. Baltimore, MD: Johns Hopkins University 1989 Press.
- [67]. Berry MW, Drmac Z and Jessup ER. *Matrices, vector spaces, and information retrieval*. SIAM Review 1999; **41**: 335-362.
- [68]. Chen JT, Kuo SR and Cheng YC. On the true and spurious eigensolutions using circulants for real-part dual BEM. In *IUTAM/IACM/IABEM Symp. Advanced Mathematical and Computational Mechanics Aspects of Boundary Element Method*, Cracow, Poland, 2000b; 77-85. Dordrecht: Kluwer.

- [69].Chen IL, Chen JT, Kuo SR and Liang MT. A new method for true and spurious eigensolutions of arbitrary cavities using the CHEEF method. The Journal of the Acoustical Society of America 2001a ; **109**: 982-999.
- [70].Kitahara M. Boundary integral equation methods in eigenvalue problems of elastodynamics and thin plates. 1985 Elsevier.
- [71].Chen JT, Lin JH, Kuo SR and Chyuan SW. Boundary element analysis for the Helmholtz eigenvalue problems with a multiply connected domain. Proceedings of the Royal Society Series A 2001; **457**: 2521-2546.
- [72].Chen JT, Liu LW and Chyuan SW. Acoustic eigenanalysis for multiply-connected problems using dual BEM. Communications in Numerical Methods in Engineering 2004; **20**: 419-440.
- [73].Chen JT, Liu LW and Hong HK. Spurious and true eigensolutions of Helmholtz BIEs and BEMs for a multiply connected problem. Proceedings of the Royal Society Series A 2003; **459**: 1891-1924.
- [74].Abramowitz M, Stegun IA. Handbook of mathematical functions with formulation graphs and mathematical tables. New York. Dover. 1972.
- [75].Saito K, Nakada M, Iijima K and Onishi K. A quasi-spectral method for Cauchy problem of 2D Laplace equation on an annulus. Journal de Physique 2005; **12**: 128-139.
- [76].Chen JT, Chang MH, Chen KH and Lin SR. The boundary collocation method with meshless concept for acoustic eigenanalysis of two-dimensional cavities using radial basis function. Journal of Sound and Vibration 2002; **257**: 667-711.

Method \ Eigenvalue	RMM	BEM	FEM	PM
k_1	4.50(SS)	4.50(SS)	4.453	4.548(SS)
k_2	4.56(AS)	4.50(AS)	4.512	4.588(AS)
k_3	6.40(AA)	6.37(AA)	6.267	6.457(AA)
k_4	6.40(SA)	6.37(SA)	6.269	6.472(SA)
k_5	7.10(SS)	7.16(SS)	6.930	7.083(SS)

Table 5-1 The former five eigenvalues for a circular domain with two equal holes by using different approaches.

Method \ Eigenvalue	RMM	BEM	FEM	PM
k_1	4.50(SS)	4.47(SS)	4.443	4.655(SS)
k_2	5.38(AS)	5.37(AS)	5.316	N/A
k_3	5.38(SA)	5.37(SA)	5.320	N/A
k_4	5.55(AA)	5.54(AA)	5.486	5.561(SA)
k_5	5.95(SS)	5.95(SS)	5.884	5.868(SS)

Table 5-2 The former five eigenvalues for a circular domain with four equal holes by using different approaches.

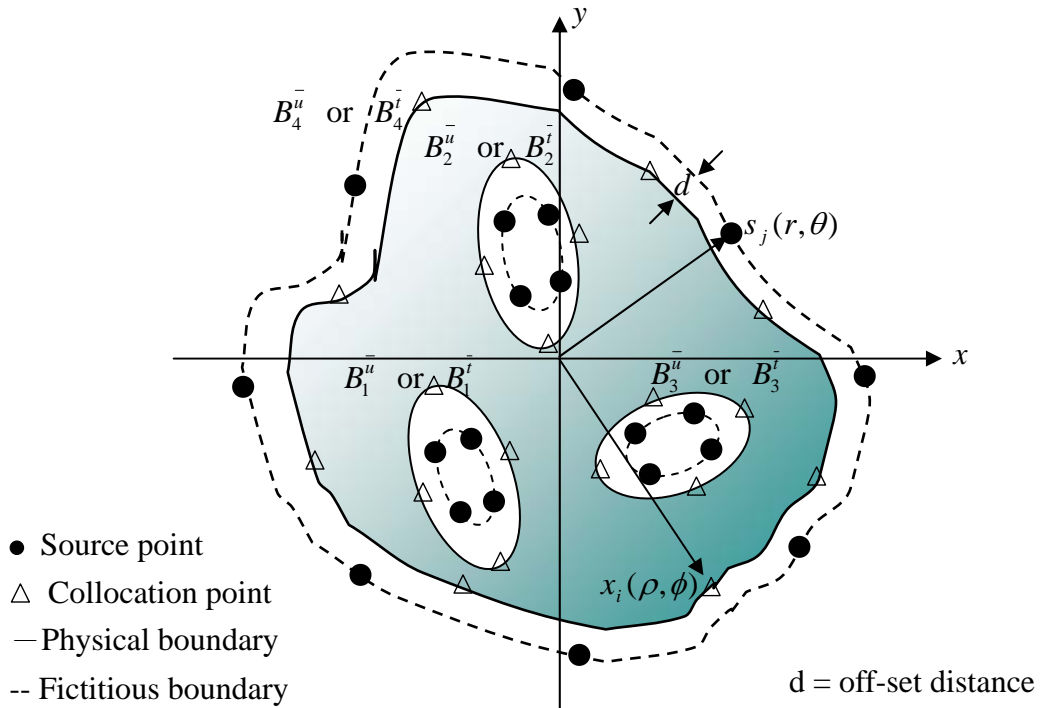


Fig. 1-1 (a)

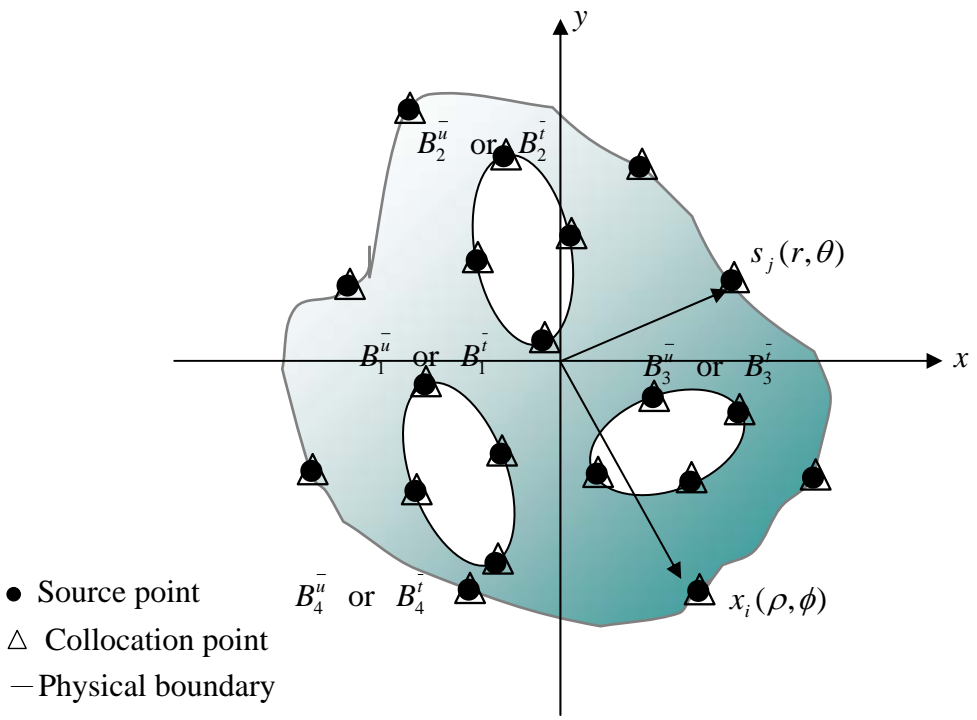


Fig. 1-1 (b)

Fig. 1-1 The conventional MFS and the RMM for the multiply-connected problems, (a) Conventional MFS, (b) RMM.

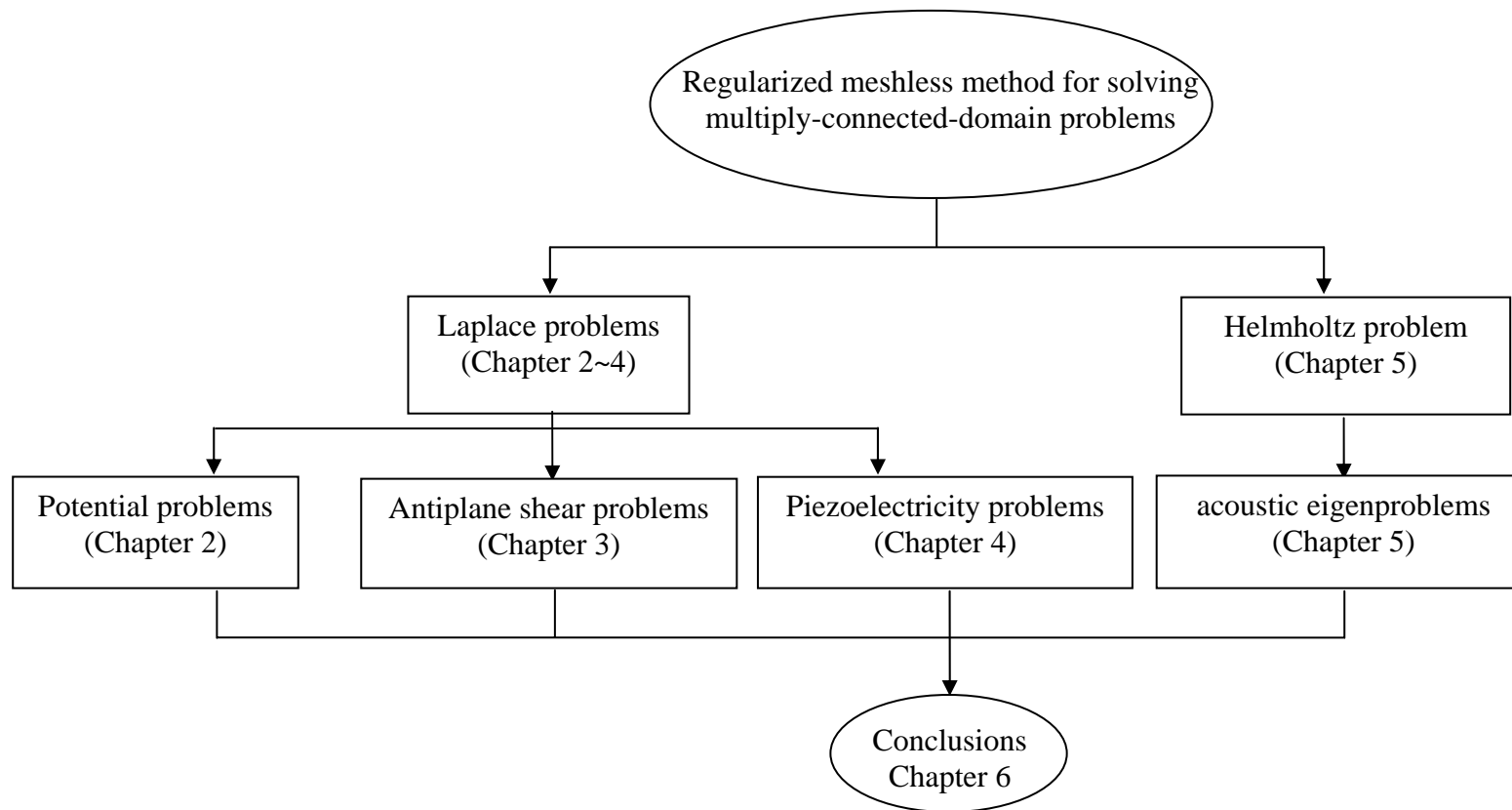


Fig. 1-2 The frame of the thesis

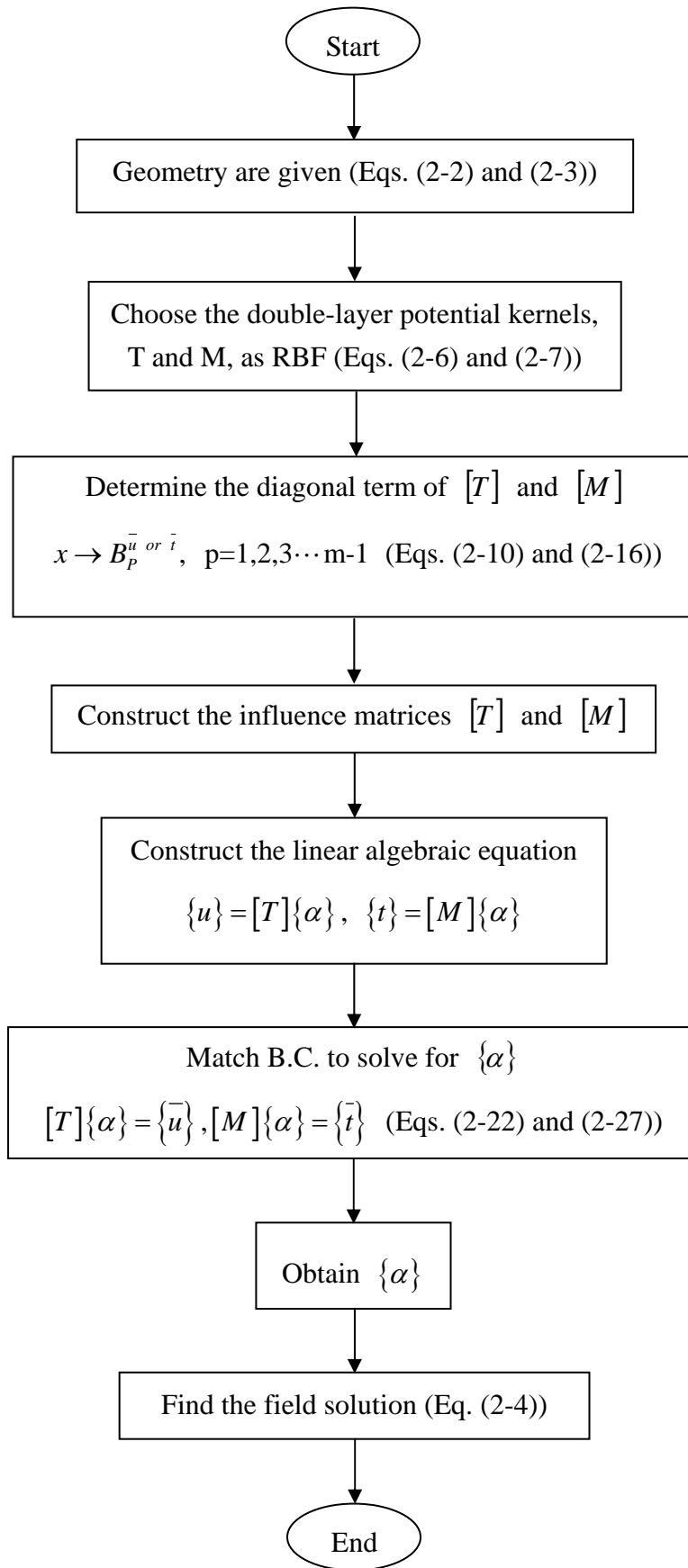


Fig. 2-1 Solution procedures.

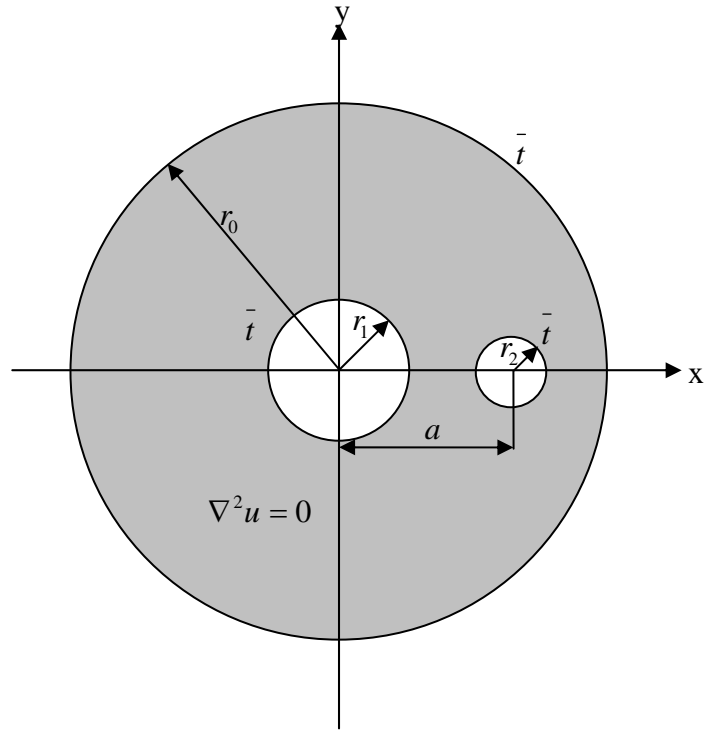


Fig. 2-2 Problem sketch for the case 2-1 ($r_0 = 2.0$, $r_1 = 0.5$, $r_2 = 0.25$ and $a = 1$).

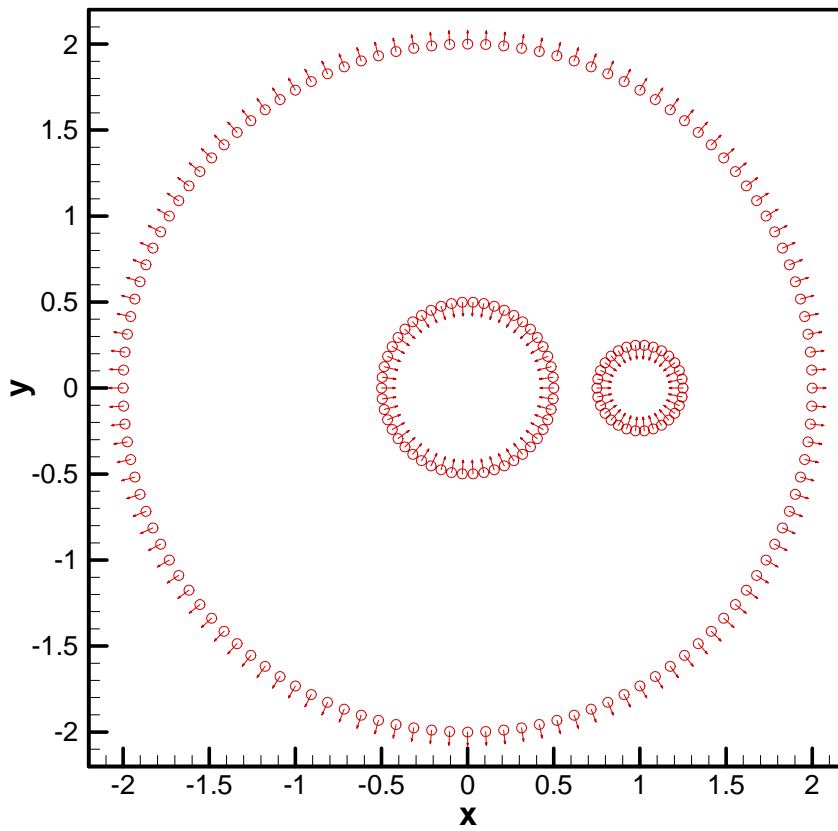


Fig. 2-3 Nodes distribution (200 nodes) for the case 2-1.

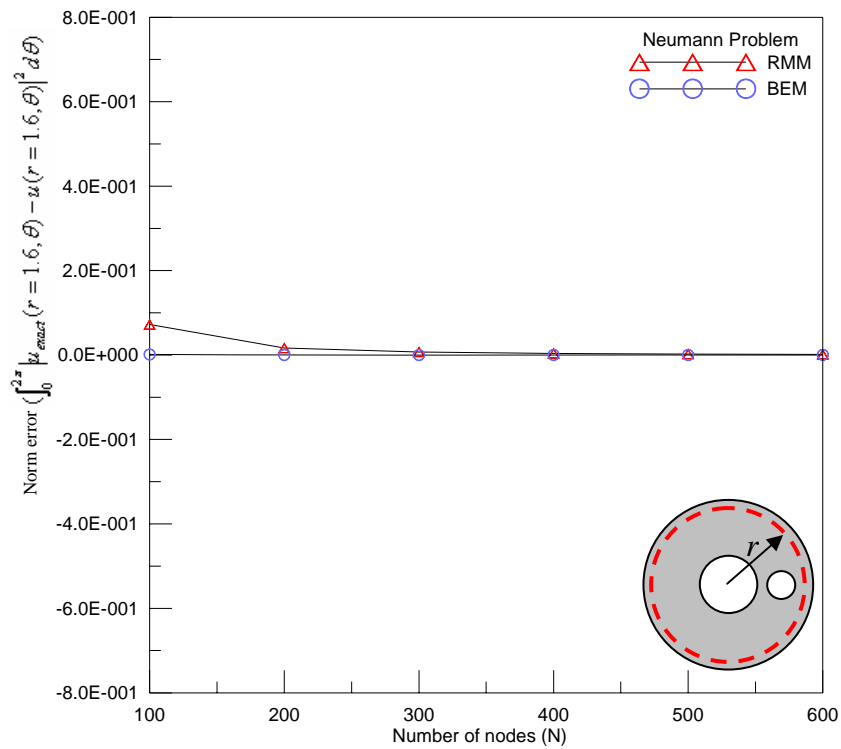


Fig. 2-4 The norm error along the radius $r = 1.6$ versus the number of nodes for the case 2-1.

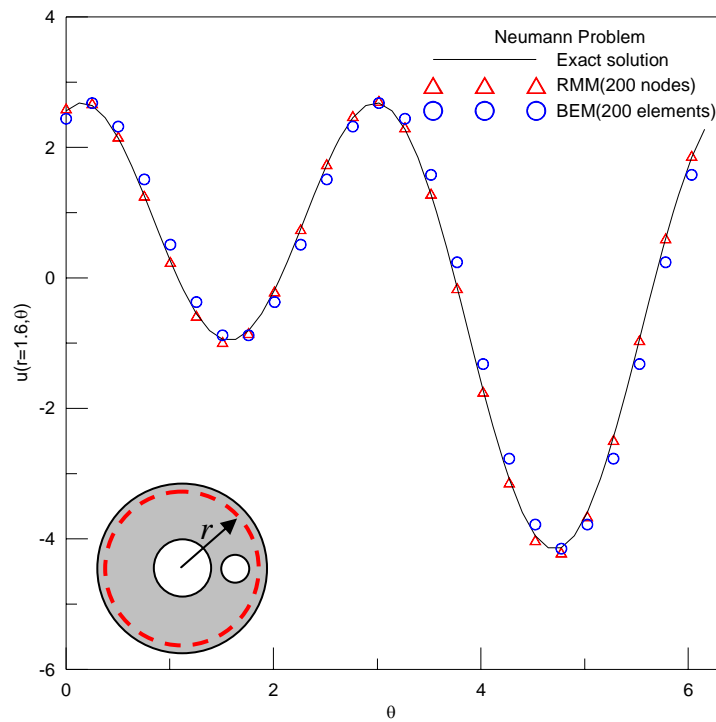


Fig.2-5 The error analysis for the field solution along the radius $r = 1.6$ by using the RMM and BEM.

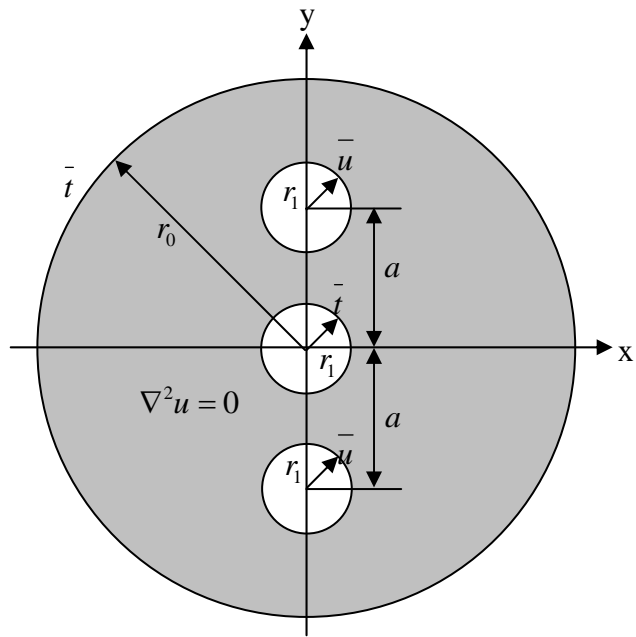


Fig. 2-6 Problem sketch for the case 2-2 ($r_0 = 2.0$, $r_1 = 0.25$ and $a = 1.0$).

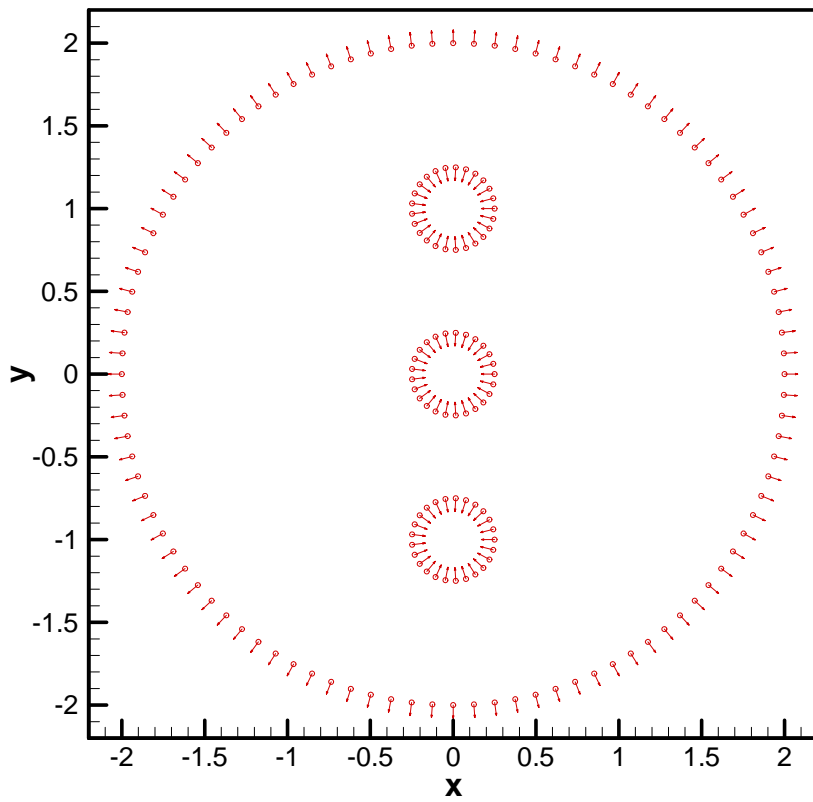


Fig. 2-7 Nodes distribution (175 nodes) for the case 2-2.

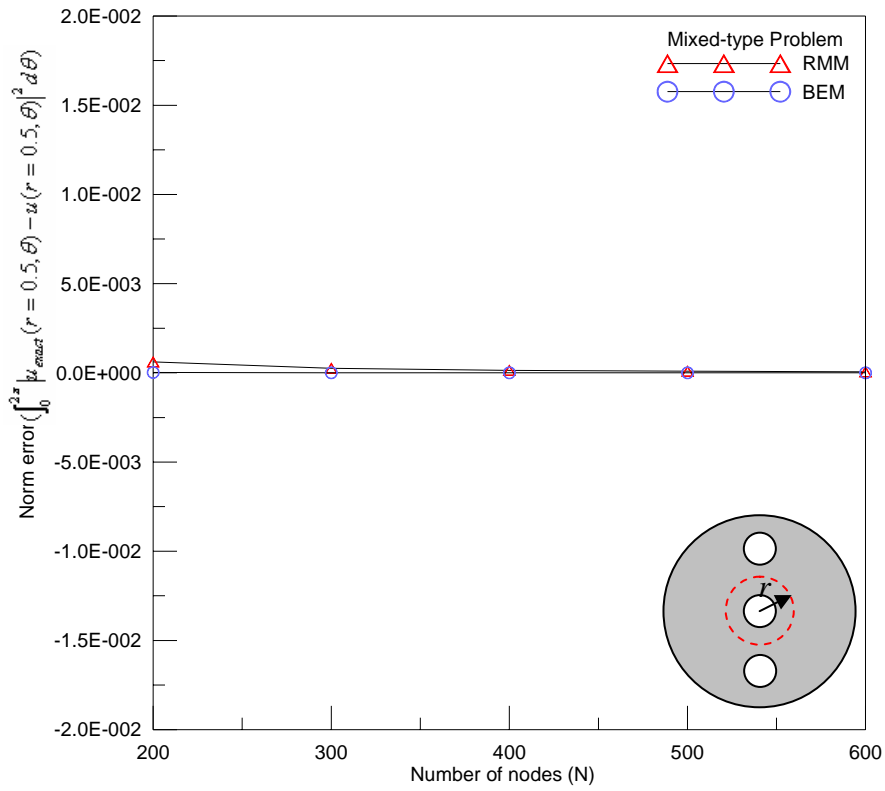


Fig.2-8 The norm error along the radius $r = 0.5$ versus the number of nodes for the case 2-2.

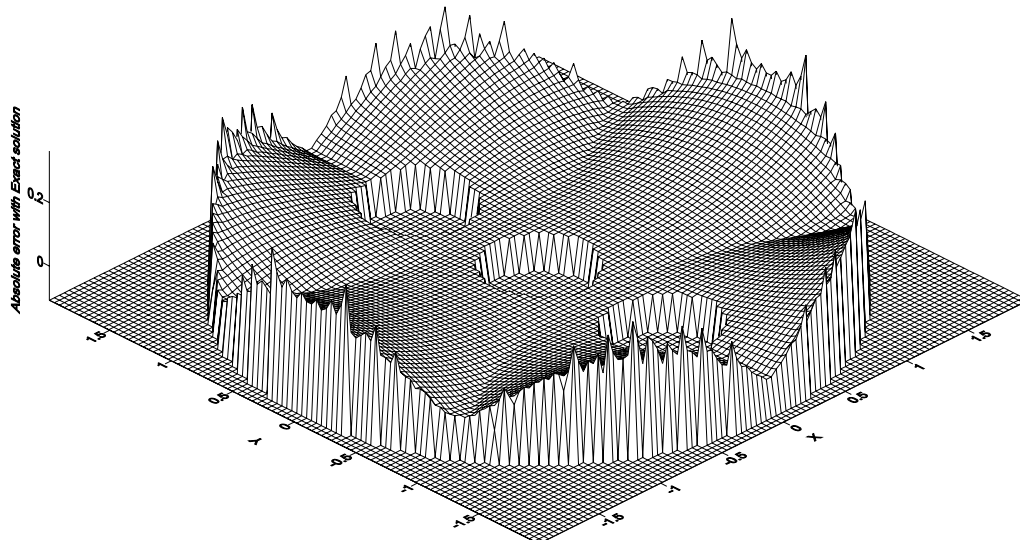


Fig. 2-9 Absolute error with the exact solution for the entire domain of the case 2-2 (400 nodes).

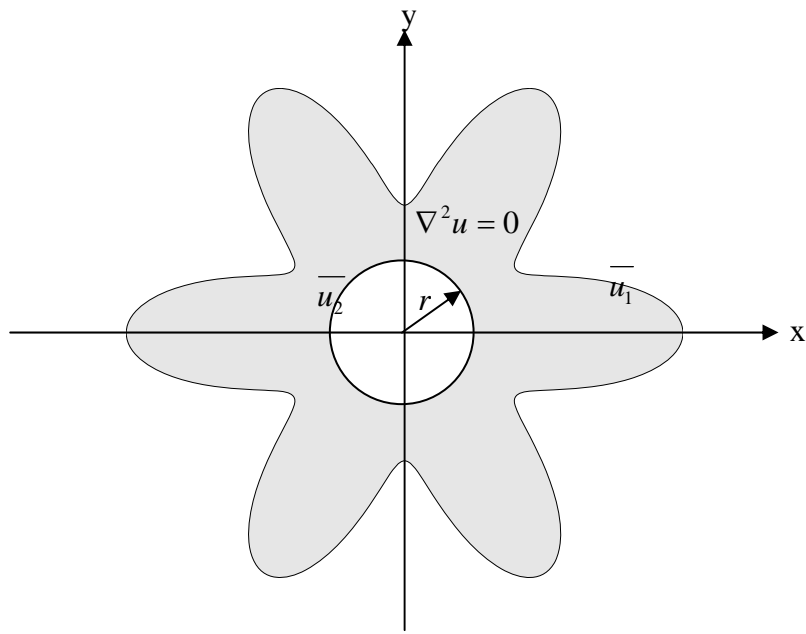


Fig. 2-10 (a)

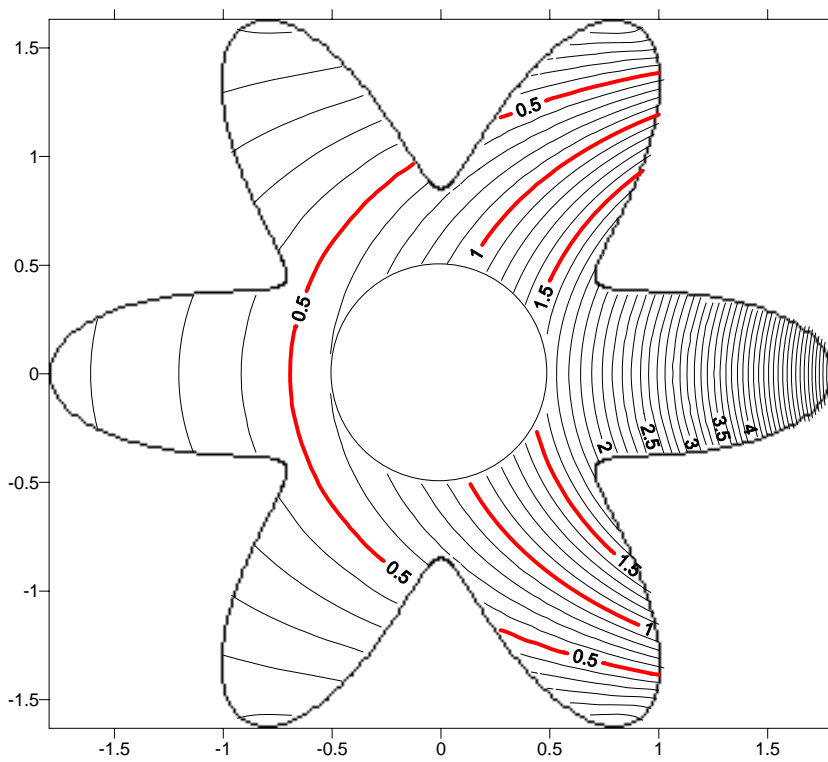


Fig. 2-10 (b)

Fig. 2-10 Problem sketch and the exact solution for the case 2-3, (a) problem sketch $r = 0.5$, (b) the field potential of the exact solution.

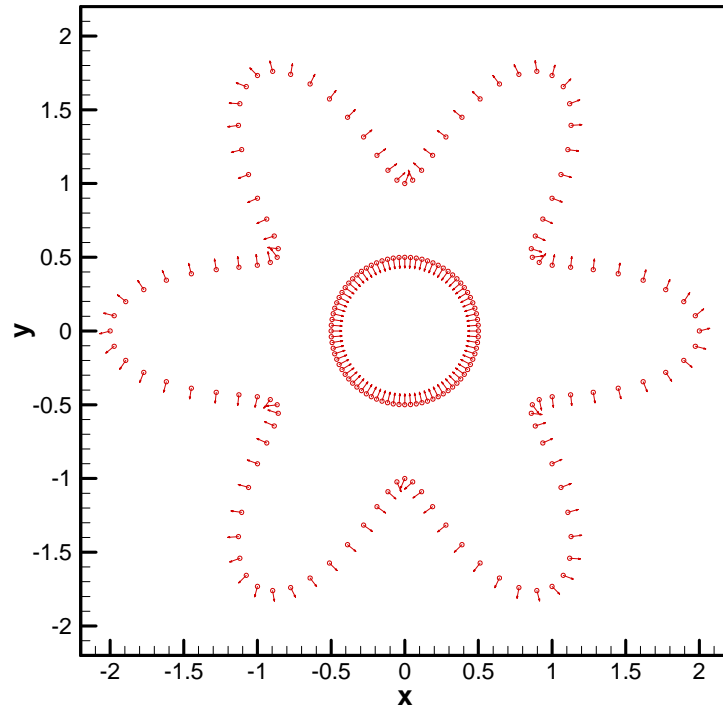


Fig. 2-11 Nodes distribution (200 nodes) for the case 2-3.

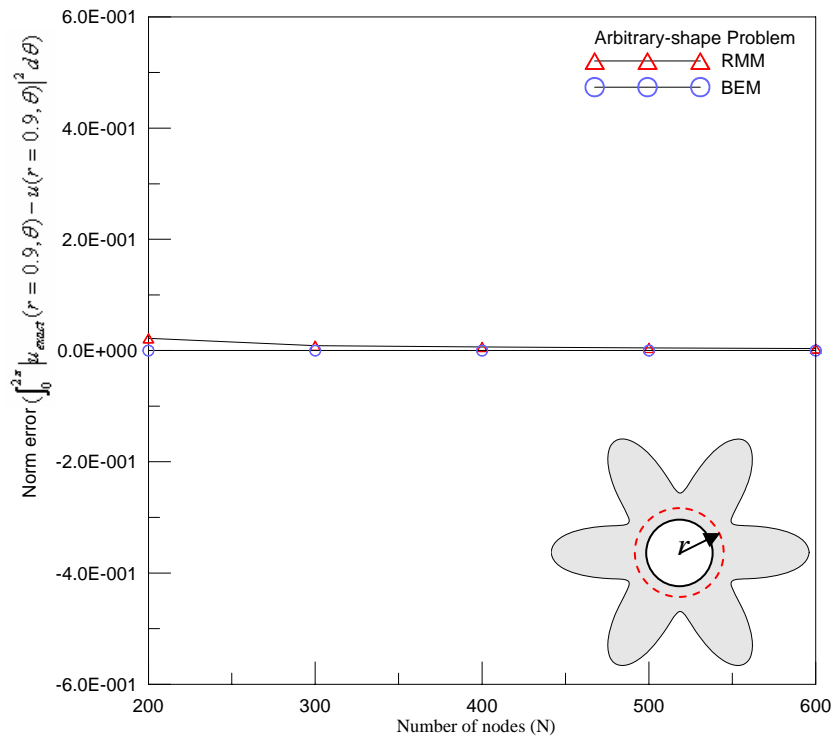


Fig. 2-12 The norm error along the radius $r = 0.9$ versus the number of nodes for the case 2-3.

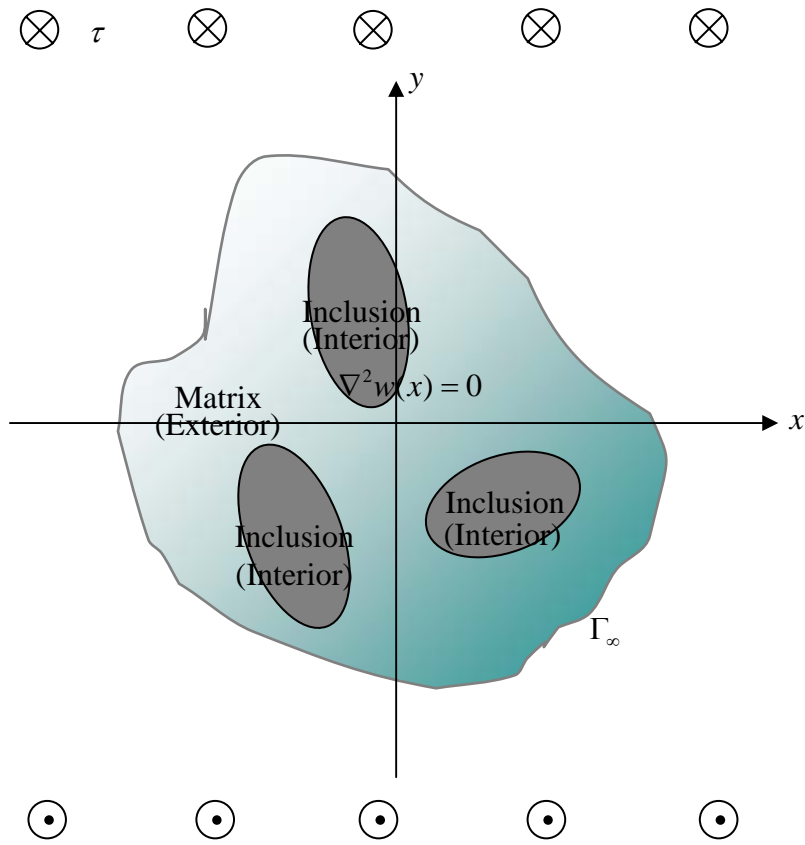


Fig. 3-1 Problem sketch for a multiple inclusions problem under remote shear.

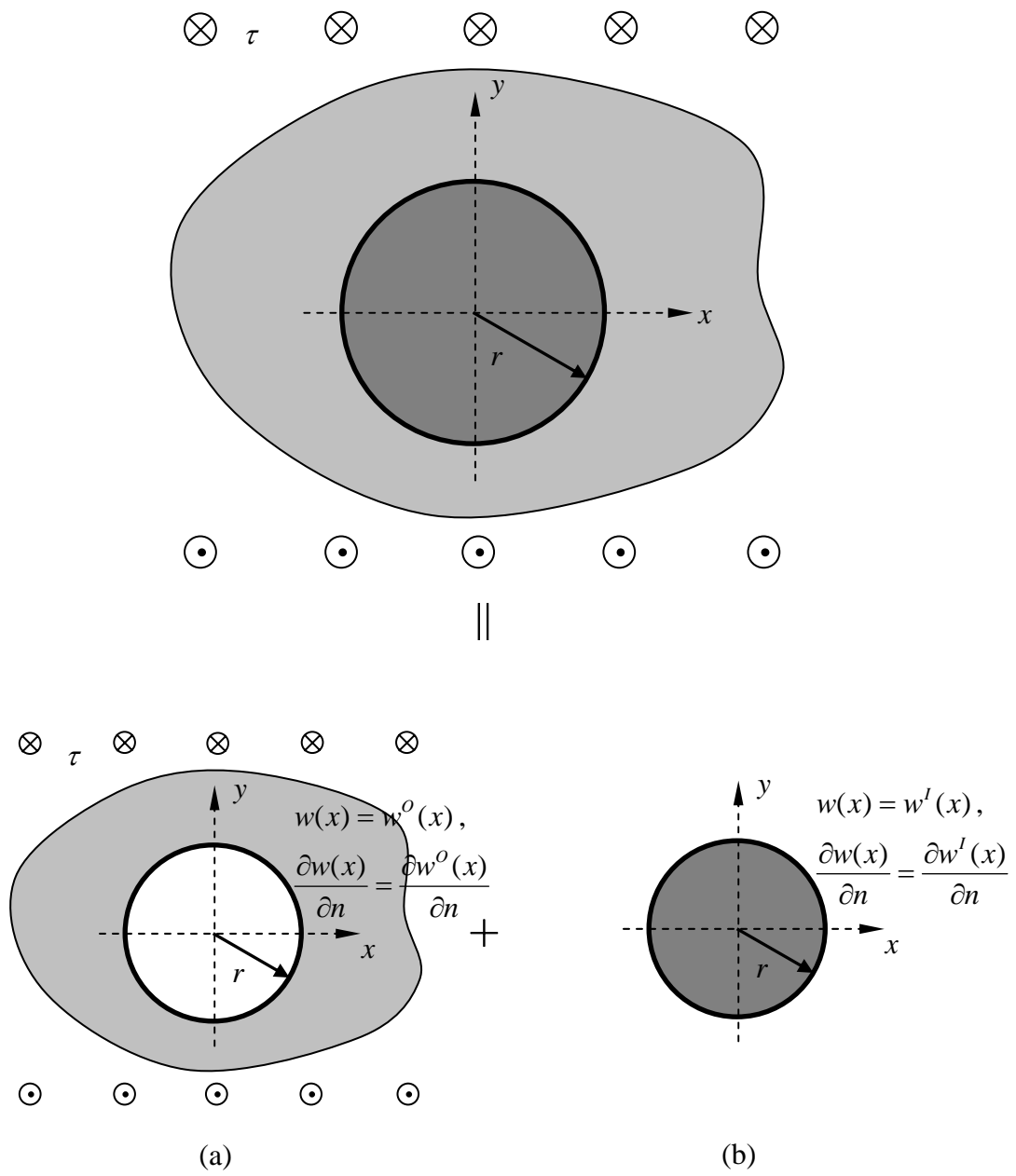


Fig. 3-2 Decomposition of the problem.

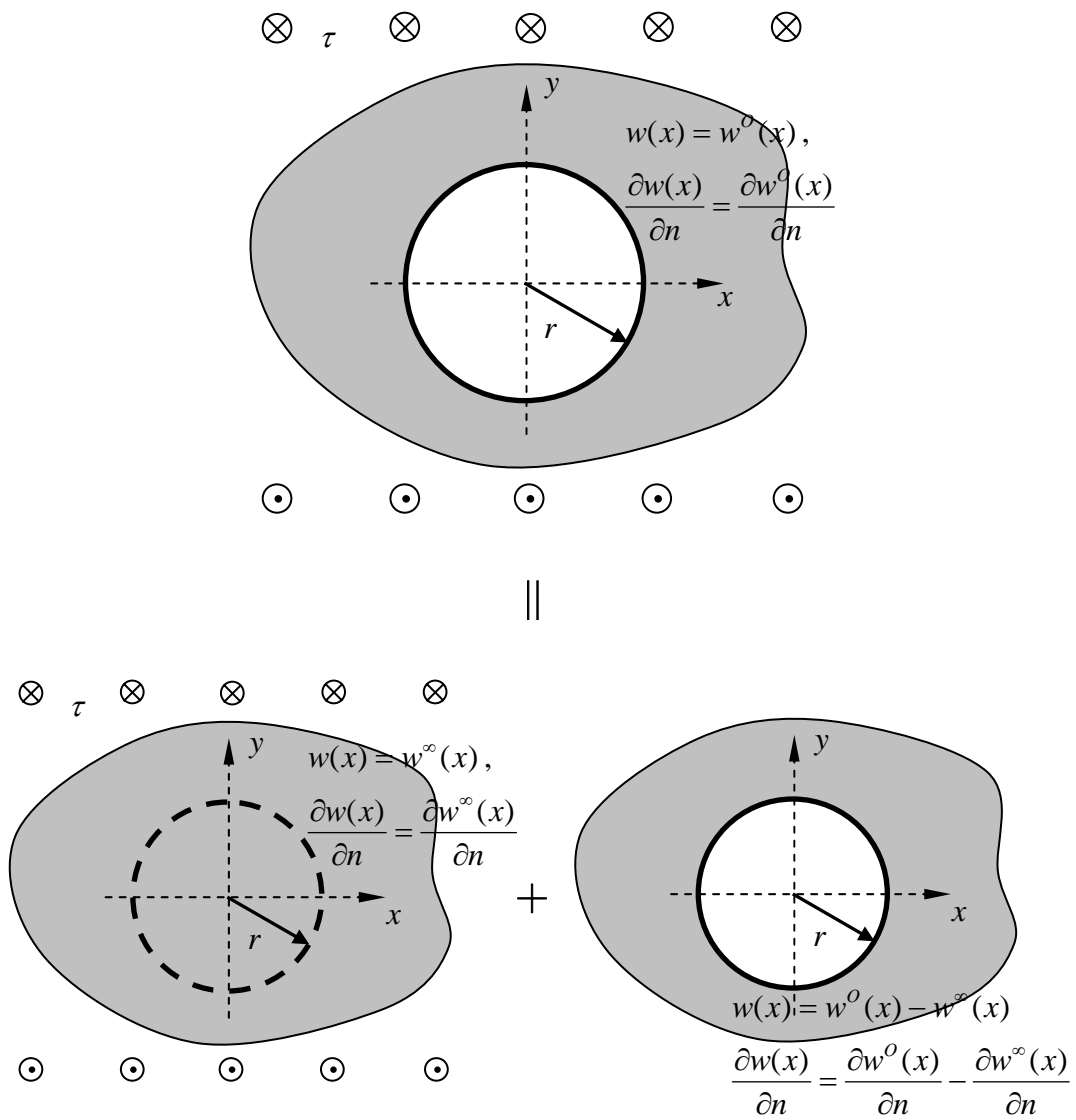


Fig. 3-3 Decomposition of the problem of Fig. 3-2 (a).

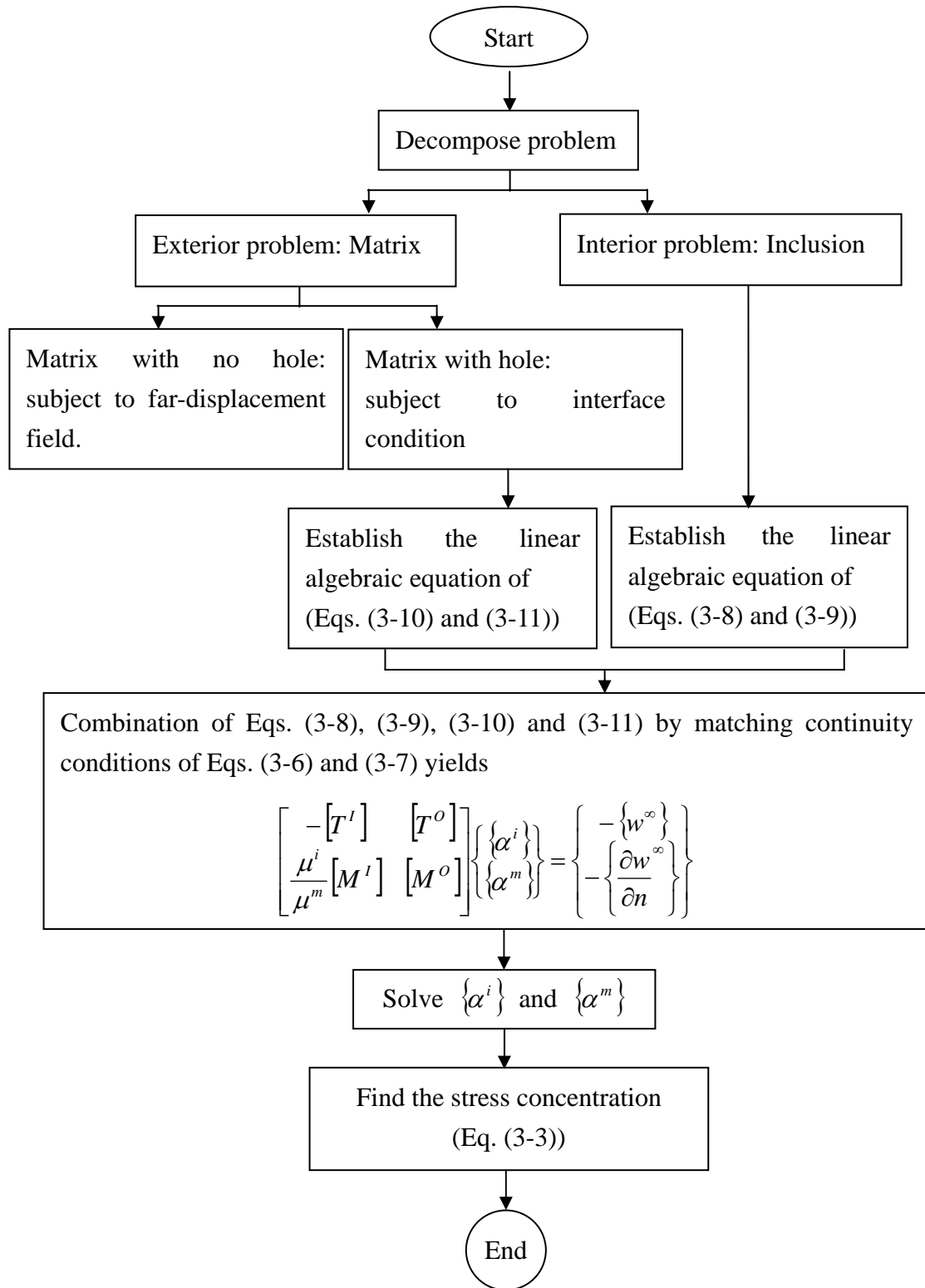


Fig. 3-4 Flowchart of solution procedures.

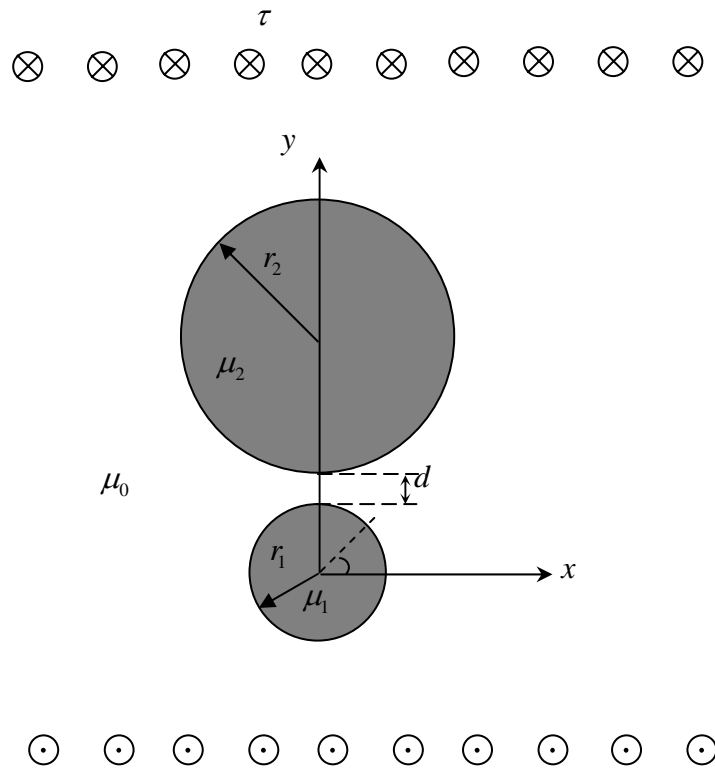


Fig. 3-5 Problem sketch of double inclusions under antiplane shear.

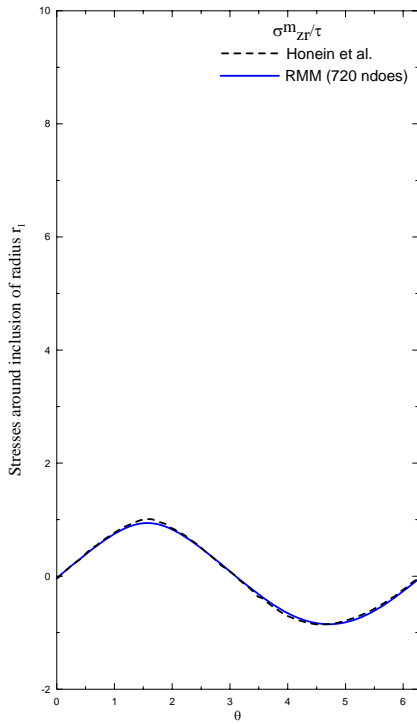


Fig. 3-6 (a)

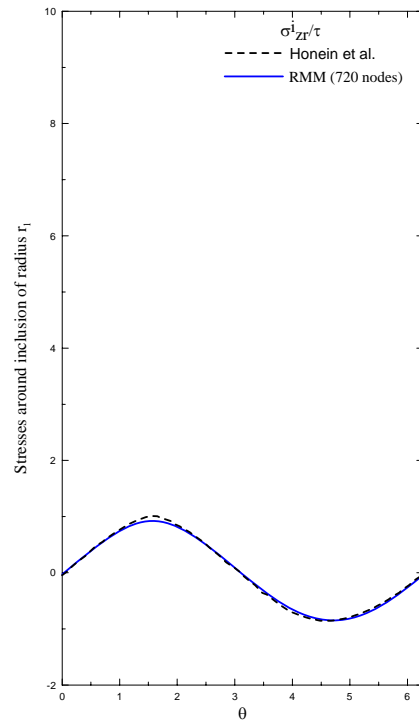


Fig. 3-6 (b)

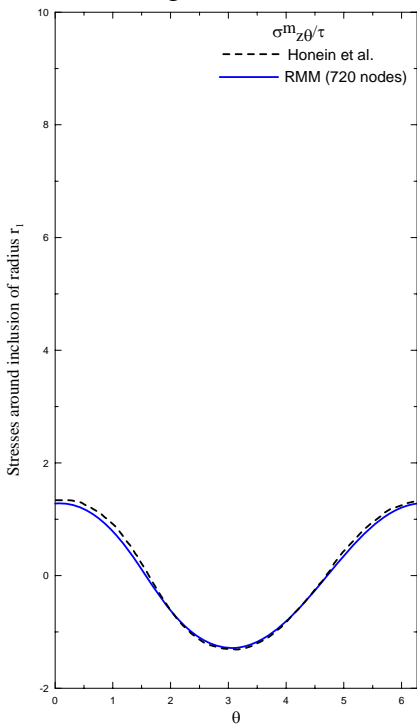


Fig. 3-6 (c)

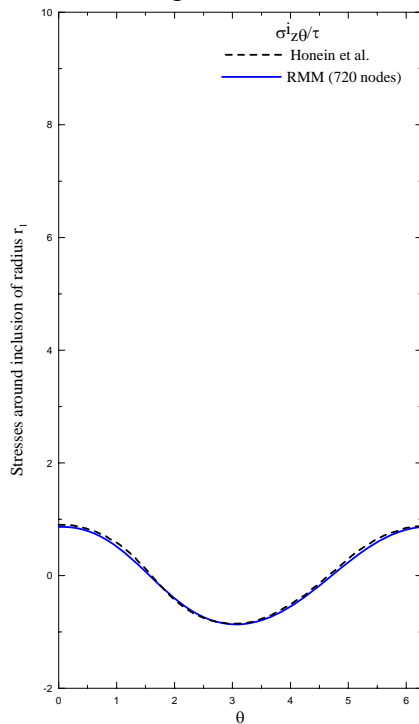


Fig. 3-6 (d)

Fig. 3-6 Stress concentration along the boundaries of both the matrix and the smaller inclusion, (a) σ_{zr}^m / τ , (b) σ_{zr}^i / τ , (c) $\sigma_{z\theta}^m / \tau$, (d) $\sigma_{z\theta}^i / \tau$.

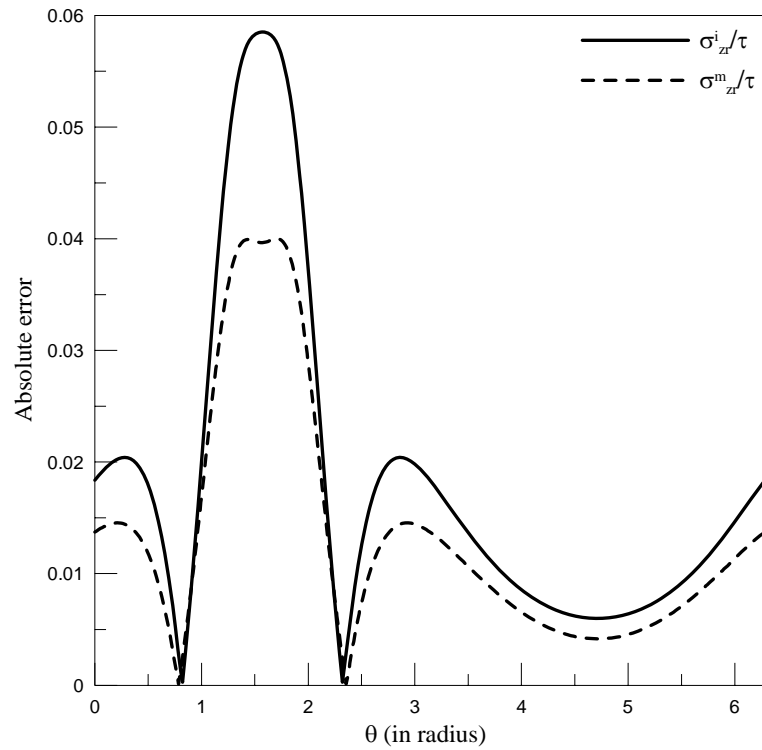


Fig. 3-7 (a)

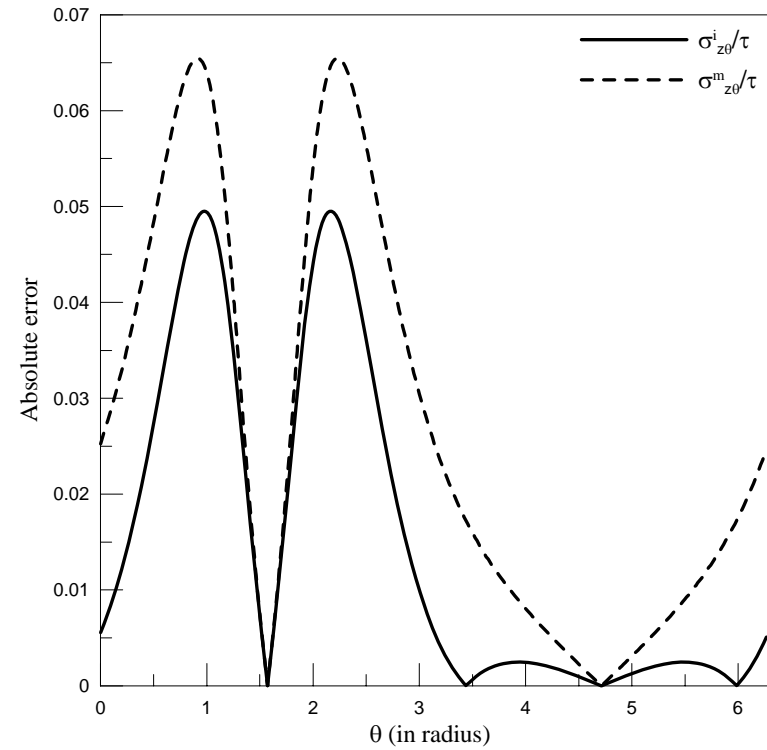


Fig. 3-7 (b)

Fig. 3-7 The absolute error of stress concentration along the boundaries of both the matrix and the smaller inclusion, (a) σ_{zr}^m/τ and σ_{zr}^i/τ , (b) $\sigma_{z\theta}^m/\tau$ and $\sigma_{z\theta}^i/\tau$.

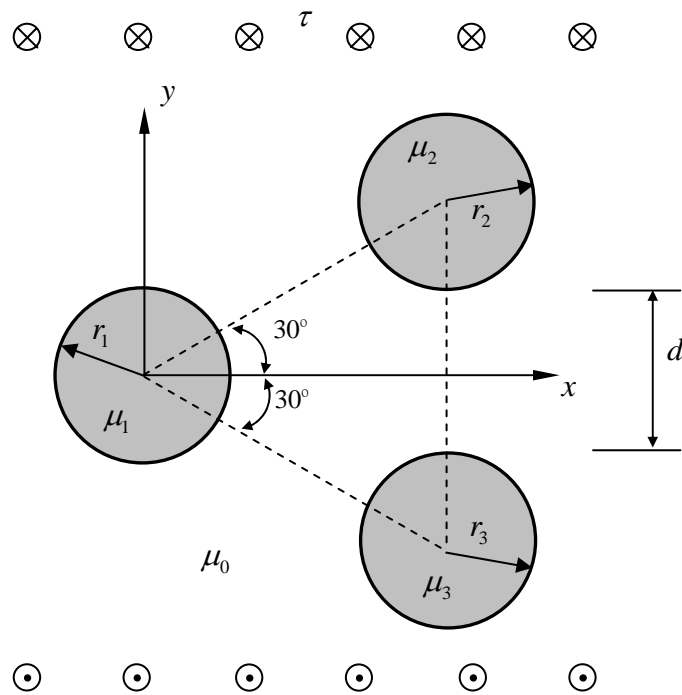


Fig. 3-8 Problem sketch of three inclusions under antiplane shear.

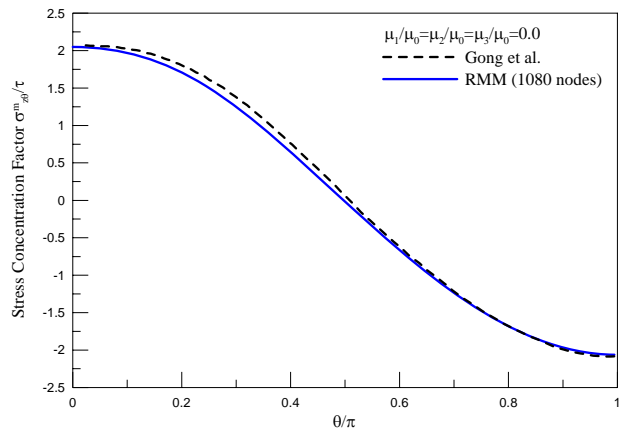


Fig. 3-9 (a)

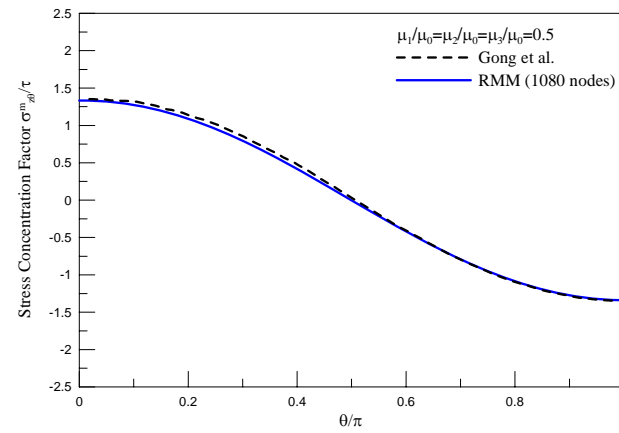


Fig. 3-9 (b)

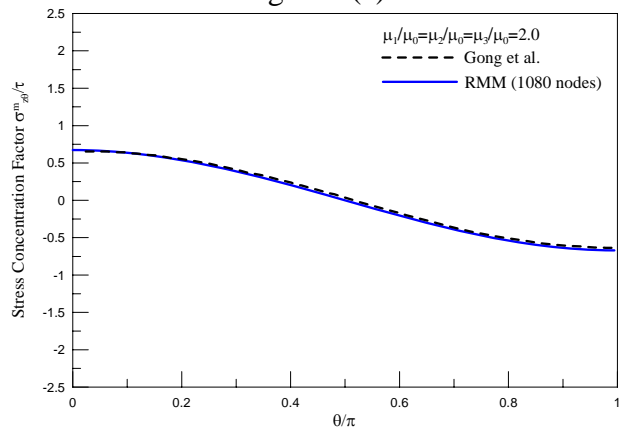


Fig. 3-9 (c)

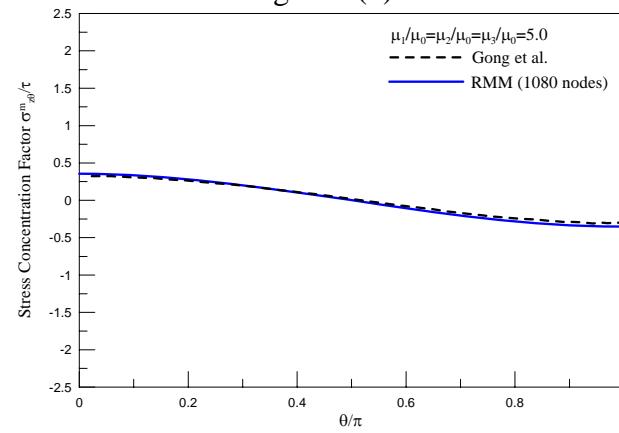


Fig. 3-9 (d)

Fig. 3-9 Stress concentration factor $\sigma_{z\theta}^m / \tau$ along the boundaries of both the left inclusion and matrix for various shear modulus ratios, (a) $\mu_1 / \mu_0 = \mu_2 / \mu_0 = \mu_3 / \mu_0 = 0.0$, (b) $\mu_1 / \mu_0 = \mu_2 / \mu_0 = \mu_3 / \mu_0 = 0.5$, (c) $\mu_1 / \mu_0 = \mu_2 / \mu_0 = \mu_3 / \mu_0 = 2.0$, (d) $\mu_1 / \mu_0 = \mu_2 / \mu_0 = \mu_3 / \mu_0 = 5.0$.

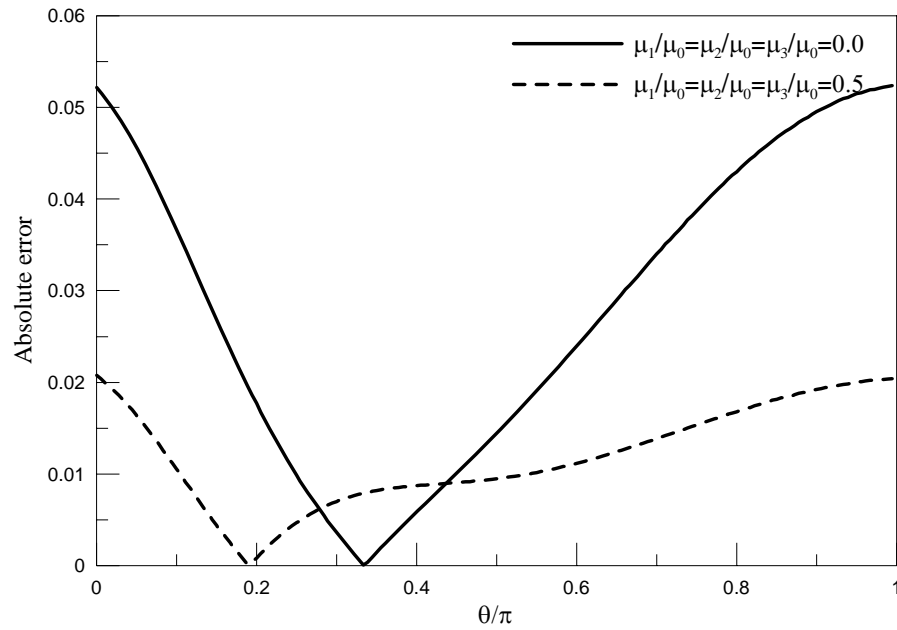


Fig. 3-10 (a)

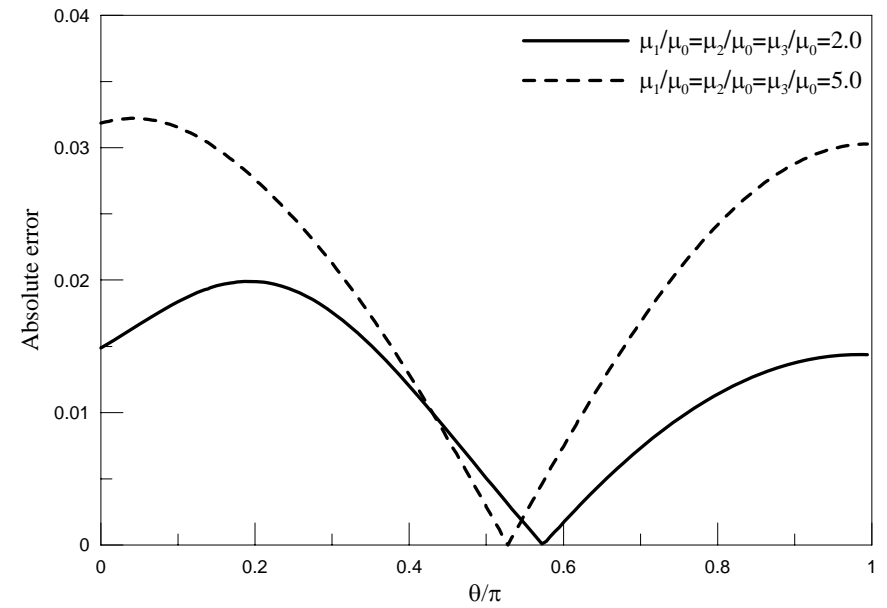


Fig. 3-10 (b)

Fig. 3-10 The absolute error result of stress concentration along the boundaries of both the matrix and the left inclusion for various shear modulus ratios, (a) $\mu_1/\mu_0 = \mu_2/\mu_0 = \mu_3/\mu_0 = 0.0$ and $\mu_1/\mu_0 = \mu_2/\mu_0 = \mu_3/\mu_0 = 0.5$, (b) $\mu_1/\mu_0 = \mu_2/\mu_0 = \mu_3/\mu_0 = 2.0$ and $\mu_1/\mu_0 = \mu_2/\mu_0 = \mu_3/\mu_0 = 5.0$.

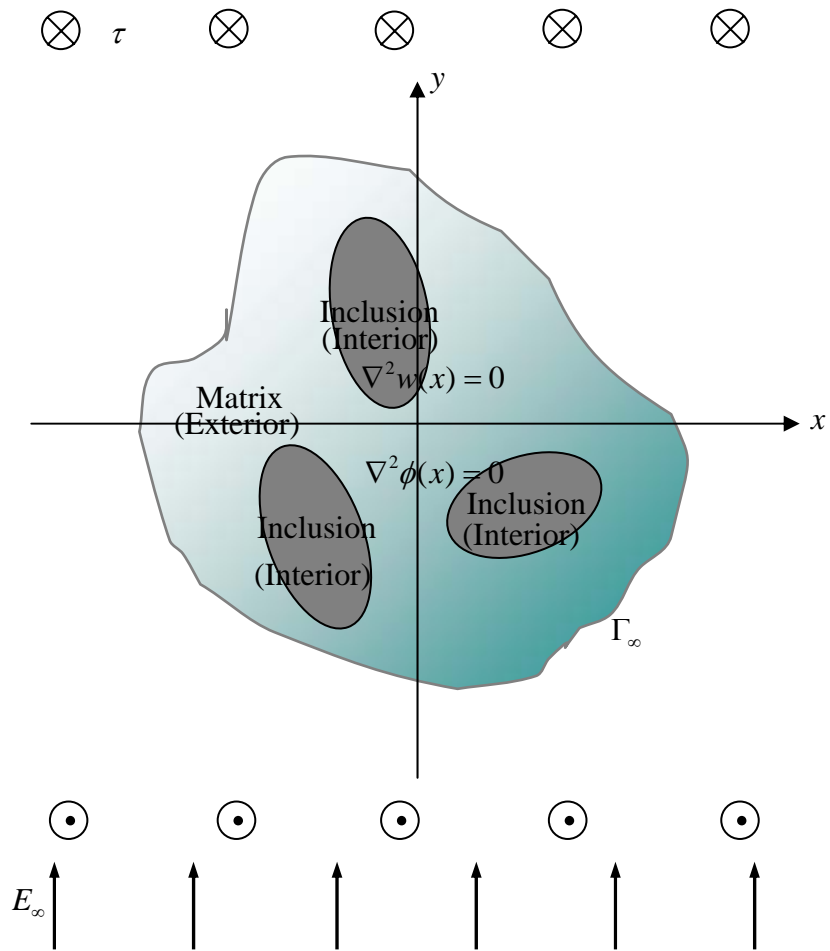


Fig. 4-1 Problem sketch.

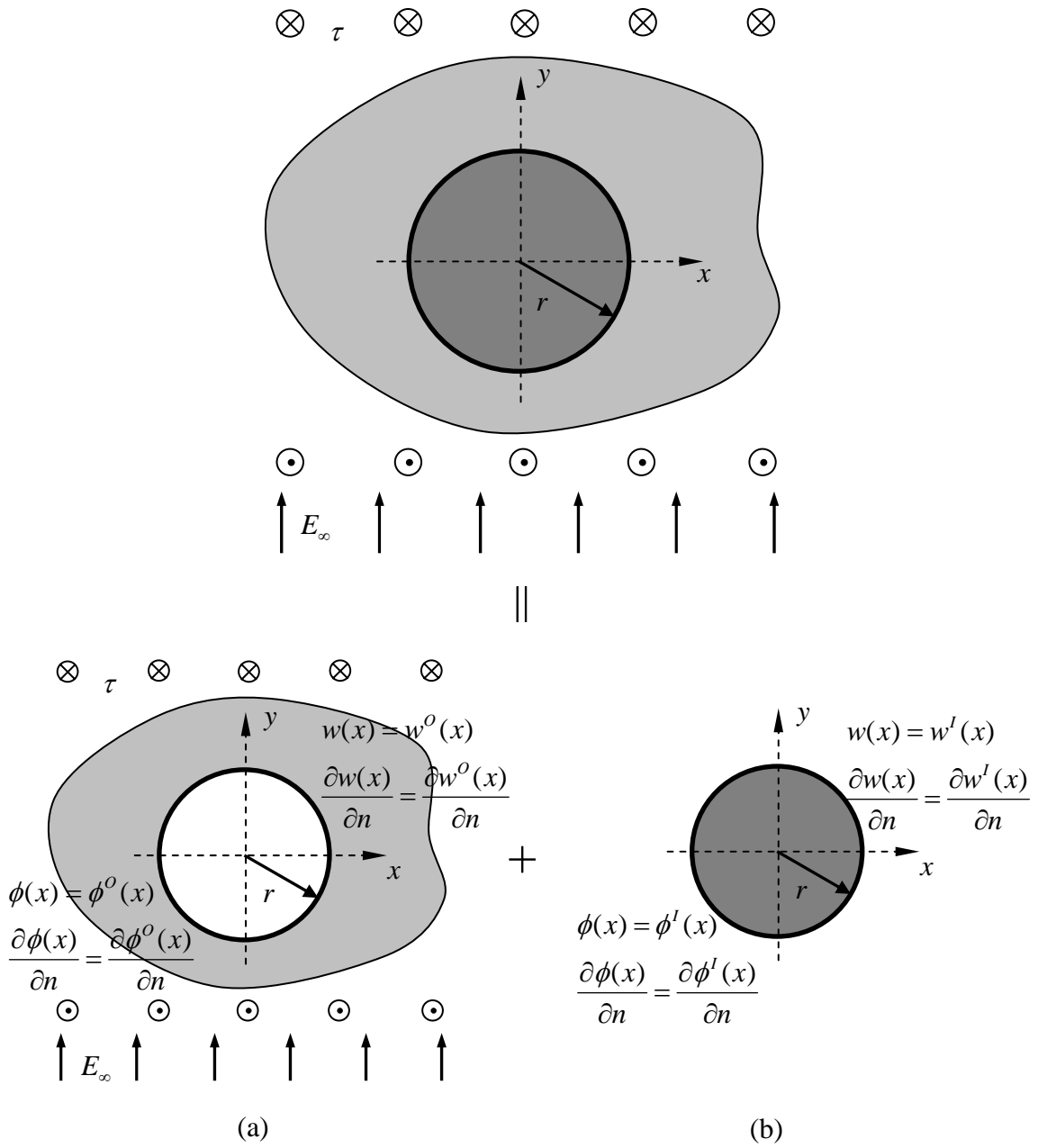


Fig. 4-2 Decomposition of the problem.

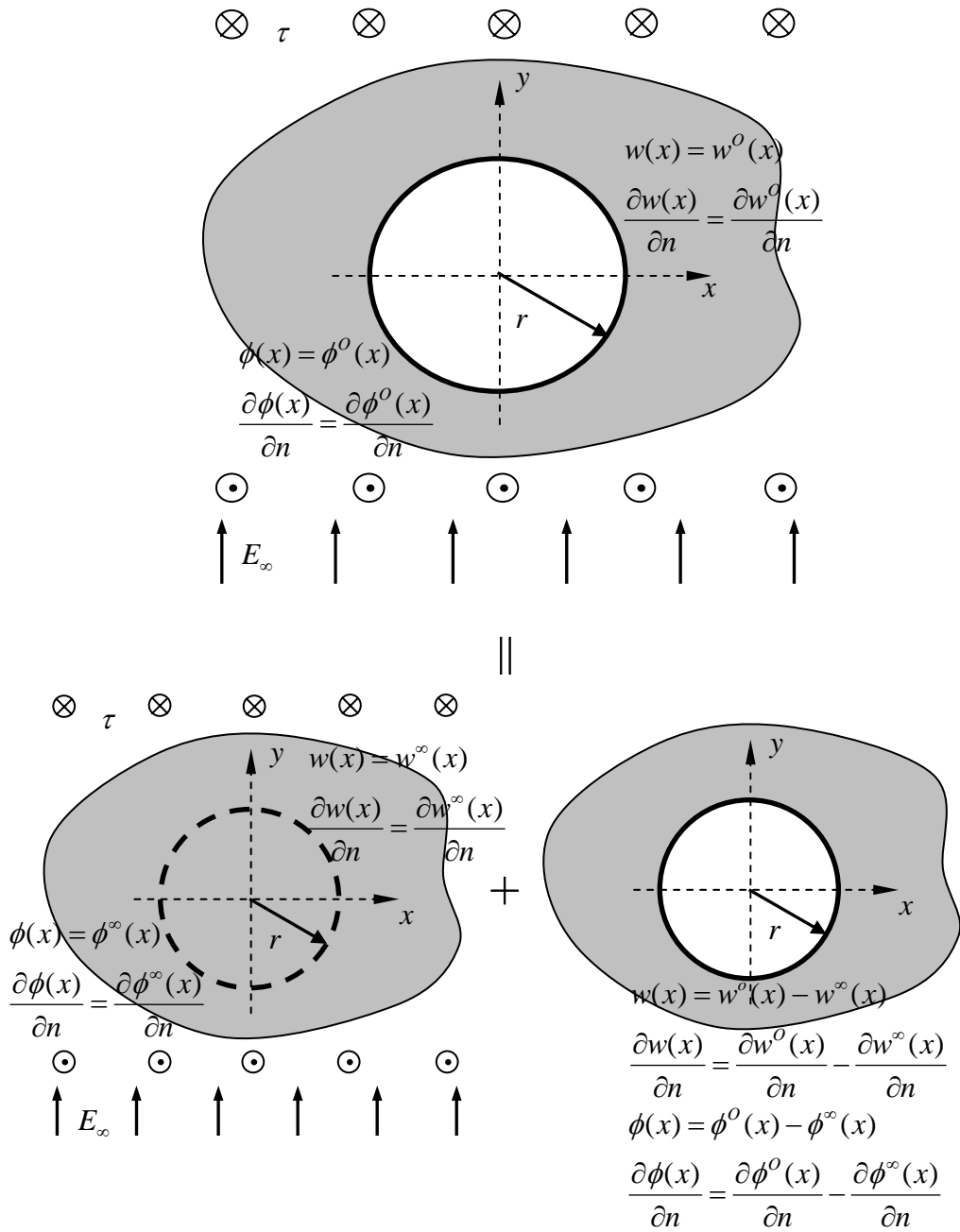


Fig. 4-3 Decomposition of the problem of Fig. 4-2 (a).

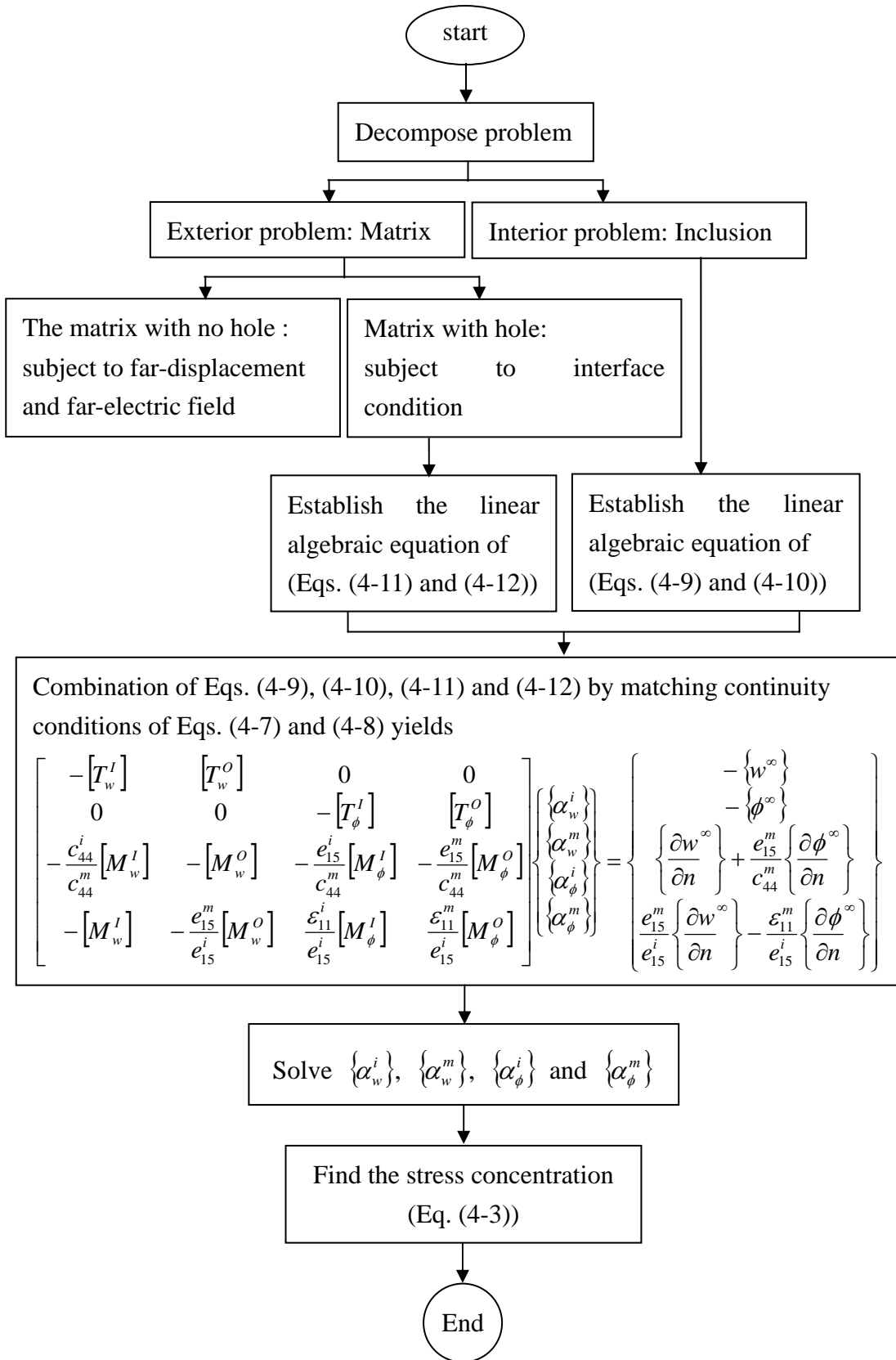


Fig. 4-4 Flowchart of solution procedures.

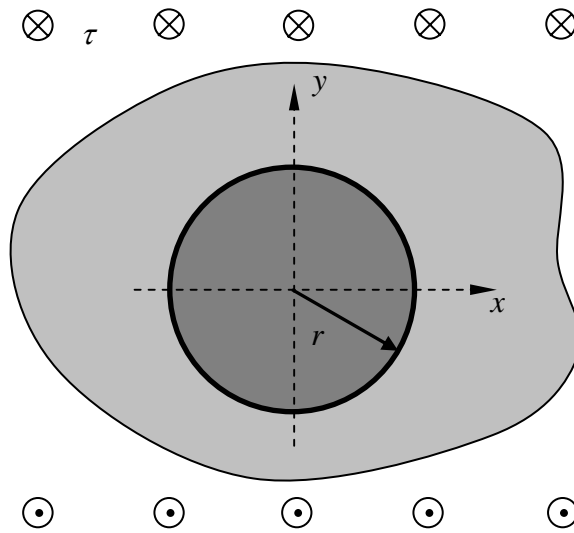


Fig. 4-5 Problem sketch of elastic dielectric matrix with an inclusion.

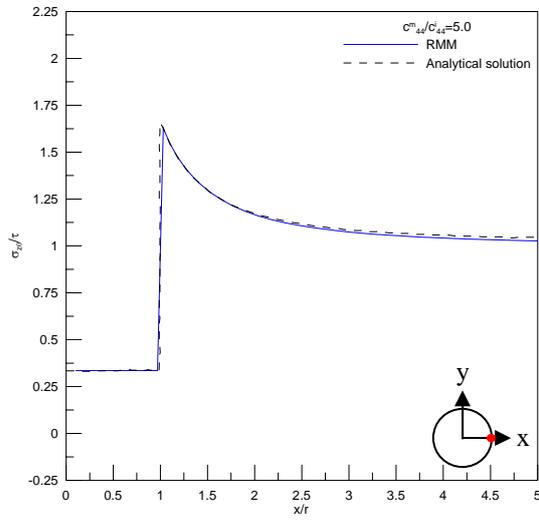


Fig. 4-6 (a)

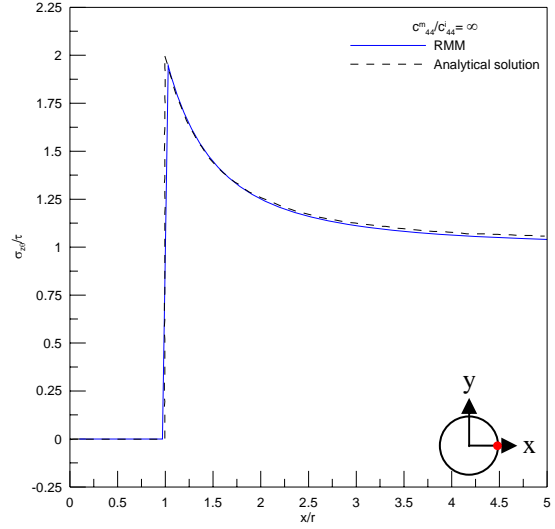


Fig. 4-6 (b)

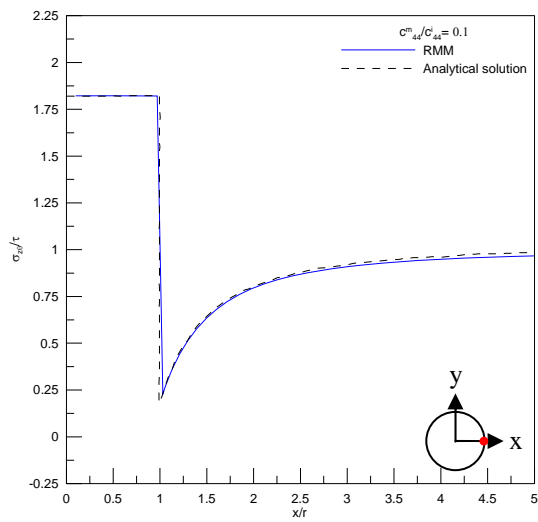


Fig. 4-6 (c)

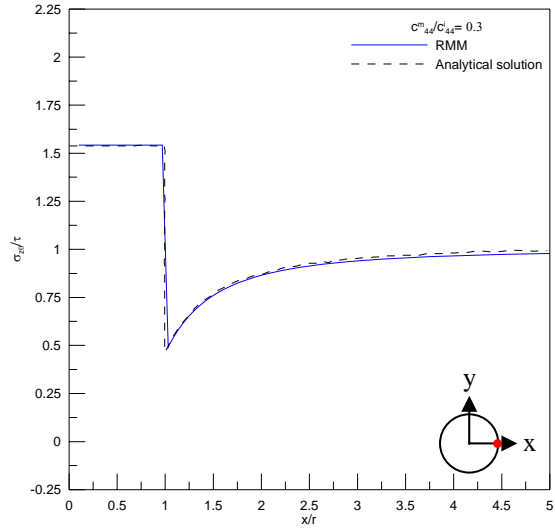


Fig. 4-6 (d)

Fig. 4-6 Stress concentration result along the line at $\theta = 0$ versus different elastic modulus ratios for single elastic dielectric inclusion in elastic dielectric matrix, (a) elastic modulus ratio $c_{44}^m / c_{44}^i = 5$, (b) elastic modulus ratio $c_{44}^m / c_{44}^i = \infty$, (c) elastic modulus ratio $c_{44}^m / c_{44}^i = 0.1$, (d) elastic modulus ratio $c_{44}^m / c_{44}^i = 0.3$.

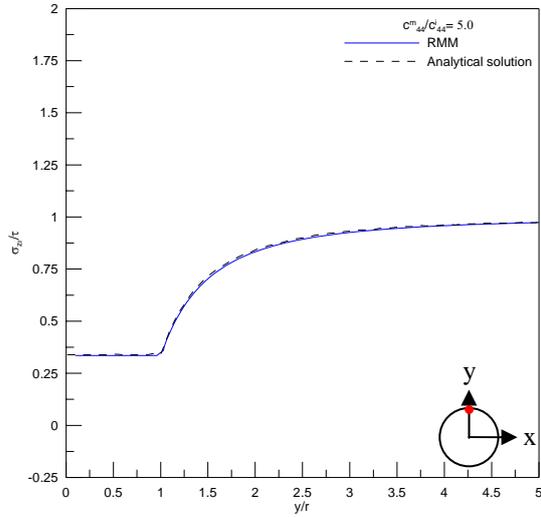


Fig. 4-7 (a)

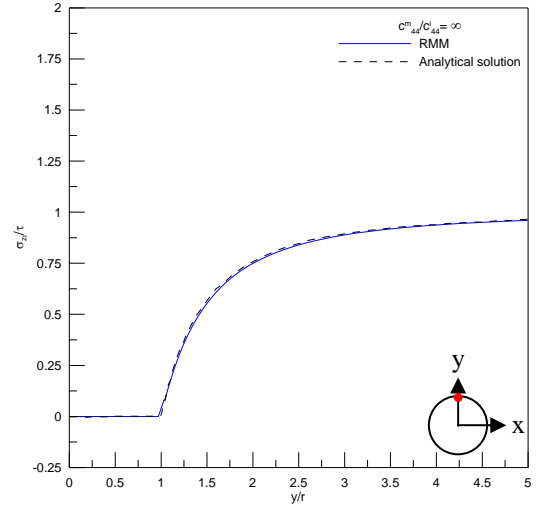


Fig. 4-7 (b)

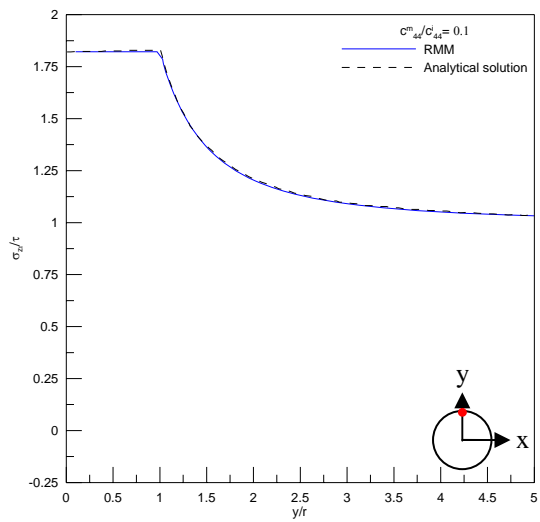


Fig. 4-7 (c)

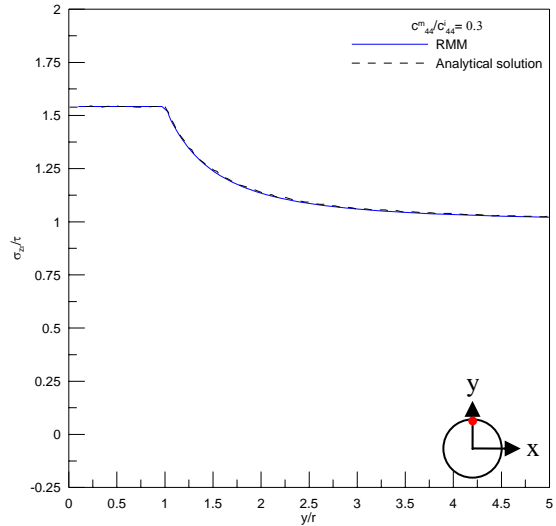


Fig. 4-7 (d)

Fig. 4-7 Stress concentration result along the line at $\theta = \pi/2$ versus different elastic modulus ratios for single elastic dielectric inclusion in elastic dielectric matrix, (a) elastic modulus ratio $c_{44}^m / c_{44}^i = 5$, (b) elastic modulus ratio $c_{44}^m / c_{44}^i = \infty$, (c) elastic modulus ratio $c_{44}^m / c_{44}^i = 0.1$, (d) elastic modulus ratio $c_{44}^m / c_{44}^i = 0.3$.

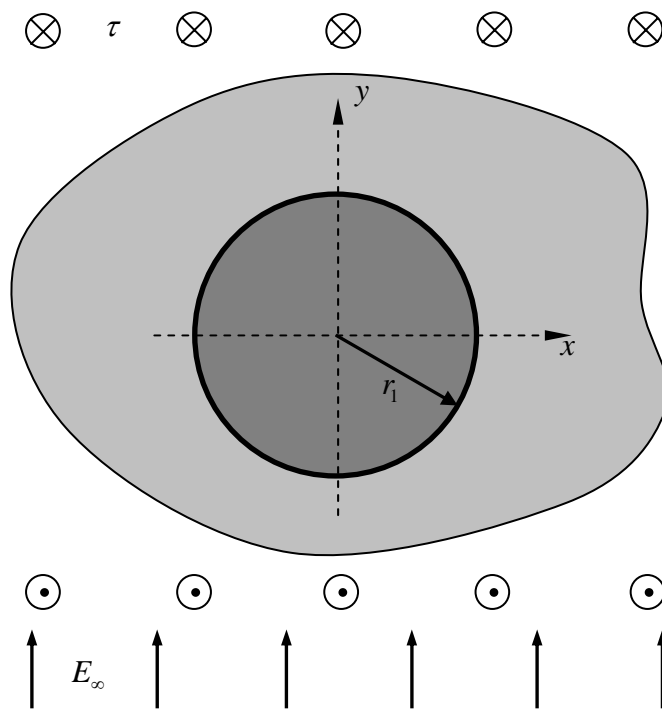


Fig. 4-8 Problem sketch of single piezoelectric inclusion.

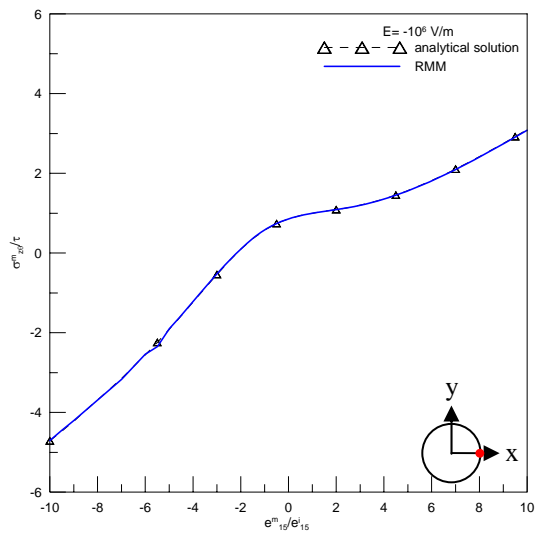


Fig. 4-9 (a)

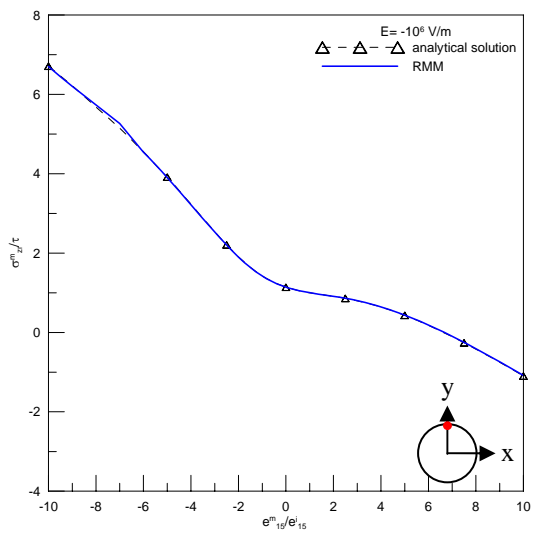


Fig. 4-9 (b)

Fig. 4-9 Stress concentration result of single piezoelectric inclusion in piezoelectric matrix for different piezoelectric modulus ratios when $E = -10^6$ V/m, (a) stress concentration at $\theta = 0$, (b) stress concentration at $\theta = \pi/2$.

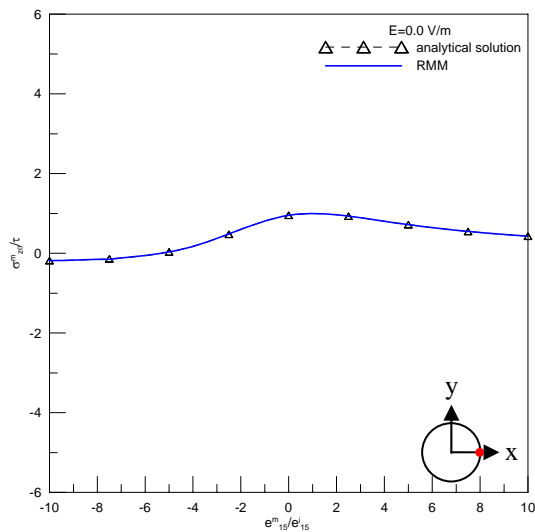


Fig. 4-10 (a)

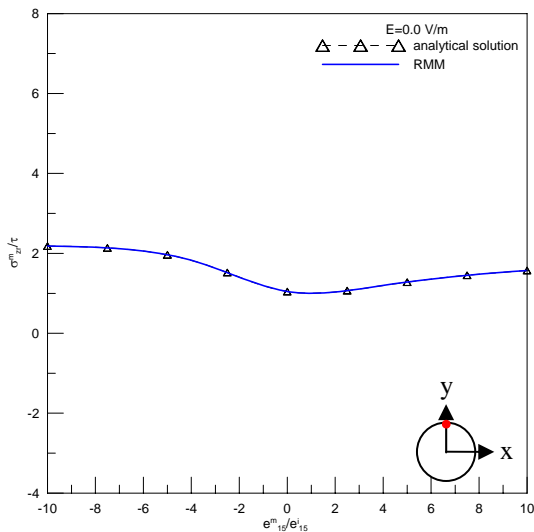


Fig. 4-10 (b)

Fig. 4-10 Stress concentration result of single piezoelectric inclusion in piezoelectric matrix for different piezoelectric modulus ratios when $E = 0$ V/m, (a) stress concentration at $\theta = 0$, (b) stress concentration at $\theta = \pi/2$.

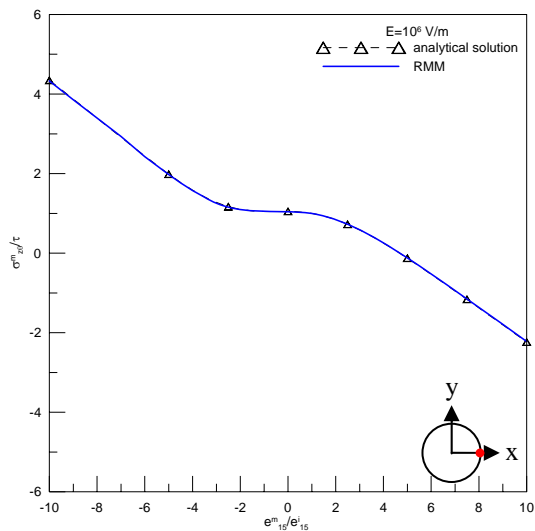


Fig. 4-11 (a)

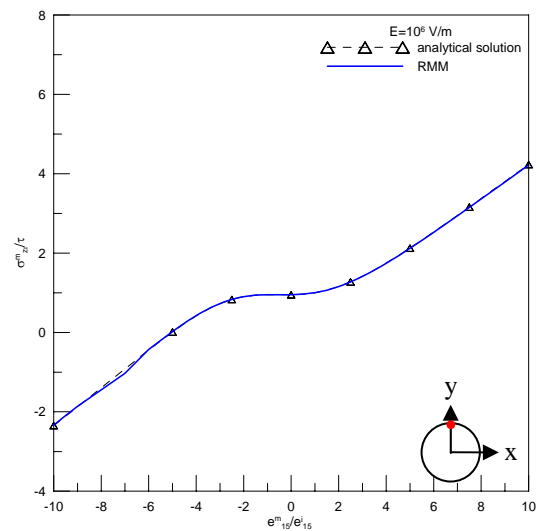


Fig. 4-11 (b)

Fig. 4-11 Stress concentration result of single piezoelectric inclusion in piezoelectric matrix for different piezoelectric modulus ratios when $E = 10^6$ V/m, (a) stress concentration at $\theta = 0$, (b) stress concentration at $\theta = \pi/2$.

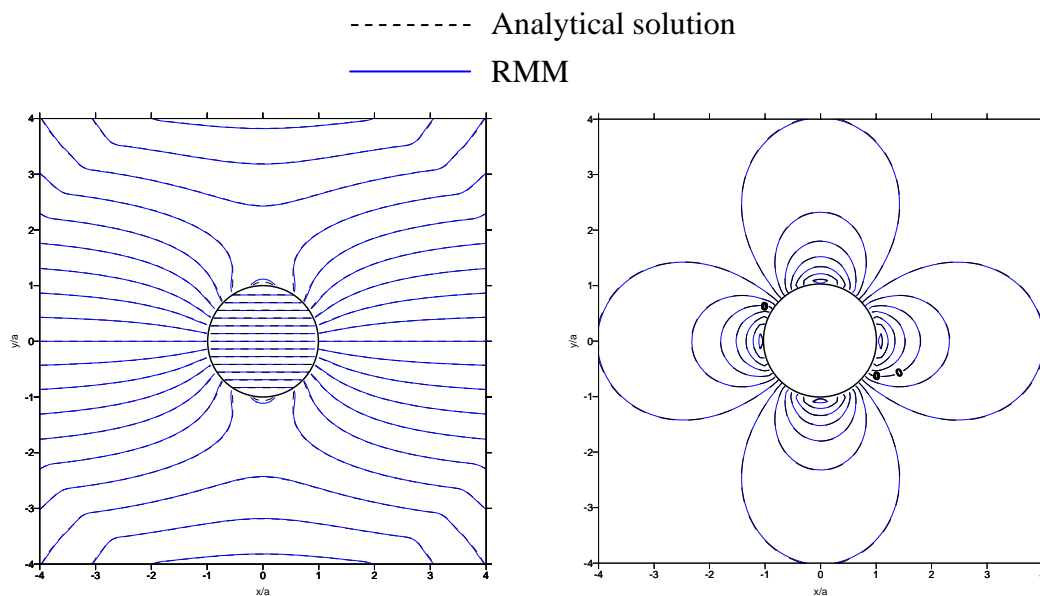


Fig. 4-12 (a)

Fig. 4-12 (b)

Fig. 4-12 Contours result of single piezoelectric inclusion in piezoelectric matrix, (a) electric potential ϕ , (b) shear stress σ^m_{zy} .

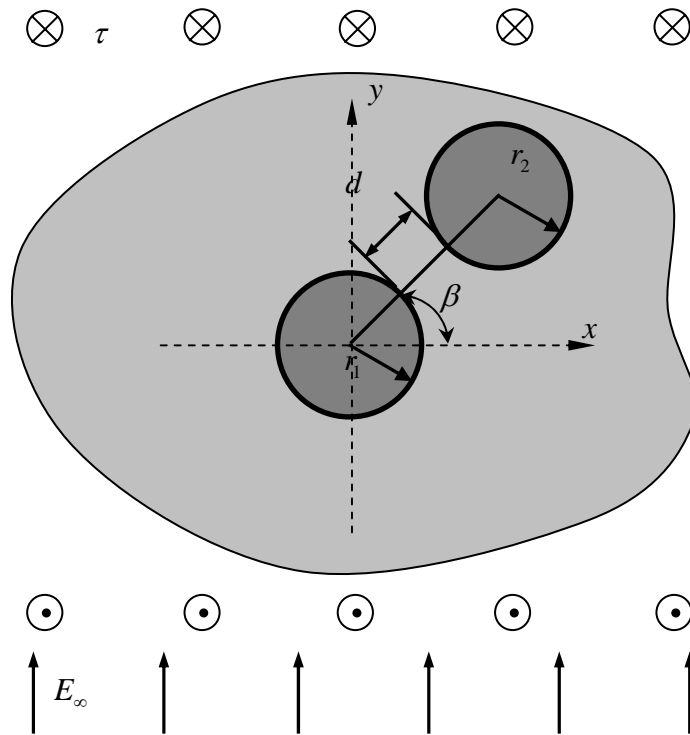


Fig. 4-13 Problem sketch of double piezoelectric inclusions.

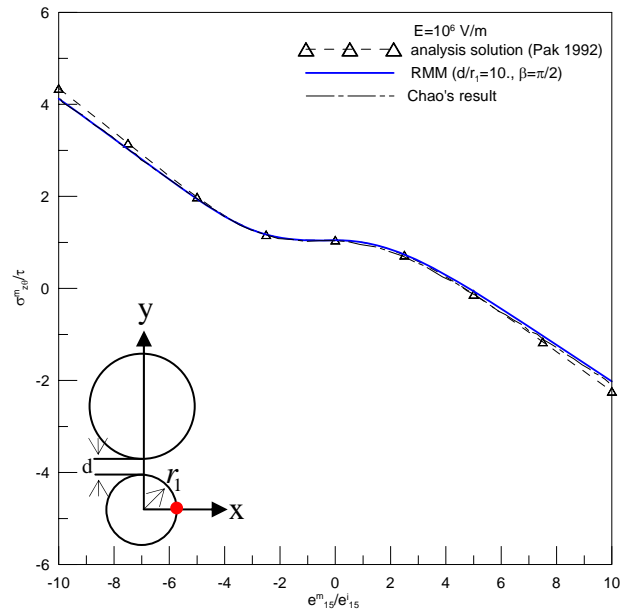


Fig. 4-14 (a)

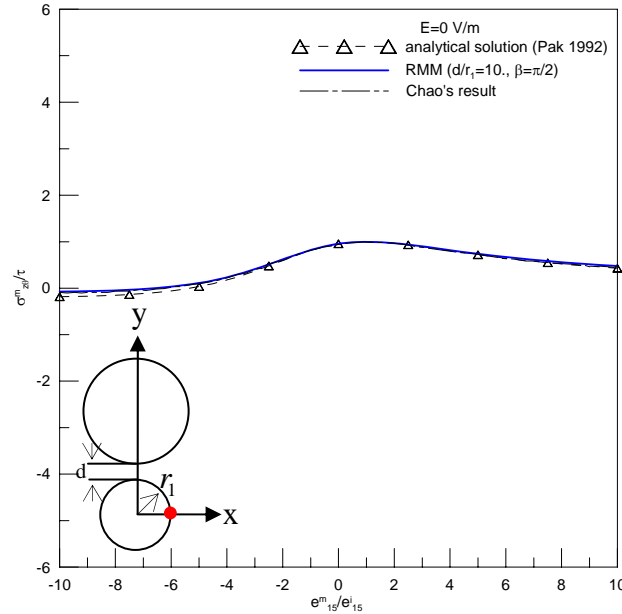


Fig. 4-14 (b)

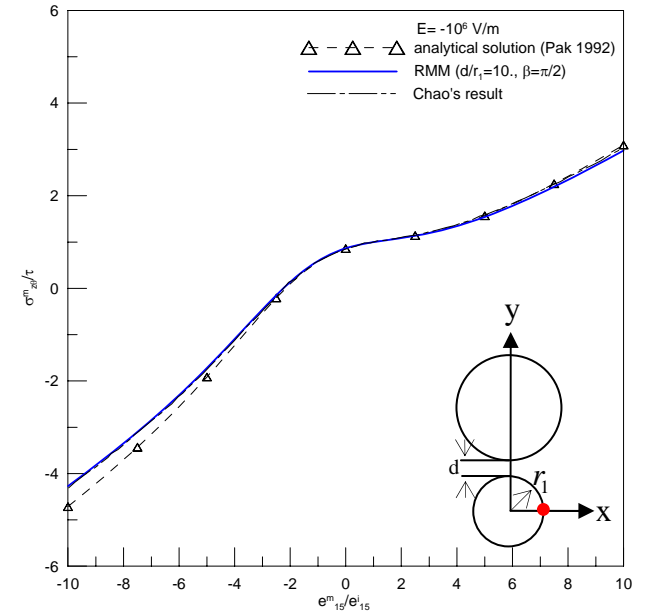


Fig. 4-14 (c)

Fig. 4-14 Stress concentration $\sigma_{z\theta}^m / \tau$ result of double piezoelectric inclusions in piezoelectric matrix for different piezoelectric module ratios and electric field, (a) $E_\infty = 10^6 \text{ V/m}$, (b) $E_\infty = 0.0 \text{ V/m}$, (c) $E_\infty = -10^6 \text{ V/m}$.

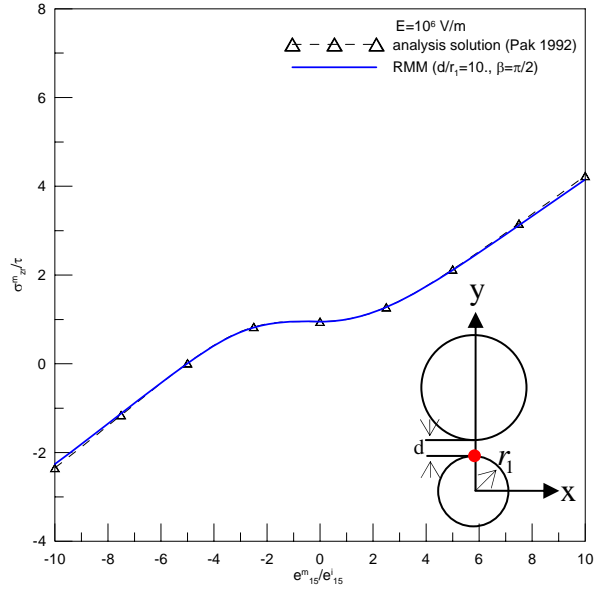


Fig. 4-15 (a)

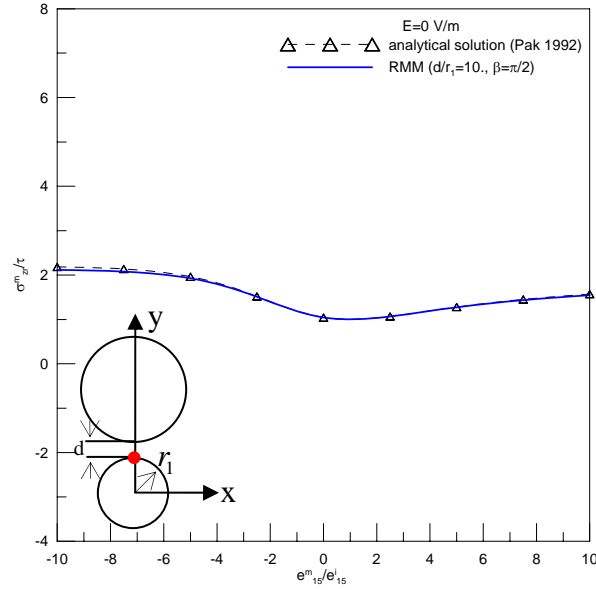


Fig. 4-15 (b)

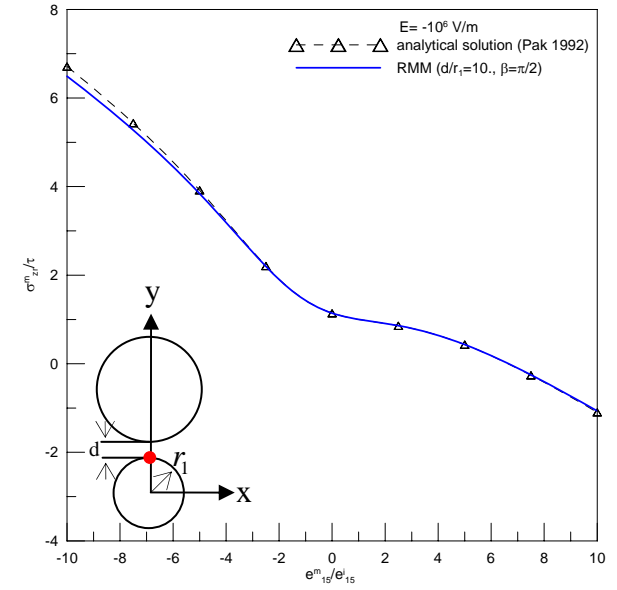


Fig. 4-15 (c)

Fig. 4-15 Stress concentration σ_{zr}^m / τ result of double piezoelectric inclusions in piezoelectric matrix for different piezoelectric module ratios and electric field, (a) $E_\infty = 10^6$ V/m, (b) $E_\infty = 0.0$ V/m, (c) $E_\infty = -10^6$ V/m.

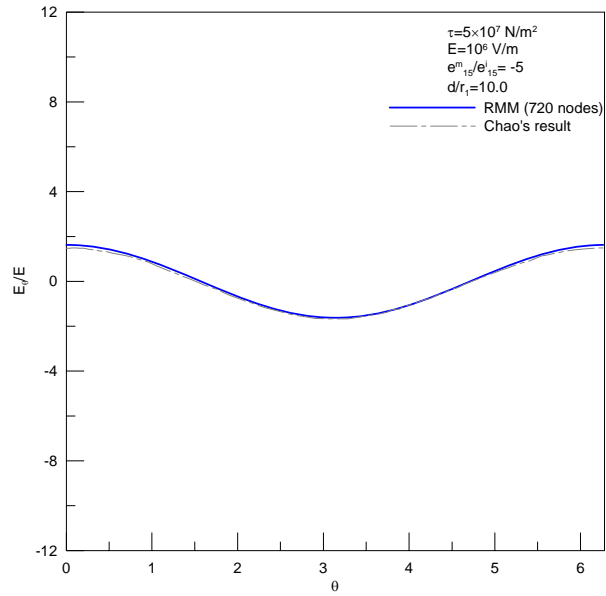


Fig. 4-16 (a)

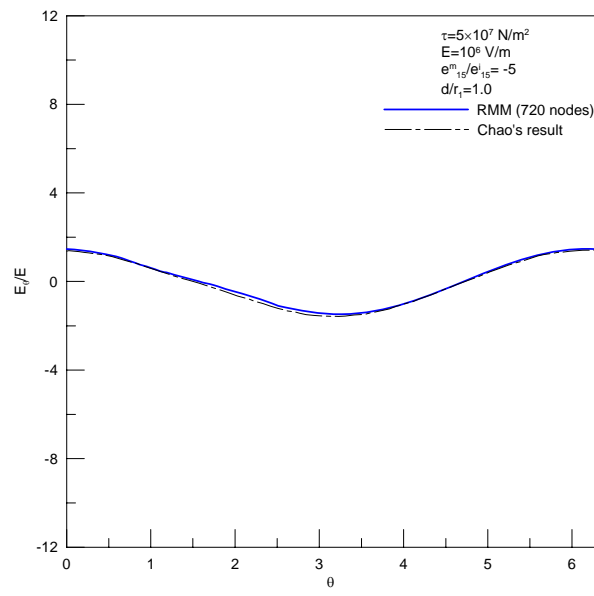


Fig. 4-16 (b)

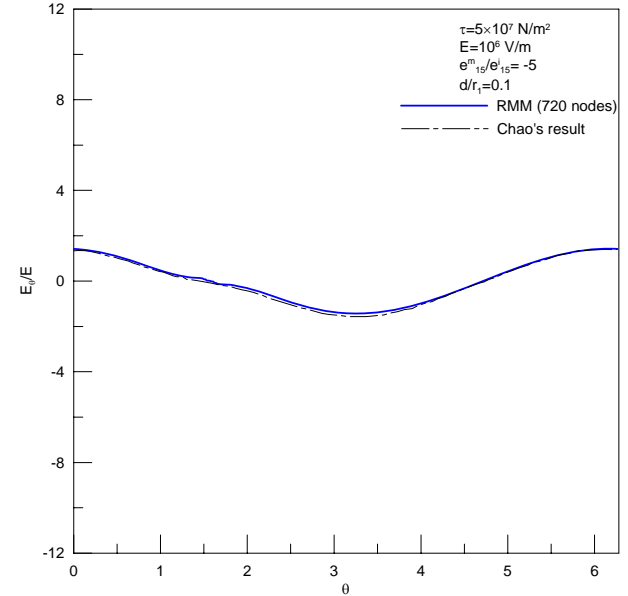


Fig. 4-16 (c)

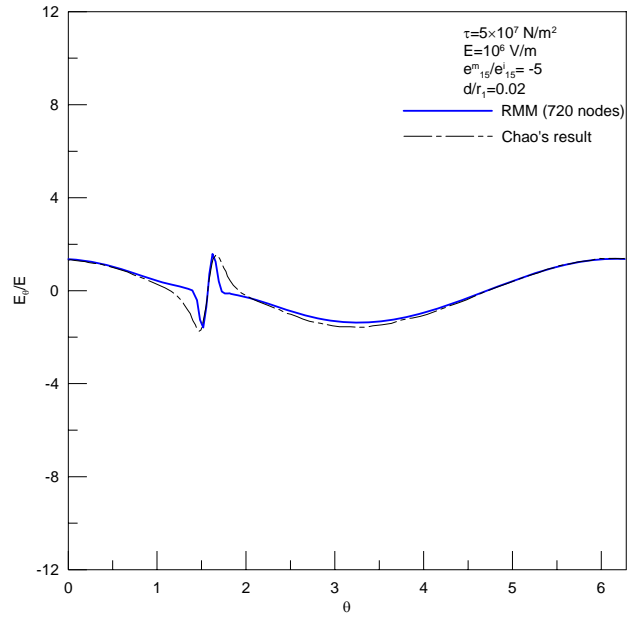


Fig. 4-16 (d)

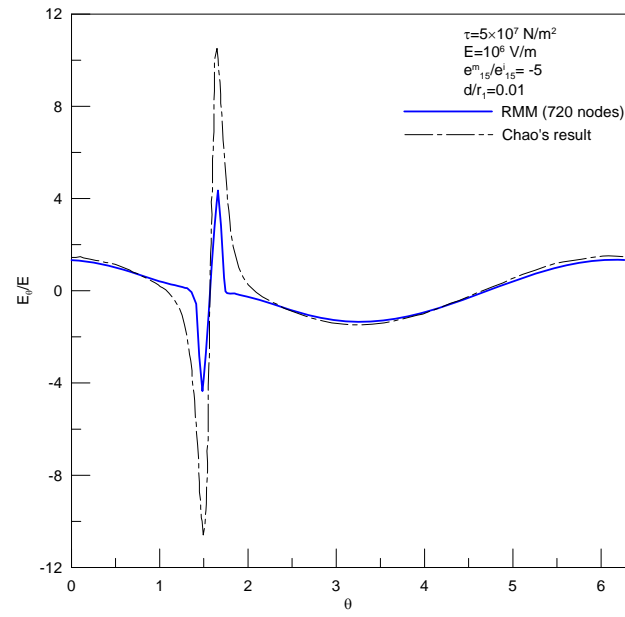


Fig. 4-16 (e)

Fig. 4-16 Tangential electric field distribution along the boundaries of first inclusion for different ratios d/r_1 with $\beta = \pi/2$, (a) $d/r_1 = 10.0$, (b) $d/r_1 = 1.0$, (c) $d/r_1 = 0.1$, (d) $d/r_1 = 0.02$, (e) $d/r_1 = 0.01$.

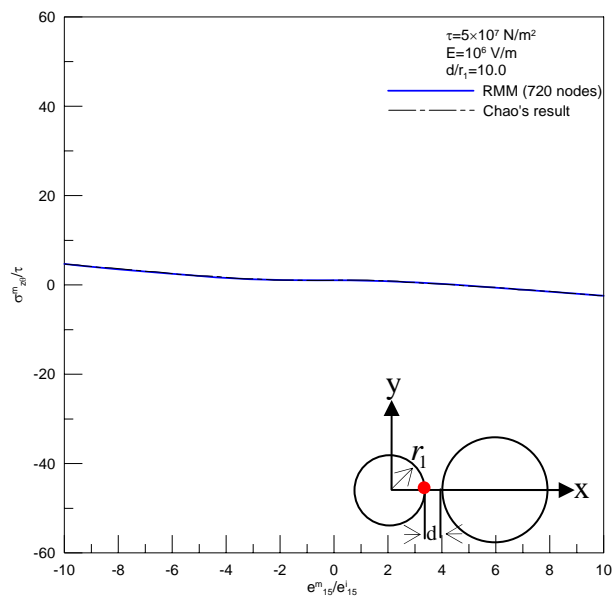


Fig. 4-17 (a)

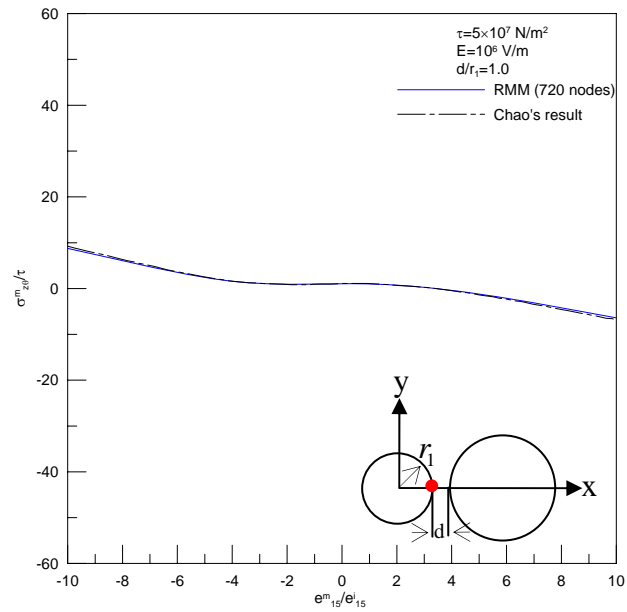


Fig. 4-17 (b)

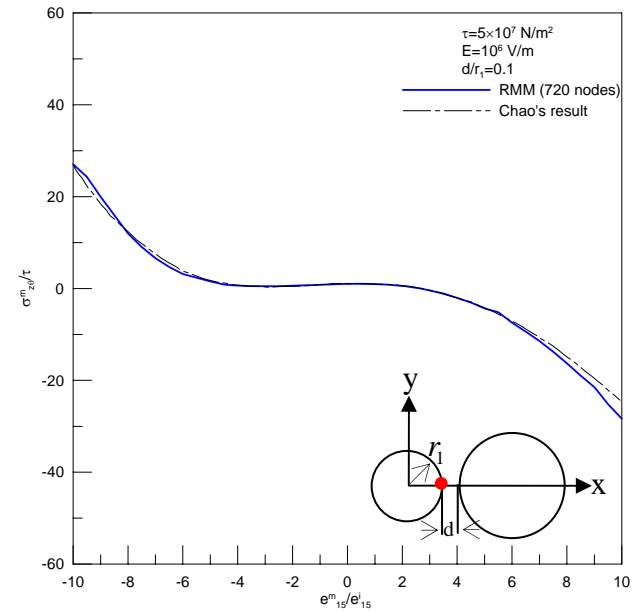


Fig. 4-17 (c)

Fig. 4-17 Stress concentration for different ratios d/r_1 of piezoelectric constants with $\beta=0$, (a) $d/r_1=10.0$, (b) $d/r_1=1.0$, (c) $d/r_1=0.1$.

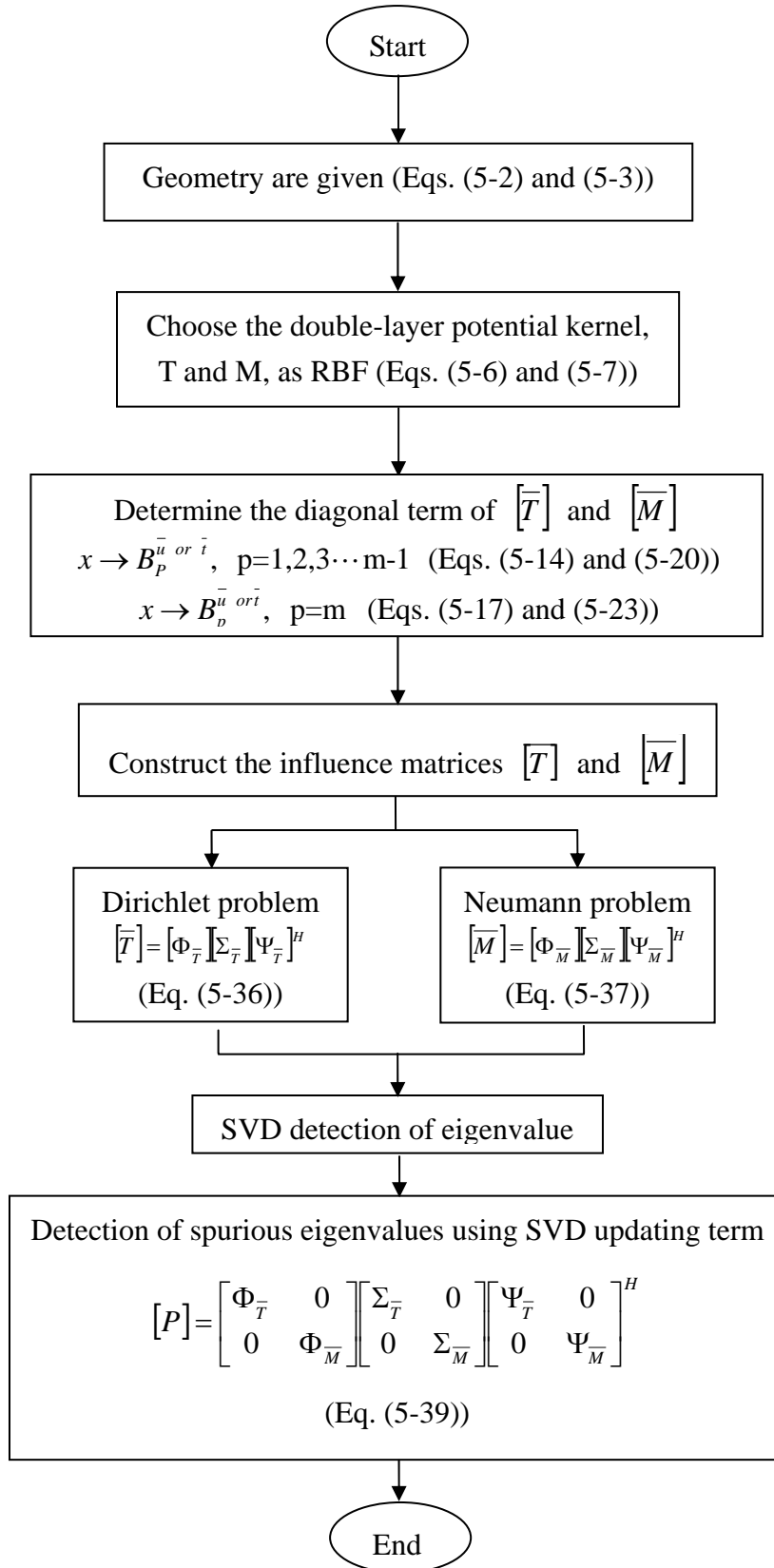


Fig. 5-1 Flowchart of solution procedures.

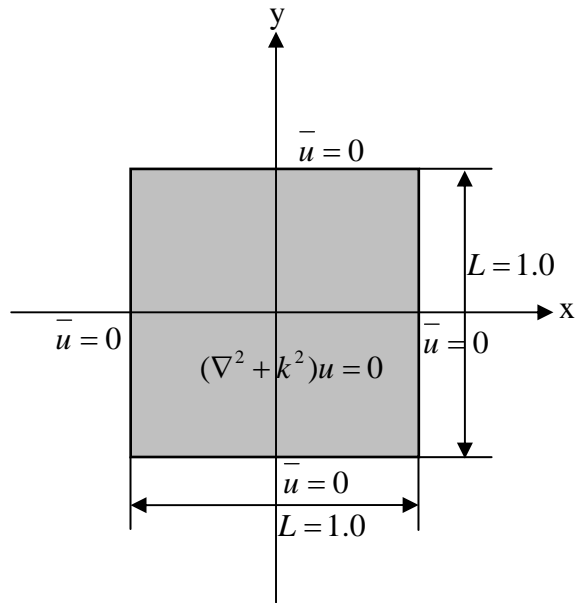


Fig. 5-2 Problem sketch for the case 1.

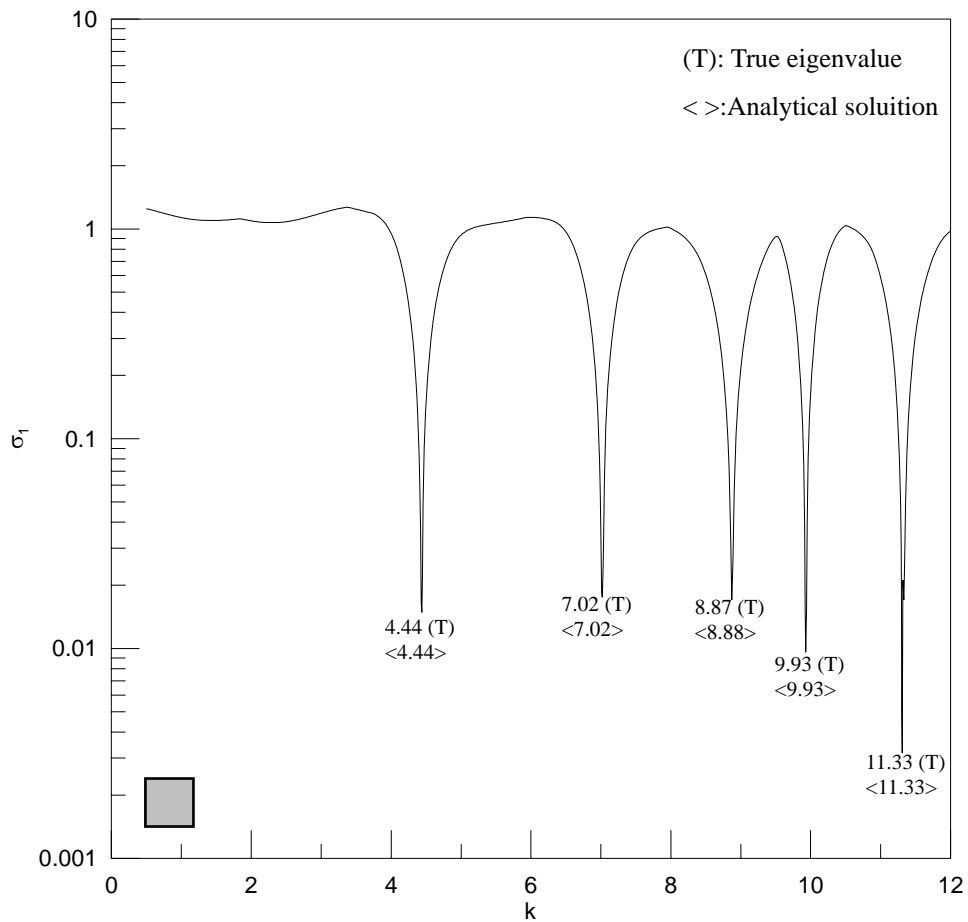


Fig. 5-3 The first minimum singular value versus wave number.

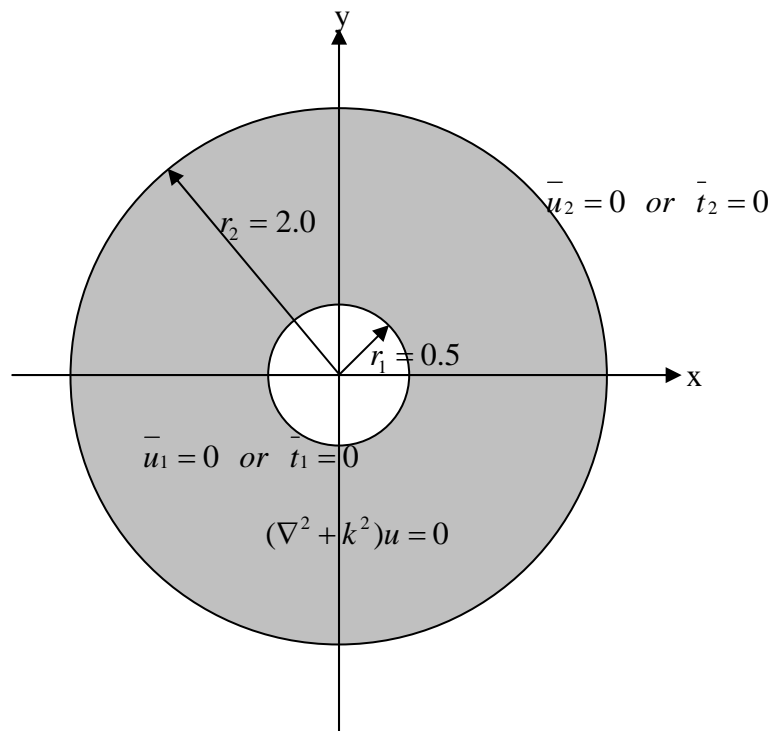


Fig. 5-4 Problem sketch for the case 5-2.

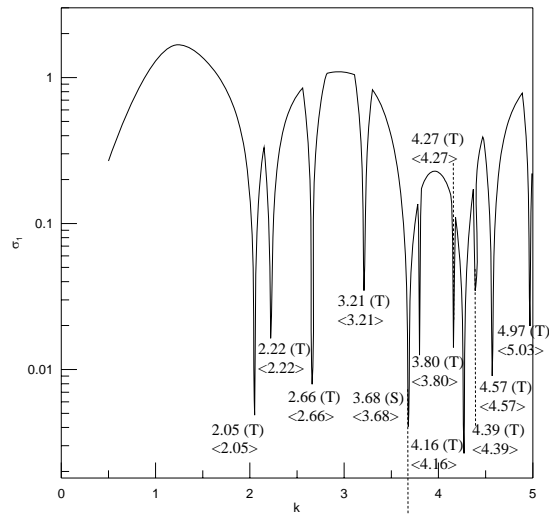


Fig. 5-5 (a)

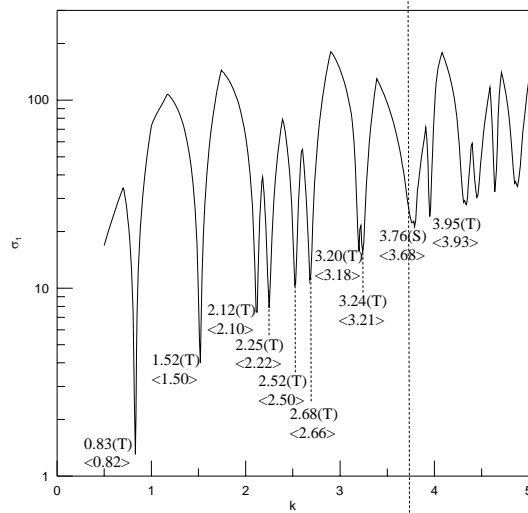


Fig. 5-5 (b)

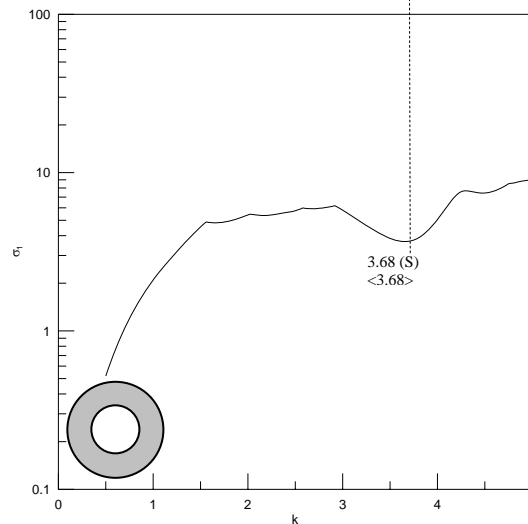


Fig. 5-5 (c)

(T): True eigenvalue
 (S): Spurious eigenvalue
 <>: Analytical solution

Fig. 5-5 The first minimum singular value versus wave number, (a) The result of RMM and analytical solution for the Dirichlet BC, (b) The result of RMM and analytical solution for the Neumann BC, (c) The result of RMM approach + SVD updating term.

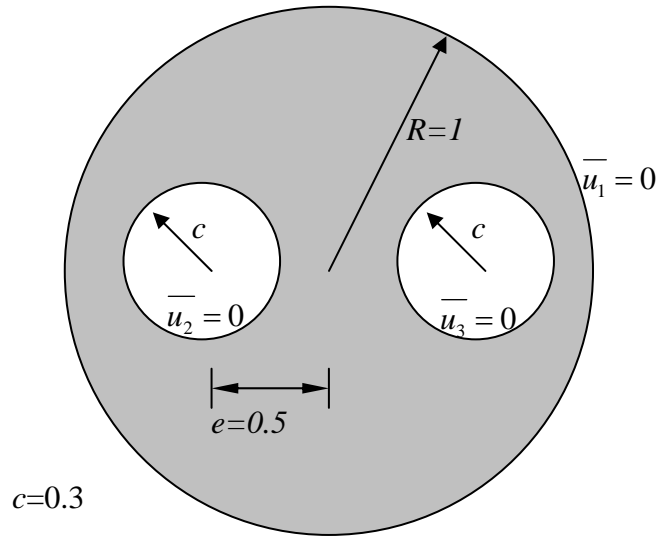


Fig. 5-6 Problem sketch for the case 5-3.

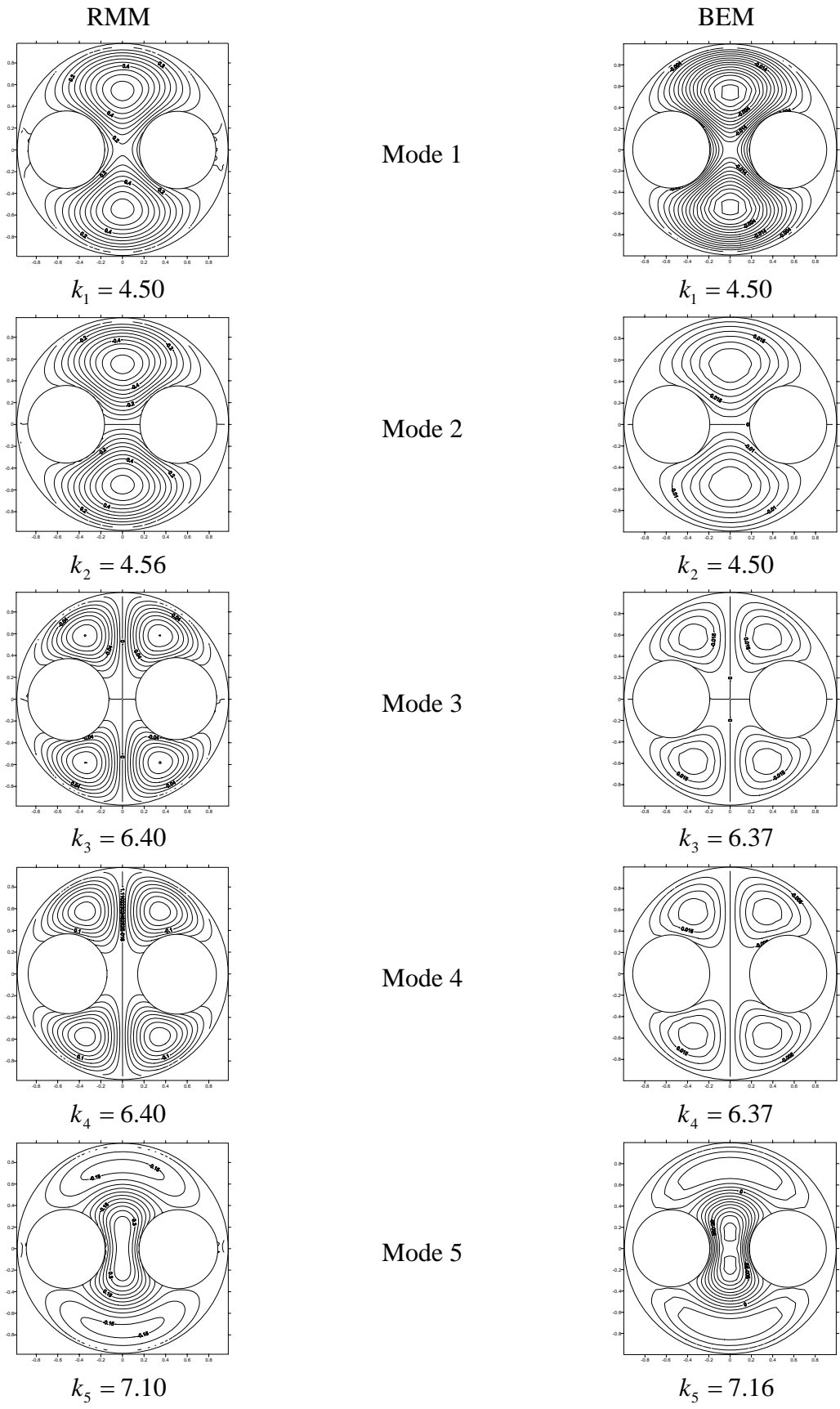


Fig. 5-7 The eigenmode result of the RMM and BEM for the case 5-3.

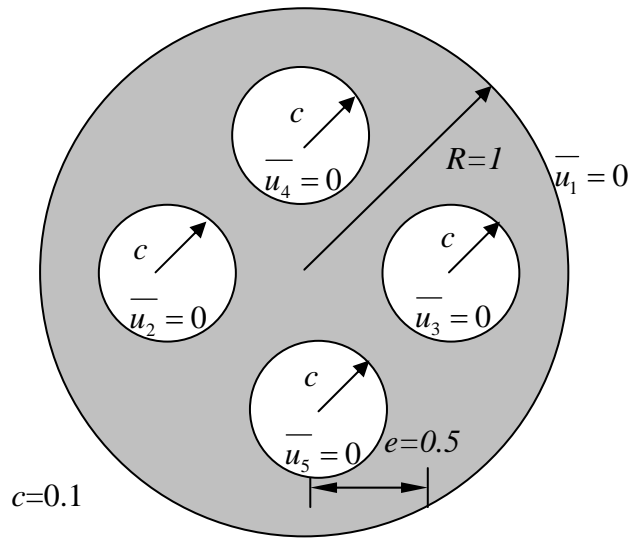


Fig. 5-8 Problem sketch for the case 5-4.

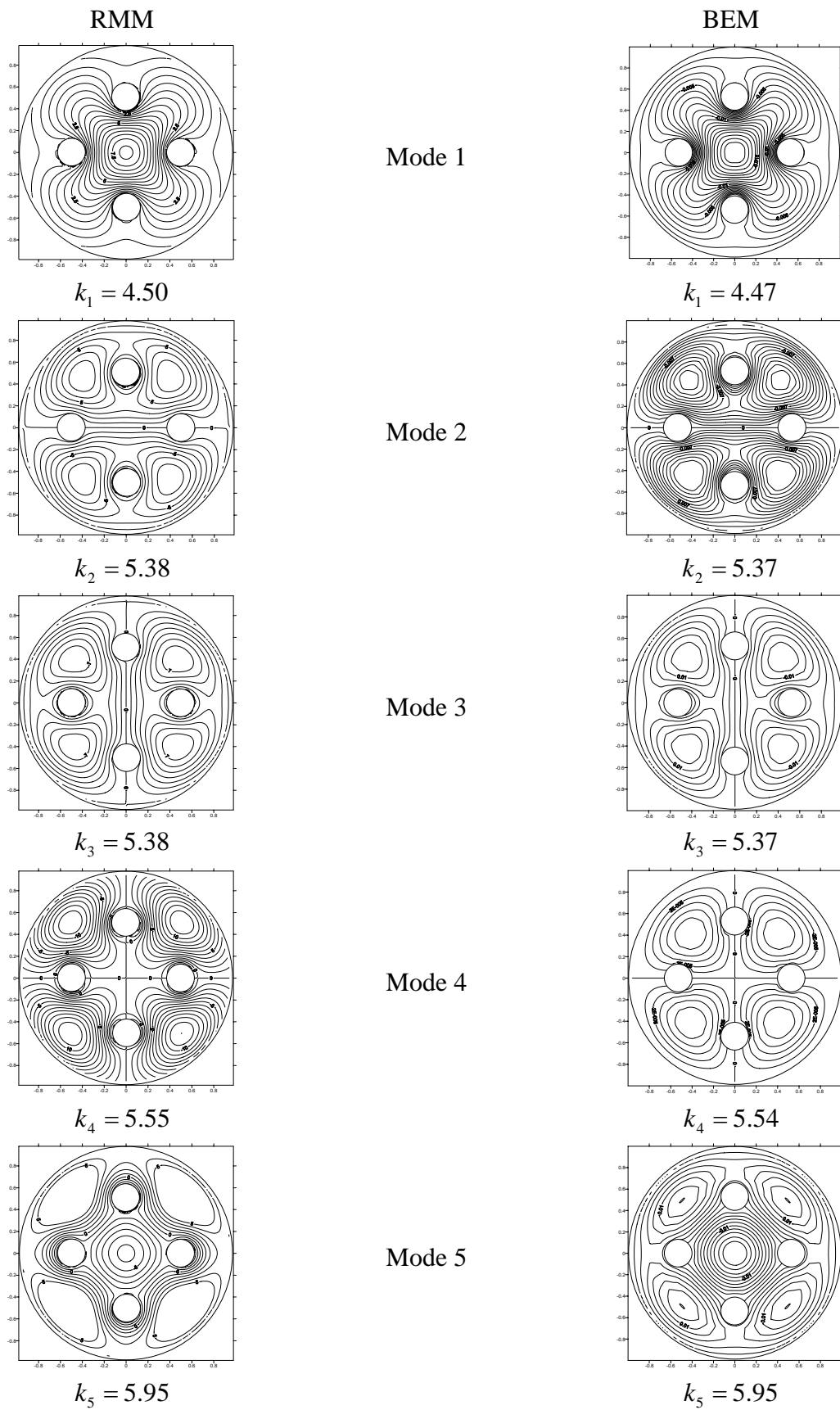


Fig. 5-9 The eigenmode result of the RMM and BEM for the case 5-4.

作者簡歷

中文姓名：高政宏
英文姓名：Jeng-Hung Kao
出生日期：民國 68 年 06 月 26 日
籍貫：台灣省台中縣
聯絡地址：台中市南屯區東興路三段 199 號
聯絡電話：(04)23207845
行動電話：0911-118835
E-mail address: jenghung.kao@gmail.com



學歷：

- 國立台灣海洋大學河海工程研究所碩士 (2004.9 ~ 2006.6)
- 國立雲林科技大學營建工程系學士 (2002.9 ~ 2004.6)

著作：

(A) 期刊論文

- 1 Chen KH, Kao JH, Chen JT, Young DL and Lu MC, 2006, Regularized meshless method for multiply-connected-domain Laplace problem, Engineering Analysis with Boundary Elements, Accepted.
- 2 Chen KH, Chen JT and Kao JH, Regularized meshless method for solving acoustic eigenproblem with multiply-connected domain, Submitted.
- 3 Chen KH, Chen JT and Kao JH, Regularized meshless method for antiplane shear problems with multiple inclusions, Submitted.
- 4 Chen KH, Kao JH and Chen JT, Regularized meshless method for antiplane piezoelectricity problems with multiple inclusions, Submitted.
- 5 Chen JT, Chen KH and Kao JH, The multiple boundary integral equations for oblique incident wave problem, Submitted.

(B) 會議論文

- 1 Kao JH, Chen KH and Chen JT, 2005, Regularized meshless method for solving Laplace problems with holes, 中華民國力學學會第二十九屆全國力學會議, 新竹.
- 2 Kao JH, Chen KH and Chen JT, 2006, Regularized meshless method for solving anti-plane problems with inclusions, 中華民國第八屆結構工程研討會, 日月潭.
- 3 Chen KH and Kao JH, 2006, A study on the eigenanalysis for membranes with stringers using novel meshless method in conjunction with SVD and multi-domain techniques, respectively, 中華民國第八屆結構工程研討會, 日月潭.